



Beatriz Quaresma Chaves Alves de Moura

Licenciada em Ciências da Engenharia Química e Bioquímica

Hybrid Ionic Liquids/Metal Organic Frameworks for CO₂/CH₄ separations

Dissertação para obtenção do Grau de Mestre em
Engenharia Química e Bioquímica

Orientador: Doutora Isabel A. A. C. Esteves, Investigadora
Auxiliar, FCT- UNL

Co-orientador: Doutor José M. S. S. Esperança,
Investigador Principal, FCT-UNL

Co-orientador: Doutora Luísa A. Neves, Investigadora
Auxiliar, FCT-UNL

Presidente: Doutor Mário F. J. Eusébio, Professor Auxiliar, FCT-UNL

Arguente: Doutor Rui P. P. L. Ribeiro, Investigador Pós-Doc, FCT-UNL

Vogal: Doutora Isabel A. A. C. Esteves, Investigadora Auxiliar, FCT- UNL



Outubro 2018

Beatriz Quaresma Chaves Alves de Moura

Licenciada em Ciências da Engenharia Química e Bioquímica

**Hybrid Ionic Liquids/Metal Organic Frameworks for
CO₂/CH₄ separations**

Dissertação para obtenção do Grau de Mestre em
Engenharia Química e Bioquímica

Orientador: Doutora Isabel A. A. C. Esteves, Investigadora Auxiliar, FCT- UNL
Co-orientador: Doutor José M. S. S. Esperança, Investigador Principal, FCT-UNL
Co-orientador: Doutora Luísa A. Neves, Investigadora Auxiliar, FCT-UNL

Presidente: Doutor Mário F. J. Eusébio, Professor Auxiliar, FCT-UNL
Arguente: Doutor Rui P. P. L. Ribeiro, Investigador Pós-Doc, FCT-UNL
Vogal: Doutora Isabel A. A. C. Esteves, Investigadora Auxiliar, FCT- UNL

Outubro 2018

Copyright © Beatriz Quaresma Chaves Alves de Moura, Faculdade de Ciências e Tecnologia, Universidade Nova de Lisboa

A Faculdade de Ciências e Tecnologia e a Universidade Nova de Lisboa têm o direito, perpétuo e sem limites geográficos, de arquivar e publicar esta dissertação através de exemplares impressos reproduzidos em papel ou de forma digital, ou por qualquer outro meio conhecido ou que venha a ser inventado, e de a divulgar através de repositórios científicos e de admitir a sua cópia e distribuição com objetivos educacionais ou de investigação, não comerciais, desde que seja dado crédito ao autor e editor.

Faculdade de Ciências e Tecnologia and Universidade Nova de Lisboa have the perpetual right with no geographical boundaries, to archive and publish this dissertation through printed copies reproduced in paper or digital form, or by any means known or to be invented, and to divulge through scientific repositories and admit its copy and distribution for educational purposes or research, non-commercial, as long as the credit is given to the author and publisher.

Acknowledgements

E ao fim de tantos anos, dou por mim sem saber o que escrever. Expressar os meus sentimentos não é inato em mim, mas vou dar o meu melhor. Afinal de contas, há pessoas que valem a pena.

Gostaria de começar por agradecer à Doutora Isabel Esteves, que esteve comigo anos antes, no Programa de Introdução à Investigação Científica, pela oportunidade e confiança depositadas em mim, assim como por toda a orientação ao longo destes meses. Agradeço ainda ao Doutor José Esperança todo sentido crítico construtivo, e à Doutora Luísa Neves toda a paciência que teve para me orientar na permeação gasosa, assim como toda a disponibilidade demonstrada.

O meu segundo agradecimento vai para a minha Mãe, que se viu sozinha com duas crianças e que fez de tudo para que nunca nos faltasse nada. Quero que saibas que continuo a batalhar para que um dia possa fazer por ti um pouco do que fizeste por mim. À Filipa, a minha irmã mais nova, agradeço a paciência para me aturar durante todos estes anos e a cumplicidade que desenvolvemos. Agradeço ainda ao Rui Alves, que é parte da nossa família, por todas as discussões, debates e troca de ideias.

Não posso deixar de agradecer às minhas queridas colegas Isabel Moreira, Lourdes Silva e Cristina Lemos, do serviço de voluntariado hospitalar da Liga Portuguesa Contra o Cancro, no Instituto Português de Oncologia de Lisboa. Agradeço a forma calorosa como me receberam na equipa, e como me apoiaram desde que decidi dedicar-me a fazer mais pelos outros. Já passaram quatro anos desde que estou convosco, e sinto que me ajudaram a crescer enquanto pessoa. Todas sabemos que o que fazemos não é fácil, e que confrontar aquilo que é a realidade de vida para muitas – demasiadas – pessoas, é destroçante. Mas convosco aprendi que gestos simples como ajeitar a almofada, fazer chegar uma garrafa de água, ou parar para ouvir o que os doentes muitas vezes não têm coragem de dizer aos familiares, faz toda a diferença naquela que é a batalha mais dura da vida – a luta pela sobrevivência. Agradeço ainda à nossa querida ‘Chefe’, Graça Almeida, que além de me ter acompanhado com todo o amor e sabedoria que lhe são característicos, me permitiu ter sempre flexibilidade de horário para poder conjugar o serviço de voluntariado com a faculdade. Um beijinho enorme para todas.

Ao meu Pai... contigo aprendi que saber escutar, e poder crescer com a sabedoria dos mais velhos é uma arte. Aprendi a não fazer distinções entre o valor das pessoas com base nas suas origens, crenças ou vivências. Aprendi que somos todos iguais em direitos, e deveres, e que ser humilde e saber calar o ego é uma parte crucial da nossa caminhada pela vida. Lembro-me que quando comecei a falar, uma das primeiras coisas que me ensinaste a dizer foi *o quadrado da hipotenusa é igual à soma dos quadrados dos catetos*. Ensinares-me o Teorema de Pitágoras antes dos três anos de idade, e todos os estímulos intelectuais que me incumbiste em pequena, ajudaram-me a crescer com amor a tudo que é lógico e racional. Obrigada.

À minha avó Maria Violeta, que nasceu em 1924 e viveu até às 93 primaveras, agradeço a inspiração e as histórias que sempre me contou sobre os tempos em que teve a sua pequena farmácia, e sobre todas as vezes que teve que consultar o *Manual Pharmacotechnico* de 1910, que está hoje nas minhas mãos, porque alguém batia à porta a pedir *Xarope das Cinco Raízes*, e ela não se lembrava das quantidades exatas a utilizar. Sei que estaria orgulhosa de mim, dos 15 netos fui a única a seguir-lhe as pisadas, e a enveredar pela química.

Ao meu querido amigo Tiago Ferreira - não há palavras. Disse muito do que queria dizer, na fita que te escrevi. Agradeço-te, do fundo do coração, todos os debates e trocas de ideias, assim como todo o apoio incondicional que me deste durante a tese. Não falhaste, e estiveste sempre lá para segurar as pontas. Já diziam os teus queridos Beatles *'Oh I get by with a little help from my friends... Gonna try with a little help from my friends'*. Muito Obrigada!

Às irmãs que a vida me deu: Daniela Agostinho, Ana Rita Pecorelli e Joanna Correia, agradeço terem crescido comigo. Agradeço todas as gargalhadas, mas agradeço sobretudo todas as vezes que me disseram que estava errada. Aprendemos muito mais com os nossos erros, do que com os nossos sucessos. E vocês foram, e são, fundamentais na minha formação enquanto pessoa. A vocês dedico uma frase da minha querida Florbela Espanca, que nasceu a 8 de Dezembro de 1894 (exatamente 100 anos antes de mim), e que diz o seguinte: *'A amizade é o maior sentimento que não morre'*. Um beijinho enorme.

Aos meus amigos Miguel Ferreira e João Filipe, obrigada por terem estado comigo 'no inferno', e por me terem motivado a continuar a avançar, mesmo sendo difícil. Ao Pedro Melo, à Ivania Macedo, ao Luís Barros e à Jéssica Costa, agradeço todo o companheirismo ao longo destes anos, e durante os serões de estudo intensivo.

Agradeço à Inês Ferreira, pelo apoio que me deu durante a tese, quer a nível laboratorial, quer a nível da caracterização das membranas sintetizadas. Um obrigado ainda ao Professor Vítor Alves, pela disponibilidade aquando da visita ao ISA para testar as propriedades mecânicas das membranas.

I also wish to thank the love of my life, Mohammad Mazaheri. Thank you for all the support you have always given me. Thank you for staying by my side on my darkest days, and for loving me still. I would like to honour you, by remembering this beautiful poem you once wrote:

طلوعت به غروبم دوخته شد
ازینجاست تا آنسوی دریاها بین الحرمینم
خیاط سرنوشت چه دوخت
کز مناست تا کعبه هر روز بین المشرقینم

E agora o mais difícil. Ao meu querido Avô, que foi tantas vezes Pai, agradeço por ter sido o meu pilar e a minha estabilidade. Tal como eu, tem sempre mais sentimentos do que palavras para os descrever, mas sei que está orgulhoso de mim. À minha querida Avó Tita, que ainda hoje me dá colinho como mais ninguém, agradeço todo o amor, toda a preocupação e todos os sacrifícios que fez, e ainda faz, por mim. A vossa vida não foi fácil, começaram a trabalhar antes dos 14 anos, e nunca tiveram possibilidade de ir à escola. Naquela altura os tempos eram outros, mais duros, implacáveis e cruéis. E hoje, ambos com mais de 80 anos, sofrem na pele as consequências de anos e anos de trabalho sem descanso. Quero que saibam que consegui. Que estudei, e que dou valor à oportunidade que tive para o poder fazer. Não me vou nunca esquecer, que a educação que tive é um luxo que muitos podem apenas sonhar alguma vez ter. A vocês dedico esta tese.

Muito obrigada.

Abstract

In this thesis, composite materials resulting from the impregnation of ionic liquids (ILs) in the porous structure of the Zeolitic Imidazolate Framework-8 (ZIF-8), known as IL@ZIF-8, were studied to investigate their potential as alternative adsorbents in gas separation processes (e.g. biogas upgrading to biomethane).

Three brand-new IL@ZIF-8 composites were synthesized, by incorporating the same molar amount of IL in the ZIF-8 framework to allow the proper comparison of these the materials. Their carbon dioxide (CO₂) and methane (CH₄) uptake capacity, as well as CO₂/CH₄ ideal selectivity, were obtained through adsorption equilibrium experiments, using a gravimetric method at 30°C of temperature and in the pressure range of 0-16 bar. In addition, these composites were fully characterized through Helium (He) pycnometry, N₂ adsorption-desorption at 77 K, Powder X-Ray Diffraction (PXRD), and Fourier Transform Infrared Spectroscopy (FT-IR). Adsorption equilibrium measurements showed that none of the prepared IL@ZIF-8 surpassed the pristine ZIF-8 in CH₄ and CO₂ uptake capacity, suffering a loss of 19-50% at 1 bar, and 17-53% at 16 bar. Furthermore, one composite showed improvements in CO₂/CH₄ ideal selectivity up to 5 bar with an increase of 7.16-7.60% at subatmospheric pressure and 5.42% at 5 bar. The same composite also showed an increase of 4.24% and 5.14%, at 10 and 16 bar, respectively.

In addition, two of the IL@ZIF-8 composites previously prepared and studied by T. Ferreira [1] were incorporated at different loadings in Matrimid®5218. The main goal was to understand how these fillers would impact the CO₂ and CH₄ permeability of the membranes, and consequently their CO₂/CH₄ ideal selectivity. These studies were performed at the temperature of 30°C and 0.7 bar of relative pressure. The prepared mixed-matrix membranes (MMMs) were also characterized to evaluate their mechanical properties and hydrophobicity.

Gas permeation results showed a paired growth in both CO₂ and CH₄ permeability, and CO₂/CH₄ ideal selectivity, with an increase in filler loading, with one of membranes surpassing the CO₂/CH₄ Robeson Upper Bound. Results also showed that with upon the incorporation of ZIF-8, the membranes become more rigid and hydrophobic than the pristine Matrimid®5218 membrane. Moreover, this effect is more pronounced when using IL@ZIF-8 as fillers, turning the membranes even more fragile and hydrophobic. Considering this, and despite the promising results obtained in the gas permeation experiments, the optimization of the mechanical properties of these membranes is fundamental for their feasible and future application in industrial gas separation processes.

Keywords: Zeolitic Imidazolate Framework-8 (ZIF-8), IL@ZIF-8 composites, Matrimid®5218, mixed-matrix membranes (MMMs), ionic liquids (ILs), gas permeation, gas adsorption.

Resumo

Nesta tese, materiais compósitos resultantes da impregnação de líquidos iônicos (LIs) na estrutura porosa do Zeolitic Imidazolate Framework-8 (ZIF-8), denominados IL@ZIF-8, foram estudados para investigar o seu potencial como adsorventes alternativos em processos de separação gasosa (e.g. condicionamento de biogás a biometano).

Três novos compósitos IL@ZIF-8 foram preparados, incorporando a mesma quantidade molar de LI na estrutura do ZIF-8, permitindo a sua válida comparação. A sua capacidade para adsorção de dióxido de carbono (CO₂) e metano (CH₄), assim como a sua seletividade ideal para CO₂/CH₄, foram obtidas através da medição de equilíbrios de adsorção usando um método gravimétrico a 30°C de temperatura e na gama de pressão de 0-16 bar. Estes compósitos foram detalhadamente caracterizados através de picnometria de Hélio (He), adsorção-dessorção de N₂ a 77 K, difração de raios-X de pó (PXRD) e espectroscopia de infravermelho (FT-IR). As medições de equilíbrio de adsorção mostram que nenhum dos compósitos IL@MOF ultrapassou o ZIF-8 relativamente à sua capacidade de adsorção de CO₂ e CH₄, tendo sofrido uma perda de 19-50% a 1 bar, e 17-53% a 16 bar. Adicionalmente, um dos compósitos mostrou vantagens na seletividade ideal CO₂/CH₄ até 5 bar, com um aumento de 7.13-7.60% a pressão subatmosférica e 5.29% a 5 bar. O mesmo compósito mostrou ainda um aumento de 4.24% e 5.12%, a 10 e 16 bar, respetivamente.

Adicionalmente, dois dos compósitos anteriormente preparados e estudados por T. Ferreira [1], foram incorporados em diferentes quantidades em Matrimid®5218. O objetivo foi perceber o impacto destes compósitos na permeabilidade de CO₂ e CH₄, e na seletividade ideal para CO₂/CH₄ das membranas. Estes ensaios foram efetuados a uma temperatura de 30°C e a uma pressão relativa transmembranar de 0.7 bar. As membranas sintetizadas foram ainda caracterizadas para avaliar as suas propriedades mecânicas e hidrofobicidade.

Os resultados de permeação gasosa mostraram um crescimento em par da permeabilidade de CO₂ e CH₄, e da seletividade ideal CO₂/CH₄, com uma das membranas a ultrapassar o Limite Superior de Robeson para CO₂/CH₄. Os resultados obtidos mostram ainda que com a incorporação de ZIF-8 as membranas tornaram-se mais rígidas e hidrofóbicas quando comparadas com Matrimid®5218. Este efeito é mais evidente quando se utiliza IL@ZIF-8, uma vez que a membranas tornaram-se ainda mais frágeis e hidrofóbicas. Considerando isto, e apesar dos resultados promissores obtidos na permeação gasosa, a otimização das propriedades mecânicas destas membranas é fundamental para que estas possam ser implementadas em processos industriais de separação de gases.

Palavras-Chave: Zeolitic Imidazolate Framework-8 (ZIF-8), compósitos IL@ZIF-8, Matrimid®5218, membranas de matriz mista (MMMs), líquidos iônicos (LIs), permeação gasosa, adsorção gasosa.

Table of Contents

1. Introduction.....	1
1.1. Motivation	1
1.2. Theoretical Concepts.....	4
1.2.1. Gas Mixtures of Interest	4
1.2.2. Gas Absorption.....	5
1.2.3. Gas Adsorption.....	6
1.2.4. Gas Permeation.....	15
2. Experimental Work	19
2.1. Adsorption Equilibria in IL@MOF Composites.....	19
2.1.1. Materials and Preparation	19
2.1.2. Characterization Techniques.....	22
2.1.3. Experimental Methodology.....	24
2.1.4. Adsorption Quantities	25
2.2. Gas Permeation in Mixed-Matrix Membranes.....	27
2.2.1. Materials and Preparation	27
2.2.2. Characterization Techniques.....	30
2.2.3. Experimental Methodology.....	32
3. Results and Discussion	37
3.1. IL@MOF Composites.....	37
3.1.1. He Pycnometry	37
3.1.2. N ₂ Adsorption-Desorption Isotherms at 77K	37
3.1.3. Powder X-Ray Diffraction	40
3.1.4. Fourier Transform Infrared Spectroscopy	41
3.1.4. Adsorption Equilibria for CO ₂ and CH ₄	43
3.2. Mixed-Matrix Membranes.....	47
3.2.1. Contact Angles	47
3.2.2. Mechanical Properties	48
3.2.3. CO ₂ and CH ₄ Permeation	50
4. Conclusion.....	53
5. Future Work.....	55
6. References	57
7. Appendixes.....	71
7.1. Appendix A – He Pycnometry Data.....	71
7.2. Appendix B – Polynomial Fitting Parameters.....	73

List of Figures

Figure 1.1. A possible and simple four-step PSA configuration for the upgrading of biogas in order to obtain biomethane	7
Figure 1.2. IUPAC's recommendations for the classification of the six types of isotherms	8
Figure 1.3. Dynamic behaviours of MOFs when interacting with guest molecules: (a) 1-dimension (b) 2-dimension (c) 3-dimension, where the red dots represent metal clusters and the black lines stand for the organic ligands.	11
Figure 1.4. (a) Comparison of gravimetric CO ₂ capacities for several MOFs (and an activated carbon as a reference) at ambient temperature and pressures up to 42 bar; (b) Comparison of the volumetric CO ₂ capacity of MOF177, zeolite 13X pellets, and MAXSORB carbon powder	12
Figure 1.5. Structural representation of ZIF-8, with the yellow sphere illustrating its pore size	13
Figure 1.6. Illustration of porous and nonporous membranes and their separation mechanisms ...	15
Figure 1.7. Revised Robeson upper bound correlation for CO ₂ /CH ₄ separation at 30°C for polymeric membranes, with $n = -2.636$ and $k = 5369140$ Barrers. Red dots represent polymeric membranes and blue dots represent thermally rearranged (TR) polymers	18
Figure 2.1. Preparation of IL@MOFs: (a) weighing the mass of IL, (b) addition of 10 mL of acetone to the IL, (c) stirring at room temperature.....	21
Figure 2.2. Preparation of IL@MOFs: (a) lidless ZIF-8 + IL + acetone vials being stirred, (b) heating up the mixture to ensure solvent evaporation, (c) sample after being dried.	21
Figure 2.3. Scheme of the adsorption operating unit: MSB - high-pressure magnetic-suspension microbalance; MKS – pressure transducer for 0-1bar; PT2 – pressure transducer for 0-10 bar; PT3 – pressure transducer for 0-35 bar.....	24
Figure 2.4. Illustration of the three tensions involved in the determination of a contact angle in a solid's surface.....	30
Figure 2.5. Illustrative example of the curves obtained for Run 1 (see Table 2.5), where the three colours represent three replicas.....	31
Figure 2.6. Illustration of the permeation apparatus: 1 - feed compartment, 2 - permeate compartment, 3 - water bath, 4 - gas feed, TC - temperature controller, PI1 & PI2 - pressure indicators, V1 & V2 - exhaust valves, V3 & V4 - inlet valves.....	32
Figure 2.7. Illustration of the gas permeation measurement cell (a) opened and (b) sealed.....	32
Figure 2.8. Illustrative example of the Feed (green) and Permeate (blue) curves obtained for CO ₂ Run 9 (see Table 2.5).....	33
Figure 2.9. Illustrative example of the curve obtained for CO ₂ , Run 12 (see Table 2.5).....	34
Figure 3.1. N ₂ adsorption-desorption isotherms at 77 K for the ZIF-8 used in this thesis (black), literature ZIF-8 data (red) and the IL@MOF composites (blue).....	38

Figure 3.2. Pore size distribution obtained through NLDFT analysis of the ZIF-8 and the IL@ZIF-8 composites.	39
Figure 3.3. PXRD spectra for the ZIF-8 reported in literature (green), the ZIF-8 used in this thesis (black), and for the synthesized IL@MOF composites (blue).	40
Figure 3.4. Obtained FT-IR spectra for the studied ILs (red), the ZIF-8 (black) and the synthesized IL@MOF composites (blue) between (a) 4000-450 cm^{-1} and (b) 1650-450 cm^{-1}	42
Figure 3.5. Example of the poor fitting provided by the Sips model for CO_2 adsorption by ZIF-8, between 0 and 1 bar. Open symbols are desorption and close symbols are adsorption. Straight line represents the Sips fitting.	43
Figure 3.6. CH_4 and CO_2 adsorption/desorption isotherms at 30°C for ZIF-8 and its comparison with literature, and the IL@ZIF-8 composites. Open symbols are desorption and close symbols are adsorption. Straight lines represent the polynomial fitting.	44
Figure 3.7. CH_4 and CO_2 adsorption-desorption isotherms at 30°C for ZIF-8 and the studied ILs. Open symbols are desorption and closed symbols are adsorption. Straight lines represent the polynomial fitting.	45
Figure 3.8. Ideal CO_2/CH_4 selectivity at 30°C for ZIF-8 and the IL@ZIF-8 composites, compared with $[\text{C}_2\text{MIM}][\text{Ac}]$ reported by T. Ferreira, and using a polynomial fitting.	46
Figure 3.9. Obtained contact angles for Matrimid®5218, Matrimid®5218/ZIF-8, Matrimid®5218/ $[\text{C}_6\text{MIM}][\text{NTf}_2]$ @ZIF-8 and Matrimid®5218/ $[\text{C}_2\text{MIM}][\text{Ac}]$ @ZIF-8.	47
Figure 3.10. CO_2/CH_4 selectivity as function of the CO_2 permeability (Barrers) at 30°C.	52

List of Tables

Table 2.1. Obtained results for IL masses to be weighed and their corresponding IL loading.....	19
Table 2.2. Chemical formula, nomenclature, name, molecular weight and structure of the chosen ILs and MOF.....	20
Table 2.3. IL and ZIF-8 loading for each composite acting as filler.	28
Table 2.4. Chemical Formula, nomenclature, name, molecular weight and structure of the chosen ILs to synthesize the IL@MOF composites, and the polymer used in MMMs.	29
Table 2.5. Work plan and summary of the conducted permeation experiments.	35
Table 3.1. Experimental determined values for the density of the solid matrix of the IL@MOF composites.	37
Table 3.2. Values for BET specific surface and its c constant; Langmuir specific surface area, total pore volume and partial pressure, obtained using <i>MicroActive</i> software.....	38
Table 3.3. Sips adsorption model parameters and Average Relative Error (%) for ZIF-8 and each IL@ZIF-8 composite.	43
Table 3.4. CH ₄ and CO ₂ uptake capacity at 30°C for ZIF-8 and the IL@ZIF-8 composites, as well as the percentage of capacity loss at 1 bar using ZIF-8 as reference.	45
Table 3.5. CH ₄ and CO ₂ uptake capacity at 30°C for ZIF-8 and the IL@ZIF-8 composites, as well as the percentage of capacity loss at 16 bar using ZIF-8 as reference.	45
Table 3.6. Puncture test results for the Matrimid®5218/ZIF-8 membranes.	48
Table 3.7. Puncture test results for the Matrimid®5218/[C ₆ MIM][NTf ₂]@ZIF-8 membranes.....	49
Table 3.8. Puncture test results for the Matrimid®5218/[C ₂ MIM][Ac]@ZIF-8 membranes.....	49
Table 3.9. CO ₂ /CH ₄ ideal selectivity and CH ₄ and CO ₂ permeability results for Matrimid®5218/[C ₂ MIM][Ac]@ZIF-8.....	50
Table 3.10. CO ₂ /CH ₄ ideal selectivity and CH ₄ and CO ₂ permeability results for Matrimid®5218/[C ₆ MIM][NTf ₂]@ZIF-8.....	51
Table 7.1. Parameters of the polynomial fitting.	73

List of Abbreviations

CFCs – Chlorofluorocarbons

EDS – Energy-Dispersive X-Ray Spectroscopy

FT-IR – Fourier Transform Infrared Spectroscopy

GHG – Greenhouse Gas/Gases

GW – Global Warming

IEA – International Energy Agency

IL – Ionic Liquid

IL@MOF – Composite of Ionic Liquid impregnated in Metal Organic Framework

ILMs – Ionic Liquid Membranes

IUPAC - International Union of Pure and Applied Chemistry

MMMs – Mixed-Matrix Membranes

MOF – Metal-Organic Framework

NG – Natural Gas

PILs – Polyionic Liquids

PSA – Pressure Swing Adsorption

PXRD – Powder X-Ray Diffraction

RTILs – Room-Temperature Ionic Liquids

SEM – Scanning Electron Microscopy

TGA – Thermal Gravimetric Analysis

TSA – Temperature Swing Adsorption

TSILs – Task-Specific Ionic Liquids

UV – Ultra-Violet

ZIF-8 – Zeolitic Imidazolate Framework

List of Symbols

A - membrane area

b – affinity constant

F – force

l – thickness

m – ‘apparent’ weighed mass

m_s – mass of solid

m_{sc} – mass of the measurement cell

M_w – molecular weight

n – heterogeneity parameter

P – permeability

p – total pressure

P_A – permeability of gas A

P_B – permeability of gas B

p_{Feed} – pressure of the feed

p_{Perm} – pressure of the permeate

q – specific amount adsorbed

q_{exc} – specific excess adsorption

q_{net} – specific net adsorption

q_s – maximum specific amount

q_t – specific total adsorption

r – probe radius

S_c – cross sectional area

S_{CO_2/CH_4} – ideal CO_2/CH_4 selectivity in adsorption

T – temperature

t – time

V_{cell} – volume of the adsorption measurement cell

V_{Feed} – volume of the gas permeation feed compartment

V_n – volume of the adsorption measurement cell sample holder

V_p – total pore volume

V_{Perm} – volume of the gas permeation permeate compartment

V_{REF} – reference volume

V_s – solid volume

V_{sc} – volume of the gas permeation measurement cell

List of Greek Letters

$\alpha_{\text{CO}_2/\text{CH}_4}$ – ideal CO_2/CH_4 selectivity in gas permeation

β – geometric parameter of the gas permeation measuring cell

ρ_g – density of the gas in the adsorption measurement cell

ρ_h – density of the adsorption measurement cell sample holder

ρ_s – solid matrix density of the adsorbent

σ – tensile strength

1. Introduction

1.1. Motivation

While debating the world's current situation with my sister, who studies Environmental Engineering, she pointed that one of the biggest challenges of the 21st century will be learning to live with the enormous social, economic and environmental consequences of Global Warming (GW). These convictions and worries are shared by many scientists [2] upon the realization that GW has a preponderant role in some of the planet's most extreme events (*e.g.* droughts, severe wildfire seasons and rising of the sea level [3,4]).

In addition, extreme climatic changes caused by GW can cause the disruption of basic food supplies, such as fresh water, cereals and cattle, as well as the increase of health costs due to insect-borne diseases spreading, causing intense allergy seasons and chronic respiratory problems [3,4].

GW and its impacts, are a consequence of the augmentation of the air pollution caused by the continuous emission of anthropogenic greenhouse gases (GHGs), enhanced by population and economic growth [5]. Those emissions, alongside the *El Niño* phenomenon [6,7], were directly responsible for the warming of the Earth's surface since 1983, and for weakening the stratospheric ozone (O₃) layer that shields the Earth from biologically-harmful solar ultraviolet (UV) radiation [5,8].

The main GHGs include methane (CH₄), nitrous oxide (N₂O), chlorofluorocarbons (CFCs) and carbon dioxide (CO₂), with the latest being the most important long-lived greenhouse gas [6,9]. It is estimated that around 78% of the increase in GHG emissions since 1970 are associated with the release of CO₂ into the atmosphere, due to anthropogenic activities, such as fossil fuel combustion processes [5,10].

Some GHG, in natural-occurring conditions, prevent a portion of the outgoing thermal radiation from escaping the planet and allow most of the incoming heat to penetrate the atmosphere of the Earth, thus keeping its temperature stable at approximately 15°C [9]. However, the atmospheric concentration of these gases has been increasing, largely exceeding their natural-existent amounts.

Measured data suggest that in 2016 the global average atmospheric concentration of anthropogenic CO₂ reached 403.3 ppm, corresponding to a 145% increase of the data registered pre-industrially, and that the concentrations of CH₄ and N₂O were approximately 1853 ppb and 328.9 ppb, respectively [5].

The continuous and incessant awareness raised over this subject, along with the provided evidential data, propelled governments worldwide to draw new and more efficient strategies to address these issues. The latest of these efforts was the 2015 Paris Climate Accord where, as of this writing, 174 nations ratified the agreement to implement specific measures that would restrict GW to an increase of 1.5-2°C [10-12]. In addition to the signature of this climate agreement, China and India – the world's most pollutant countries – slowed down their economic growth, leading to an expected reduction of anthropogenic CO₂ emissions of 2-3 Gton, by 2030 [12].

Atop of the implementation of the prementioned agreed measures, the slow rise in GW between 2014 and 2016 is also due to the enhanced financial investment in low-carbon renewable energies e.g. solar power and biomass combustion, as alternatives for energy production [10-13]. Despite all the efforts to implement these renewable technologies, their high production and maintenance costs delay a larger worldwide application [15].

Despite the world's conjoined attempts to reduce CO₂ emissions, the recent political changes in the United States have become a cause of great concern in the world's scientific community. While more than 170 nations are still committed to respect the 2015 Paris Climate Pact and its pledges, the United States have withdrawn their position, affecting the world's effort to minimize GW and its consequences [12].

The International Energy Agency (IEA) estimated that between 2014 and 2016, the CO₂ anthropogenic emissions remained flat at approximately 32.1 Gton, while global economy grew around 3.1% [16]. However, in 2017 a record amount of 32.5 Gton in CO₂ emissions was reached, due to higher energy demands and slower energy efficiency improvements [17].

In April and May of 2018, the Mauna Loa Observatory in Hawaii recorded an average concentration of atmospheric CO₂ above 410 ppm, the highest monthly average ever recorded in history [18]. This tendency, and the continuous misuse of highly pollutant energy sources, support the predictions that even larger amounts of atmospheric CO₂ will be registered by the end of 2018 [14].

Consequently, it is expected that by the end of the 21st century, the average atmospheric temperatures will have suffered an increase of more than 2°C due to anthropogenic GHG emissions. The ongoing emissions of these gases will cause further warming and provoke larger changes than those observed in the 20th century [19,20]. These issues led scientists to develop new processes that include the application of non-biological methodologies, to prevent CO₂ inclusion in the atmosphere by capturing it from exhaust pipes, compressing it to a supercritical fluid for transport, and storing it in profound reservoirs e.g. mineralization and ocean storage [15].

The most common methods for capturing CO₂, as an alternative to the conventional cryogenic separation, are absorption e.g. with amine solutions by scrubbing, adsorption e.g. through Pressure Swing Adsorption (PSA) and gas membrane permeation [20-22]. Adsorption has been the focus of several studies, especially concerning the capacity and selectivity for CO₂ capture of different materials, such as activated carbons and zeolites, since it is an energetically less intensive option that presents high performance levels considering gas purity and recovery. However, the associated regeneration costs of the used materials can act as a limitation, since the employed adsorbent materials are fundamental to an optimal conditioning/separation process [24,25]. Over the years there has been a growing necessity to shape these materials into granules or pellets of different shapes and sizes, even though they offer slower kinetics [26], to counteract the excessive loss of pressure in the adsorption columns upon the use of powders [27].

Alternative materials, such as recent metal-organic frameworks (MOFs), e.g. ZIF-8, MIL-100 and MIL-101 [28,29], present large surface areas and pore volume that favor mass transfer from the outside to the internal sites and have been found to be efficient adsorbents due to their high CO₂ adsorption capacity [27]. Likewise, ionic liquids (ILs) known by their nonflammability, negligible volatility, high conductivity and chemical-thermal stability, have been found to have an extremely high CO₂ absorption affinity that could promote the development of alternative strategies for GHG capture [21].

Over the years, polymers such as polyamide, polyimide, polyarylether sulfone, cellulose acetate and silicon rubber have been widely used in industrial processes involving permeation, such as desalination of seawater, recovery of hydrogen from hydrocarbon gas streams, and CO₂ capture [32,33] since they provide advanced functionalities that can be employed in high performance membranes with low operating costs, ease of construction and scale-up, and excellent processability [34]. However, these materials are not an optimal solution, due to their lack of thermal-chemical stability and low trade-offs between selectivity and permeability, with an improvement in permeability being almost always obtained at the expense of the selectivity, and vice-versa [35,36].

In order to overcome the disadvantages associated with polymeric membranes, mixed-matrix membranes (MMMs) have been studied and found to be a promising alternative due to the combination of the easy processability of the polymers, with the gas separation performance of the filler materials [37]. MMMs also present high mechanical flexibility [33,36,38]. Recently, and considering the advantages of both MMMs and MOFs, MMMs with MOFs acting as fillers started to be studied, showing a great potential for future industrial applications in gas separation processes [31-35].

In addition, very recently, and because some MOFs can undergo structural changes when adsorbing different molecules [43,44] the design of new dynamic composites based on the incorporation of other materials, such as ILs, in the MOFs (IL@MOFs), and their posterior application as MMMs fillers, is a brand-new approach that could enhance both the permeability and selectivity of the newly designed MMMs.

1.2. Theoretical Concepts

1.2.1. Gas Mixtures of Interest

In 1821, William Hart found the first reservoir of natural gas (NG), a colorless, shapeless and odorless gaseous mixture rich in hydrocarbons. Nowadays, the process of combustion of this gas accounts for 23.7% of the primarily energy consumption sources [45]. NG is a safe energy source when it comes to storage, usage and transportation, and its energy has been used as heat for residential, commercial and industrial sites, as well as in the production of ethylene and ammonia in the petrochemical and fertilizer industries, respectively [46].

From the NG combustion, as well as other industrial fuel combustion processes, results a gaseous mixture, flue gas, composed mostly of N_2 and CO_2 , although traces of H_2O and O_2 can often be found [47]. Even though, in the flue gas provenient of the combustion of NG, the emission of SO_2 is non-significant and the emissions of N_2O and CO_2 are reduced by 50-60% in comparison with other fossil fuels, it still contains enormous amounts of GHGs that can be released to the atmosphere, heavily contributing to GW [48]. Due to the CO_2 emissions associated with natural gas combustion, technologies using adsorption with amines for the removal and capture of this GHG have been implemented, even though their main drawbacks include corrosion issues, which leads to increased maintenance costs, and high energy consumption [49]. In order to overcome these drawbacks, new capture and purification methods have been studied e.g. fixed-site-carrier membranes [50].

Considering the issues associated with NG, and the fact that the majority of the natural reservoirs of important energy sources are located in politically unstable regions [51], biogas obtained from the anaerobic digestion of organic materials and waste residues, has a critical role as an alternative renewable energy source to produce power and heat. With biogas being a mixture of mostly CH_4 (ranging from 55% to 70%) and CO_2 (ranging from 30% to 45%), it is possible to obtain biomethane from its upgrading, through CO_2 removal/capture, and thus conditioning biogas into a suitable substitute for natural gas [52]. Focusing on developing new materials for biogas upgrading, the goal of this thesis was to prepare brand-new composite materials resulting from the impregnation of ILs in the porous structure of ZIF-8 (MOF), and to study their CO_2 uptake capacity, CO_2/CH_4 ideal selectivity and CO_2 permeability in gas permeation experiments.

1.2.2. Gas Absorption

Gas absorption operations involve mass transfer from a gas (solute) to a non-volatile liquid (solvent), and can be classified as physical or chemical mechanisms [53]. Physical absorption is based on Henry's Law, where the capacity of the solvent increases linearly with the pressure, and its regeneration is possible through pressure reduction or temperature increment [54]. Industrial physical absorption processes to capture CO₂, occur at high partial pressures and non-reactive polar solvents with an acid gas affinity, like Selexol and Rectisol, are used [55].

On the other hand, chemical absorption is a highly selective mechanism, limited by stoichiometry, that involves reversible and irreversible chemical reactions to enhance the effectiveness of gas separation processes [56]. For this mechanism, Henry's Law can no longer be applied since different chemical components of the gas mixture can get involved in competing reactions, making it an extremely complex process [57]. Industrially, the most common chemical absorbents are alkanolamines, such as diethanolamine (DEA) [58], N-methyldiethanolamine (MDEA) [59] and monoethanolamine (MEA) [60]. MEA is the absorbent most frequently used, due to its affordability and availability, but also due to its high CO₂ reactivity [61].

The major drawbacks associated with the use of these absorbents, are their high solvent regeneration energy demands and their fast rate of degradation due to the formation of carbamates resulted from the CO₂ reaction with the amine solutions, and that can cause its neutralization and equipment corrosion [62]. In order to overcome these limitations, Ionic Liquids (ILs), have been intensively studied since the middle of the 1990s [63] as possible absorbent alternatives, and have been proved to improve the performance, economy and general efficiency of gas absorption operations [54]. ILs are often described as molten salts with hybrid organic-inorganic structures and melting points below 100°C [64]. These materials present nonflammability [65], negligible volatility [66], thermal stability [21], water immiscibility [67], solvating potential [68], electrical conductivity [69] and an outstanding recyclability [70,71].

The growing interest in these materials comes from the fact that they are foreseen as 'designer solvents' that allow the existence of almost unlimited structural combinations, since during their synthesis, the choice of anion impacts their functionality/chemistry, whilst the choice of cation is linked to its stability [64,71]. Besides their role as absorbents in gas separation, these materials can also be used in membrane processes [72], and as electrolytes in batteries [73], solvents in biocatalysis [74] and fuel additives [75]. They are often divided into different categories, depending on their specific features [64]: Room-Temperature ILs (RTILs) [76,77], Task-Specific ILs (TSILs) [78,79], Poly(ionic) Liquids (PILs) [80,81] and IL Membranes (ILMs) [72,82].

Nonetheless, the use of some ILs presents limitations that can condition a wider implementation in industrial processes, such as high production costs [83], high viscosity [72] and high energy consumption during the recycling procedures [84].

1.2.3. Gas Adsorption

Gas adsorption is a well-established technique used in chemical industries, namely for CO₂ capture/separation, that is based on the accumulation of gas molecules (adsorbate) on the pores of a solid material (adsorbent) due to a bond deficiency and imbalance of atomic forces on the molecules of the solid surface [85–88]. The opposite process of adsorption, occurring simultaneously but at a different rate, is denominated desorption [89].

Adsorption can be a physical or a chemical process. Physical adsorption is a consequence of weak interactions associated with Van Der Waal's forces, since the molecules of gas do not bind to a specific location on the adsorbent, but instead they spread along its surface, with an energy never exceeding 80 kJ/mol. Physical adsorption is an easily reversible process and often results in several layers being formed by the adsorbed molecules on the surface of the adsorbent [27,90]. On the other hand, chemical adsorption involves a covalent bond, stronger than the interactions found in physical adsorption, since electrons are shared by the surface of the adsorbent and the adsorbed molecules. Because the heats of adsorption involved in these chemical bonds are up to 800 kJ/mol, this is considered an irreversible mechanism. Unlike physical adsorption, herein the adsorbate binds to a specific site of the adsorbent, if its surface is clear of any molecules that might have been previously adsorbed, generating a single layer of adsorbed molecules [90]. In addition, the adsorption phenomenon can often be described as a physical-chemical process, where a chemisorbed layer is displayed at a higher temperature and underlying several layers of physically adsorbed molecules [85,90].

The impact of pressure variation in an adsorption process, can be explained by Le Chatelier's principle of 1888 «*Tout système en équilibre chimique éprouve, du fait de la variation d'un seul des facteurs de l'équilibre, une transformation dans un sens tel que, si elle se produisait seul, elle amènerait une variation de signe contraire du facteur considéré*» [91], meaning that when a certain stress is applied to a system in equilibrium, it will cause a shift in said equilibrium so as to counteract the effect of the constraint. Hence, adsorption is favored by an increase in pressure: when more pressure is added to the system, it will tend to decrease said pressure by favoring the reaction wherein the gas molecules are bind to the surface of the adsorbent [92,93]. The typical exothermic behavior of an adsorption process, can also be explained by the aforementioned principle: a decrease in temperature will increase the solubility of the gas molecules in the adsorbent, augmenting the extent of the adsorption equilibria [92,93].

Being a fundamental process in the chemical industry, adsorption is often used in Pressure Swing Adsorption (PSA) cyclic processes, for the separation, upgrade and fractioning of gaseous mixtures (e.g. biogas). In these processes, the achieved separation level depends on the selectivity equilibrium and ratio between the different gaseous species, with said ratio corresponding to the distribution of each component in both the adsorbed and non-adsorbed phases [27].

PSA cyclic processes can have four or more steps, and can last for a few seconds or several minutes [33]. These processes present efficiencies up to 95% [94], and their optimization in terms of operation flexibility, product purity and energy efficiency can be achieved by operating an arrangement of several adsorbers, instead of a single column, that will basically work in complementary cycles of adsorption at higher partial pressures, and desorption at lower partial pressures facilitating the use of common resources, and smoothing the production flow [95]. A simplified example of a four-step PSA system is illustrated in Figure 1.1.

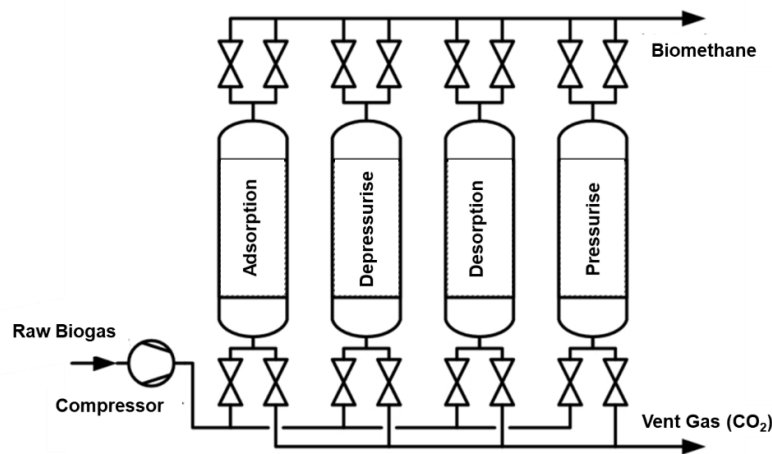


Figure 1.1. A possible and simple four-step PSA configuration for the upgrading of biogas in order to obtain biomethane. Adapted from reference [96].

Temperature Swing Adsorption (TSA) is a similar process to PSA, but rather than manipulating pressure, the temperature is modulated. TSA can be used for CO₂ capture, since it consists of complementary cycles of adsorption with temperature variation, instead of pressure alteration [96]. However, the duration of these cycles is superior, sometimes ranging from several minutes to several days [33], since it takes longer periods to attain temperature changes, rather than pressure swings [97].

Usually, a PSA system that performs several desorption cycles at subatmospheric pressure is known as Vacuum Swing Adsorption (VSA) [98].

1.2.3.1. Adsorption Equilibria

Adsorption equilibria is described, at constant temperature, through isotherms that correlate the amount of adsorbate present on the surface of the adsorbent, as a function of the gas pressure. To better understand the curvatures of isotherms, it is important to classify the adsorbent according to its pore size: micropore (width < 2 nm), mesopore (2 nm < width < 50 nm) and macropore (width > 50 nm) [99].

There are essentially six types of isotherms, recommended by IUPAC in 1985 [100], attending to the properties of the relation between the adsorbent and the adsorbate. The models of said isotherms are represented in Figure 1.2.

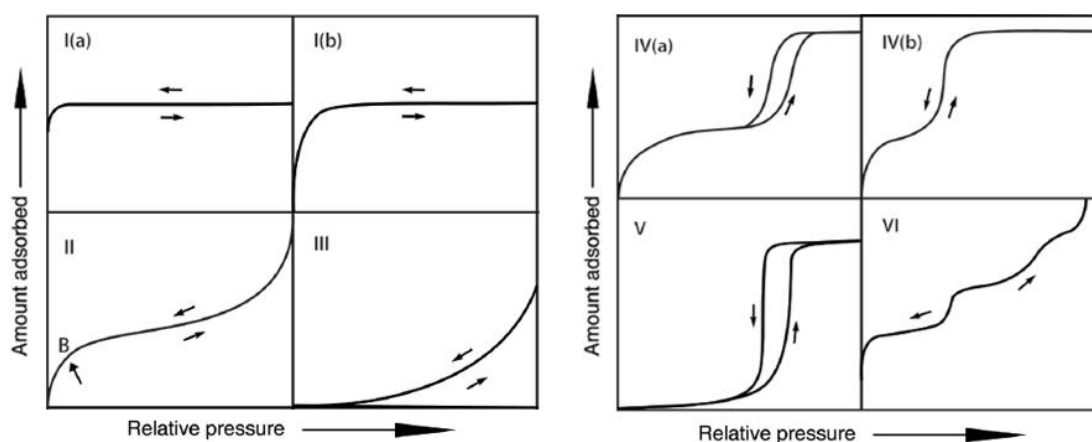


Figure 1.2. IUPAC's recommendations for the classification of the six types of physisorption isotherms [100].

Isotherm Type I describes a reversible adsorption by microporous solids, where the uptake is dependent on the available microporous volume, instead of the surface area. An abrupt uptake at low pressure is explained by the enhanced interactions between the adsorbent and adsorbate in narrow micropores, resulting in their rapid filling. Thus, isotherm Type I (a) represents materials with mainly micropores, while Type I (b) denotes materials with micropores and, possibly, mesopores.

Type II isotherm describes physical adsorption of most gases on nonporous, or macroporous, adsorbents. The shape of its curve is a consequence of a mono-multi layer adsorption process up to high pressure. In Figure 1.2 (II), point B represents the completion of the monolayer coverage, and the beginning of the multilayer adsorption process.

Isotherm Type III describes weak interactions between the adsorbate and adsorbent, and thus the adsorbed molecules are clustered around the most favorable binding sites on a nonporous, or macroporous, solid. The inexistence of point B in Figure 1.2 (III) means that the formation of a monolayer cannot be identified.

Type IV isotherm describes mesoporous materials, and an adsorption process that is impacted by not only the adsorbent-adsorbate interactions, but also by the interaction between the molecules in a condensed phase. The initial mono-multi layer in the mesopore is followed by condensation of gas molecules to a liquid-like phase, at a lower pressure than the saturation pressure of the bulk liquid.

Therefore, in isotherm Type IV (a) the capillary condensation is followed by hysteresis, since the pore width exceeds the critical width due to the influence of the adsorption mechanism and temperature, and Type IV (b) is observed in cylindrical and conical mesopores that are tapered at the end.

Isotherm Type V describes water adsorption on hydrophobic micro and mesoporous adsorbents, where at lower pressures its shape is attributed to weak adsorbent-adsorbate interactions, whilst at higher pressures occurs molecular clustering and pore filling.

Lastly, Type VI isotherm represents a layer-by-layer adsorption on an extremely nonporous and uniform surface. The sharpness of the steps represented in Figure 1.2 depends on the adsorption mechanism and its temperature, whilst the height of each step represents the uptake of each adsorbed layer.

Adsorption equilibria depends on the selectivity of the adsorbent, which represents its ability to accommodate different species considering their stronger or weaker interactions. Its steric mechanism is associated with the dimension of the pores of the adsorbent, which should be such as to favor the entrance of small molecules while excluding larger ones [86–88,101]. Lastly, kinetics is related to the resistance of intraparticle mass transfer: slow diffusion rates of adsorbate are a disadvantage and can be overcome by reducing the size of the particles, though it can cause an increase in pressure drop [86–88,101].

According to J. Willard Gibbs, the father of statistical mechanics that inspired the development of physical-chemistry/thermodynamics as a science [102], when studying adsorption, one should consider the existence of a mathematical/hypothetical surface with no volume, that separates the adsorbed molecules from the unadsorbed gas phase. The extent of said dividing surface, depends on the amount of the solid material present in the system [103].

Usually, the commonly accepted protocol to determine the Gibbs dividing surface in microporous solids involves the utilization of helium (He) as a probe molecule, since it is assumed inert under certain conditions [103,104], and setting a reference state for the adsorption measurements. The choice of pressure and temperature conditions is done arbitrarily by each experimentalist, and thus each reference state is unique and variable. This allows the measurement of different adsorption quantities *i.e.* Net, Excess and Total adsorption, further explained in section 2.1.4.

1.2.3.2. Adsorbents

The potential energy across the surface of an adsorbent depends on its density and crystalline structure [90], and thus the selection of adsorbent, considering all of its properties, is of the utmost importance when aiming for an efficient adsorption process. The most important characteristics when choosing an adsorbent are its capacity, selectivity, regenerability and compatibility [101,105,106]. A large capacity, representing the number of molecules that can be captured by the adsorbent depending on its initial condition, temperature and fluid concentration, is intrinsically related to high surface areas and microporous volumes [86].

Selectivity represents the affinity of a certain material to preferably adsorb a specific gas, in comparison to other gas species. Generally, a non-selective sorbent can capture at the same rate different gas species, whilst a highly selective material can uptake a single specific component at a faster rate [101,107]. Regenerability is the ability of an adsorbent to “go back” to its pre-adsorption state during sequential cycles, which can be achieved by thermal, pressure or chemical swing such as elution or supercritical extraction. Compatibility is linked to both chemical and physical factors that might damage and reduce the life and utility of an adsorbent, by causing excessive disintegration of its structure [101].

It is also important to consider, not only the cost of an adsorbent since it should be as inexpensive as possible, but also its surface area, that is useful when monitoring its activity and stability, and accounts for its degree of exposure to the gas molecules [108–111]. Associated with surface area, and consequently with the capacity of the adsorbent, comes its pore volume. In most materials, the pores only go a few molecules deep, thus many pores are needed to adsorb a larger amount of gas [109,110].

There are innumerable examples of adsorbents, whose both physical and chemical properties make them ideal for specific applications. Aluminas are inorganic compounds, mostly used as desiccants and catalysts due to their high thermal shock and water resistances, that present an opaque/crystalline structure and a surface area varying between 200 and 400 m²/g [101,112].

Silicas are also inorganic materials, used in humidity control and food preservation, due to their water adsorption capacity of around 40 wt% and to their easiness of regeneration, at approximately 150°C. They are usually amorphous and translucent mesoporous materials, with attrition/dusting resistance and surface areas between 300 and 900 m²/g [101,112]. Zeolites are aluminosilicates, mostly used as air purifiers and dehumidifiers, with crystalline and microporous surface areas varying between 600 and 800 m²/g. While their 3D framework structure has uniform dimensions and contains aluminum, silicon and oxygen, their small pores have cations and water that allow the adsorption of gas molecules at high temperatures [112–114].

Being developed since the mid-1970s, activated carbons are obtained by carbonization of organic compounds (e.g. bones and wood), which propels the formation of pores and gives them a black granular appearance. Despite their main disadvantage being a small yield of production, these adsorbents present internal surface areas of approximately 1000 to 1500 m²/g making them one of the most common adsorbents used in industrial processes, such as water purification and air filtration [107,109,110].

The biggest limitations for the usage of adsorbent materials are their low selectivity for a specific gas uptake and their high regeneration costs [24,25], and so, during the last decade, intensive studies have been conducted regarding Metal-Organic Frameworks (MOFs) as alternative adsorbents [22,23,29]. MOFs are crystalline solids with firm but flexible structures, due to the covalent bonds between organic ligands and inorganic clusters *i.e.* ionic/metallic centers [21,30,31]. Their highly microporous system and large surface areas beyond 6000 m²/g [115,116] favor mass transfer and diffusion from the outside, hence facilitating the access of gas molecules to the internal sites and enhancing their efficiency as adsorbents [114]. The flexibility and dynamic behavior of some of these materials can be classified in three types, as shown in Figure 1.3 (a) 1-dimension (1D), (b) 2-dimension (2D) and (c) 3-dimension (3D) [114].

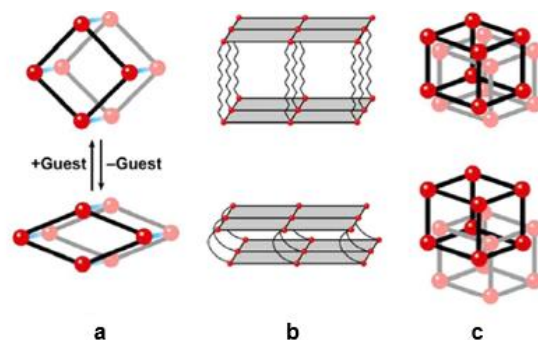


Figure 1.3. Dynamic behaviours of MOFs when interacting with guest molecules: (a) 1-dimension (b) 2-dimension (c) 3-dimension, where the red dots represent metal clusters and the black lines stand for the organic ligands. Adapted from reference [114].

In Figure 1.3 (a), the rotation of the organic ligands, induced by host-guest interactions causes a change in volume, though the frame topology remains unaltered upon adsorption. On the other hand, in Figure 1.3 (b) although there is a set of firm 2D layers, covalently bind through flexible columns, there is an expansion of the framework, caused by the lengthening of said columns. Lastly, in Figure 1.3 (c) the intrinsically connected 3D grids of the framework, slide apart opening or closing the pores of the material.

The different methods for MOF syntheses [115], accompanied by the choice/design of its inorganic cluster and organic ligands, provide these materials different structures that allow stronger/weaker binding sites for lodger molecules, thus impacting their specific properties and applications [23].

MOFs have been taking part as revolutionary materials, not only in gas storage/separation processes [117–120], but also in catalysis [121–124], sensor devices [125–127], proton conduction [128–130] and biomedicine, by having a preponderant role in drug storage/delivery [131–133]. For the past years MOFs such as MOF-177, with a BET surface area of 4500 m²/g and a CO₂ uptake capacity of 33.5 mol/kg at 35 bar, have been used for CO₂ capture, storage, transport and concentration [134]. Figure 1.4 (a) shows a comparison between several MOFs and the NoritRB2 activated carbon as reference, for CO₂ uptake up to 42 bar and Figure 1.4 (b) shows a comparison between MOF-177, Zeolite 13X and MAXSORB for CO₂ uptake.

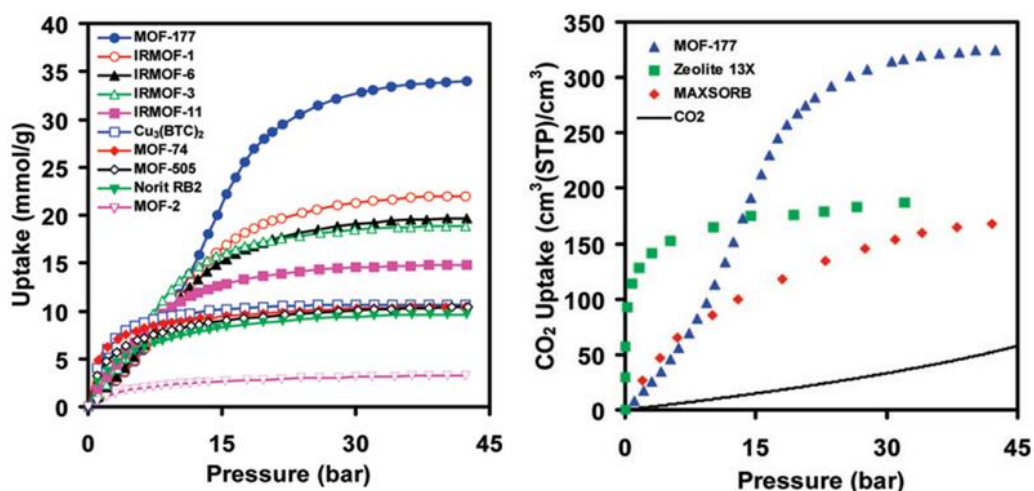


Figure 1.4. (a) Comparison of gravimetric CO₂ capacities for several MOFs (and an activated carbon as a reference) at ambient temperature and pressures up to 42 bar; (b) Comparison of the volumetric CO₂ capacity of MOF177, zeolite 13X pellets, and MAXSORB carbon powder. Adapted from reference [135].

Due to high fabrication costs and low thermal/chemical stabilities of some MOFs [136,137], new ones have been studied, concerning their CO₂ adsorption capacity and selectivity, as to evaluate their possible implementation in gas separation technologies. Llewellyn *et al.* showed that MIL-101 (Cr) has a CO₂ capacity of 18 mol/kg at 50 bar and 304 K [29], Mu *et al.* reported a CO₂ capacity of 23.5 mol/kg for the MOF UMCM-1 at 24 bar and 298 K [138] and Finsy *et al.* discovered that up to 5 bar the framework of the hydroxyl groups in the MIL-53 (Al) has a strong interaction with CO₂, causing its preferential adsorption, whilst CH₄ is unselectively adsorbed [139].

Most of these MOFs have been designed considering applications with high pressure operating conditions, which does not preclude the use of other MOFs as CO₂ capturers in mixed gas systems operating at lower pressures [135]. Wu *et al.* showed that the flexible MOF [Zn₂(bpdca)₂(bpee)]·2 DMF has a CO₂/CH₄ selectivity ratio of 257 (v/v) at subatmospheric pressures [140].

The biggest disadvantages in the production of MOFs are the use of non-renewable materials and organic solvents derived from petrochemical sources that can act as toxic contaminants [141]. In order to outgrow these limitations, Gassensmith *et al.* designed a new 'green' MOF, CD-MOF-2, made of renewable cyclic oligosaccharide γ -cyclodextrin and RbOH, that showed atypically strong affinity with CO₂, at low pressures [142–144].

There is also a newly developed subclass of MOFs, denominated Zeolitic Imidazolate Frameworks (ZIFs), that are crystalline microporous materials with high thermal-chemical stabilities, water resistance and large specific surface areas [145]. In this family, special attention is being paid to the Zeolitic Imidazolate Framework-8 (ZIF-8), whose structure is made by zinc ions coordinated by four imidazolate rings [146]. This material maintains its thermal stability up to 673 K [147], has a high chemical resistance to water, as well as to alkaline solutions and organic solvents [148], pores of 11.6 Å [149], surface area of 1300-1800 m²/g [150] and pore volume of 0.636 cm³/g [148]. The 3D crystalline structure of ZIF-8 is represented in Figure 1.5.

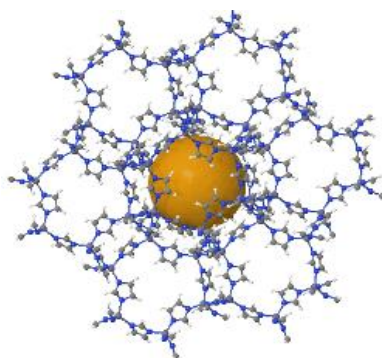


Figure 1.5. Structural representation of ZIF-8, with the yellow sphere illustrating its pore size [118].

ZIF-8 has been reported as an alternative material, not only for the capture of CO₂ [151] but also for the removal of humic acid from water [152]. It can also be used as nanoreactors in effective biocatalytic cascades, by the encapsulation of an enzyme/cofactor, or two or three enzymes, in its nanoparticles [153].

A very recent way of enhancing and improving MOFs properties, is incorporating ILs in their frameworks (IL@MOFs), as demonstrated by Kinik *et al.* who observed the doubling of the CO₂/CH₄ selectivity up to 1 bar upon impregnation of the IL [BMIM][PF₆] in ZIF-8 [28]. Also, in the experimental work developed by Sezginel *et al.* the IL [BMIM][BF₄] was incorporated in the MOF CuBTC, and an increase in CH₄ selectivity of at least 1.5 times was observed [154]. This distinct behavior implies that the combination of the tunable properties of ILs with the choice/design of the MOFs' structures, is an opportunity to develop new materials that could play a decisive role in solving future energy challenges [30].

The first technique to be developed for the synthesis of IL@MOFs was the ionothermal method, and it consists in the use of an IL, acting simultaneously as solvent and as the structure directing agent in the formation of the MOF, providing the template cations around which the inorganic frameworks are ordered [155]. The first IL@MOF was synthesized by Dybtsev *et al.* with the IL [BMIM][BF₄] [156]. This is an advantageous method, due to the absence of competition between the solvent and template upon interaction with the growing solid, when both template and solvent are the same species [157]. However, only a limited number of pairs ILs/MOFs can be used in ionothermal synthesis, due to the thermal lability of organic ligands containing functional groups, resulting in problematic solubility or coordination of metal ions [30]. Considering this, a more simple and effective strategy has been developed to incorporate ILs in MOFs, denominated Post-Impregnation, that can be divided into three different impregnation methods, as follows:

(1) Solution of ILs, where a solvent is used to disperse the IL and force it into the MOF structure, mostly through stirring [30]. Luo *et al.* successfully used this method to synthesize the ABIL-OH@HKUST-1 composite, that showed good catalytic activity [158].

(2) Postsynthetic Modification, known as 'ship-in-a-bottle' where the IL is synthesized inside the MOF frame [30], allowing the incorporation of ILs with ions larger than the MOF's aperture [73]. Ji *et al.* confined the IL BAIL into the nanocages of the MOF-101, and it showed superior catalytic performance for the acetalization of benzaldehyde with glycol [159].

(3) Capillary Action, where the impregnation of the IL happens by its diffusion into the micropores of the MOF, for which a solution of IL + MOF should be heated and stored [30]. Fujie *et al.* mixed the IL EMI-TFSA with ZIF-8, and the mixture was heated and stored overnight to enhance diffusion of the IL into micropores [73].

Considering this, one of the goals of this thesis was to prepare three brand new IL@ZIF-8 composites and test their CO₂ uptake capacity and ideal CO₂/CH₄ selectivity, in order to evaluate their potential as adsorbents in gas separation processes.

1.2.4. Gas Permeation

Membranes have been used in industrial gas separation processes since 1977 [33], and have always been in direct competition with other technologies, like PSA. The choice between these technologies in, for example, the upgrade of biogas, is done considering the desired biomethane purity level, its specific commercial applications, the quality/quantity of the raw biogas, as well as the plant site and its conditions [160,161].

When it comes to the purity level, and considering that biogas is mostly CH₄ (ranging from 55% to 70%) and CO₂ (ranging from 30% to 45%) [52], both PSA and membrane fabricants guarantee a typical methane content, in biomethane, between 95.0-99.0% (v/v) [162]. In addition, investment costs are roughly the same for both technologies, at lower throughputs, with PSA needing € 3700.00 and membranes needing between € 3500.00 - € 3700.00, both for 500 m³/h of biomethane [162]. Therefore, it is fair to admit that an optimal technology to upgrade biogas does not exist, since each process is directly dependent on its own designed specifications, goals and limitations.

In theory, a membrane is a barrier between two bulk phases, being the permeate the phase (or stream) that is transported through the membrane, and the retentate, the amount of the feed inlet current that is retained by the membrane. The performance of a membrane is related with its composition (material), robustness, thickness, durability, maintenance, structure, system design and configuration (e.g. flat or hollow fibber), while at the same time accounting for two distinct parameters: permeability (*P*) which is associated with its capacity to permeate gas components, and selectivity (*S*) which corresponds to its capacity to permeate one gas species preferably from another [32,36].

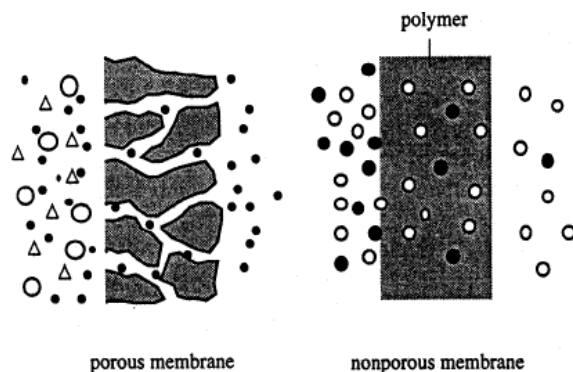


Figure 1.6. Illustration of porous and nonporous membranes and their separation mechanisms [163].

As seen in Figure 1.6, on porous membranes the separation is based on particle size, thus their main applications are microfiltration/ultrafiltration processes. On the other hand, on non-porous membranes, the separation happens considering the solubility/diffusivity of the gas in the membrane, and they are mainly used in gas separation and pervaporation processes [163].

Polymers were the earliest materials to be used in membrane fabrication, due to their highly valued advantages *i.e.* low cost, excellent processability, easy fabrication/scale-up and mechanical flexibility [35,164]. Few of the most common polymers utilized in industrial permeation processes, like desalination of seawater, recovery of hydrogen from hydrocarbon gas streams and ultrafiltration, are polyamide, polyarylether sulfone, cellulose acetate and silicon rubber [32,165] since they provide advanced functionalities that can be employed in high performance membranes [34]. However, these materials are not an optimal solution, due to their lack of thermal-chemical stability and low trade-offs between selectivity and permeability, with an improvement in selectivity being almost always obtained at the expense of the permeability, and vice-versa [35,36,166].

On the other hand, inorganic membranes (*e.g.* zeolites) can withstand organic solvents and be used under harsh operating conditions, like wide ranges of pH and temperature, while maintaining a high permeability and thermal/mechanical stability [167]. Nonetheless, their high fabrication costs alongside the difficulty to prepare defect-free membranes are the major setbacks preventing a larger implementation in industrial processes [168].

In addition, when considering gas permeation with membranes, the materials used should have a modulus high enough to allow the membrane to have mechanical resistance to bear operating pressures and pressure fluctuations. These materials should also be resistant to abrasion and breakdown/deformation, as well as resistant to chemicals in order to withstand different feed compounds and contaminants [33].

For the last few decades, and in order to find solutions to fight the performance obstacles associated with the use of both polymeric and inorganic membranes [169], various polymers have been modified with inorganic materials, such as activated carbons, zeolites and mesoporous silica [170,171], producing an innovative type of membranes, the mixed matrix membranes (MMMs), which result from the homogenous dispersion of filler molecules in a polymeric matrix, with both components affecting its separation performance and morphology [38]. These membranes are expected to present low fabrication costs while combining the flexibility of polymeric materials with the selectivity, and thermal stability, of inorganic particles [36].

Nonetheless, and despite these efforts, when filling a polymeric membrane with an inorganic compound there is often a poor polymer-filler compatibility that can result in rigid polymeric layers, blockage of pores and the appearance of voids in the polymer-filler interface, preventing the adhesion between the two phases. All of these drawbacks affect the membranes' selectivity/permeability and help understand why these membranes have not yet been commercially implemented [172,173].

In order to counteract these limitations, new kinds of 'special fillers' are being tested: high aspect ratio silica-based particles (HARs) [174], ordered mesoporous silicas (OMSs) [175] and metal-organic frameworks (MOFs) [176].

The flexibility associated with the synthesis of MOFs, mentioned in section 1.2.3.2, allows the design and fabrication of these materials with specific properties that enhance the selectivity/capacity of a membrane towards its desired application [176], which has been showed by S. Shahid who observed a 200% CO₂ permeability increase as well as 65% increase in CO₂/CH₄ selectivity in Polyimide/ZIF-8 MMMs [177], and by Dorosti *et al.* who observed an increase of 94% in CO₂ permeability and 84% in CO₂/CH₄ selectivity for a Matrimid/MIL-53 MMM with 15 wt% MOF loading [178].

However, even with the use of MOFs as fillers, there are flexibility issues due to the MOFs' crystalline nature that impacts the membranes' mechanical properties turning them more rigid and fragile, while at the same time not eliminating the formation of non-selective voids in the polymer-filler interface [179].

A possible way to outgrow these limitations, is using IL@MOF composites as MMMs fillers', and basing the choice of both ILs and MOFs on their high efficiency/affinity to capture/solubilize the gaseous species of interest. The validity of this idea was attested by Ban *et al.* who observed an increase of more than 50% in CO₂ permeability with the addition of [BMIM][NTf₂]@ZIF-8 composite to a MMM, as well as remarkable permeability and selectivity combinations that transcended the Robeson Upper Bound Limit [180].

To assess the performance of polymeric membranes, with respect to a specific gas pair, in 1991 L.M. Robeson showed that in a selectivity versus permeability plot, the data referring to said membranes lies on or below a straight line, defined as the upper bound trade-off curve, that describes the inverse relationship between permeability and selectivity, according to expression (1) [181].

$$P_i = k \alpha_{ij}^n \quad (1)$$

Where P_i is the permeability of the more permeable gaseous component through the membrane, n is the slope of the log-log limit, α_{ij}^n is the selectivity (described in terms of P_i/P_j) and k is the “front factor”. Figure 1.7, represents the revised upper bound relationship for CO₂/CH₄ in polymeric membranes at 30°C.

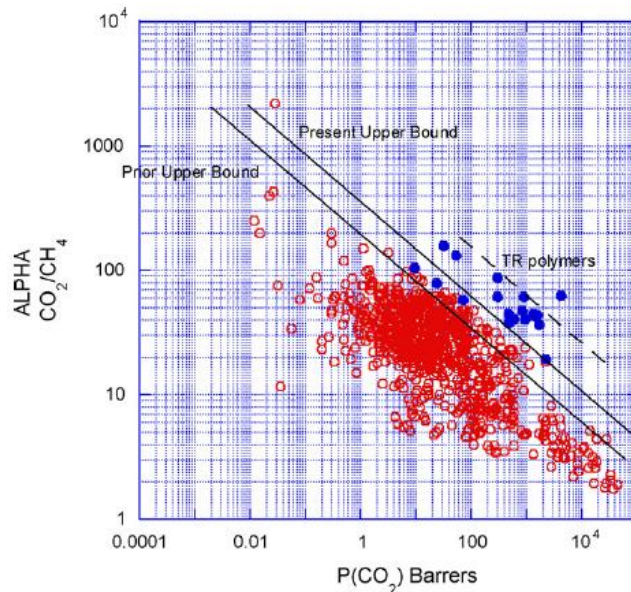


Figure 1.7. Revised Robeson upper bound correlation for CO₂/CH₄ separation at 30°C for polymeric membranes, with $n = -2.636$ and $k = 5369140$ Barrers. Red dots represent polymeric membranes and blue dots represent thermally rearranged (TR) polymers. Adapted from reference [165].

Considering this, one of the goals of this thesis was to use two of the IL@MOF composites, reported by T. Ferreira [1], as fillers in Matrimid®5218-based MMMs in order to determine their CO₂ permeability and CO₂/CH₄ selectivity, expecting that the obtained results might surpass the Robeson Upper Bound for CO₂/CH₄, which would indicate that these membranes have an excellent trade-off between permeability and selectivity.

2. Experimental Work

2.1. Adsorption Equilibria in IL@MOF Composites

2.1.1. Materials and Preparation

In order to prepare new composite materials with the impregnation of ILs in the porous structure of MOFs, to posteriorly study their CO₂ uptake capacity and CO₂/CH₄ ideal selectivity, the choice of the MOF was of the upmost importance. It was decided that the same MOF would be incorporated with different ILs, to test the effect and influence of the ILs structural differences (e.g. anionic magnetic center). The selected MOF was Zeolitic Imidazolate Framework-8, or ZIF-8 (Basolite®Z1200 by BASF), due to its advantageous properties previously reported (see section 1.2.3.2).

The chosen method to synthesise the IL@MOF composites was the Solution of ILs (see section 1.2.3.2), due to its simplicity and to the fact that ZIF-8 was available in the laboratory. This method requires the use of a solvent, and acetone (99.8% purity, Carlo Erba) was used, since it is the most common solvent mentioned in literature regarding the synthesis of IL@MOFs. To guarantee a valid comparison between all the prepared composite samples, the same number of IL moles was incorporated in the structure of the ZIF-8. Using the experimental protocol, and calculations reported in reference [1], 15 wt% of the IL with the lowest molar mass, [C₂MIM][NTf₂], for 1g of ZIF-8, was chosen as a reference. With the molar mass of [C₂MIM][NTf₂] (M_w = 391.31 g.mol⁻¹), and using equations 2 and 3, it is possible to determine the moles of IL needed, as well as the expected IL loading wt% in the MOF. The obtained values for these, are listed in Table 2.1.

$$m_{\text{IL}} = 0.15 \times (m_{\text{ZIF-8}} + m_{\text{IL}}) \Leftrightarrow 0.85 m_{\text{IL}} = 0.15 \times 1\text{g} \Leftrightarrow m_{\text{IL}} = 0.176 \text{ g} \quad (2)$$

$$n_{\text{IL}} = \frac{0.176 \text{ g}}{391.31 \text{ g.mol}^{-1}} \Leftrightarrow n_{\text{IL}} = 4.5 \times 10^{-4} \text{ mol} \quad (3)$$

Table 2.1. Obtained results for IL masses to be weighed and their corresponding IL wt% loading.

Ionic Liquid	Moles (x10 ⁻⁴ mol)	Molar Mass (g.mol ⁻¹)	IL Mass (g)	Loading (wt%)
[N _{1 2OH 2OH 2OH}][NTf ₂]	4.50	444.37	0.2000	16.70
[C ₄ MIM] ₂ [Co(SCN) ₄]	4.50	569.69	0.2564	20.40
[C ₄ MIM][FeCl ₄]	4.50	336.87	0.1516	13.20

Table 2.2, shows a list of the MOF and ILs used to synthesize the different IL@MOF composites.

Table 2.2. Chemical formula, nomenclature, name, molecular weight and structure of the chosen ILs and MOF.

Formula	Nomenclature	Name	M _w (g/mol)	Structure
C ₉ H ₁₈ F ₆ N ₂ O ₇ S ₂	[N ₁ 2OH 2OH 2OH][NTf ₂]	N,N,N-tris(2-hydroxyethyl)-N-methylammonium bis[(trifluoromethyl)sulfonyl]imide	444.37	
C ₂₀ H ₃₀ CoN ₈ S ₄	[C ₄ MIM] ₂ [Co(SCN) ₄]	1-butyl-3-methylimidazolium tetrathiocyanocobaltate(II)	569.69	
C ₈ H ₁₅ Cl ₄ FeN ₂	[C ₄ MIM][FeCl ₄]	1-butyl-3-methylimidazolium tetrachloroferrate(III)	336.87	
C ₈ H ₁₀ N ₄ Zn	ZIF-8	2-methylimidazole zinc salt	227.58	

The ILs' structure was retrieved from the NIST Ionic Liquids Database - ILThermo [182] and the structure of ZIF-8 was obtained from reference [183].

As a first step, the mass of each IL is weighed on a Sartorius analytical balance (BL 120S model, maximum weight of 120 g) into a vial containing a magnetic stirrer, as seen in Figure 2.1 (a), followed by the addition of 10 mL of acetone, as illustrated in Figure 2.1 (b). Afterwards, the sample is stirred on a magnetic stirrer (VWR VMS-C7 model) during 15 minutes at room temperature, as seen in Figure 2.1 (c), to guarantee the dissolution of the IL in the acetone.

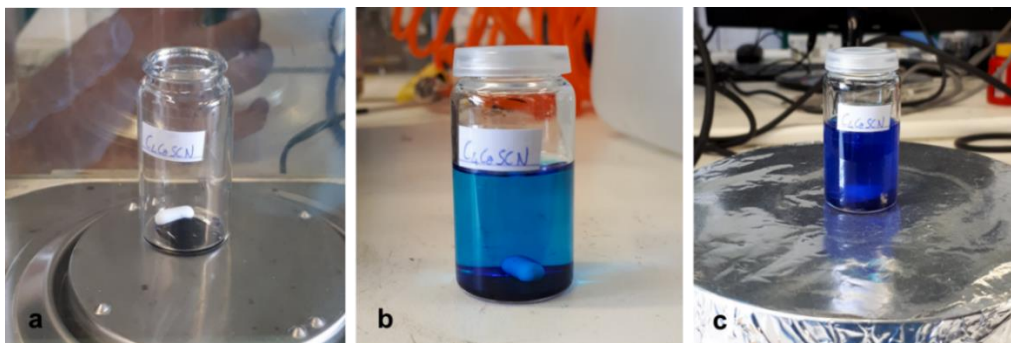


Figure 2.1. Preparation of IL@MOFs: (a) weighing the mass of IL, (b) addition of 10 mL of acetone to the IL, (c) stirring at room temperature.

As the next step, the IL and acetone solution is added to a vial containing 1 g of ZIF-8, previously degassed at 100°C for 3 hours. Posteriorly, the vial containing the mixture of ZIF-8, IL and acetone, is covered with a lid and left to be stirred overnight at room temperature. On the next day, after removing the lid, the stirring continues for another 4-5 hours as seen in Figure 2.2 (a).

Afterwards, the mixture is heated up to the boiling point of acetone, as seen in Figure 2.2 (b), to ensure its evaporation. Lastly, the sample is dried and degassed at 100°C for 3-4 hours on a Nabertherm LE14/11/B150 muffle furnace, to ensure the absence of impurities and leftover solvent. The ideal degassing-temperature indicated by the manufacturer of ZIF-8 (BASF, Germany) had been previously confirmed by T. Ferreira [1]. The dried sample is shown in Figure 2.2 (c).



Figure 2.2. Preparation of IL@MOFs: (a) lidless ZIF-8 + IL + acetone vials being stirred, (b) heating up the mixture to ensure solvent evaporation, (c) sample after being dried.

2.1.2. Characterization Techniques

To evaluate the structural/chemical properties of the IL@MOF composites, four different characterization techniques were conducted: He Pycnometry, N₂ Adsorption-Desorption Isotherm at 77K, Powder X-Ray Diffraction and Fourier Transform Infrared Spectroscopy.

2.1.2.1. He Pycnometry

The density of the solid matrix of an adsorbent is indispensable to determine the excess amount of adsorption (further explained in section 2.1.4), and can be experimentally obtained using He, assuming its particles act as probe molecules and will not be adsorbed [104,184]. The experiment to determine the density of the IL@MOFs composites was conducted at 60°C with He (>99% purity, Praxair) on an ISOSORP 2000 high-pressure magnetic-suspension microbalance (Rubotherm GmbH), the same used in adsorption equilibria measurements, whose experimental protocol is further described in section 2.1.3. For He pycnometry, the 'apparent' mass weighed by the microbalance is shown in equation (4), where m is the weighed mass, ρ_g is the density of bulk gas, ρ_h is the density of the sample holder, m_h is the mass of the sample holder, m_s is the mass of adsorbent sample, ρ_s is the density of the adsorbent's solid matrix and q_{exc} is the specific excess adsorption.

$$m = m_h \left(1 - \frac{\rho_g}{\rho_h}\right) + m_s \left(1 - \frac{\rho_g}{\rho_s} + q_{exc}\right) \quad (4)$$

As said before, He pycnometry is conducted based on the fact that He acts as a probe molecule that is not adsorbed, which simplifies and transforms equation (4) into equation (5).

$$m = m_h \left(1 - \frac{\rho_g}{\rho_h}\right) + m_s \left(1 - \frac{\rho_g}{\rho_s}\right) \quad (5)$$

From expression (5) one obtains equation (6), which is a linear type of equation ($y=mx+b$).

$$m - m_h \left(1 - \frac{\rho_g}{\rho_h}\right) = m_s - \frac{m_s}{\rho_s} \rho_g \quad (6)$$

Equation (6) illustrates the curve described by 'apparent' mass as a function of gas density, in which the mass of the solid matrix corresponds to the intercept of the prementioned linear equation, whilst the volume of the solid matrix is given by its slope. Once the mass and volume of the solid matrix are obtained, the determination of the solid matrix density is done dividing these two parameters.

2.1.2.2. N₂ Adsorption-Desorption Isotherm at 77K

The N₂ Adsorption-Desorption Isotherm at 77 K allows the determination of several important and intrinsic characteristics of a solid compound, such as its specific surface area, pore size distribution (assuming the pores have a slit shape), total pore volume and micropore volume [185]. The measurements were carried out in a Micromeritics Accelerated Surface Area and Porosimetry System (ASAP) 2010 static volumetric unit.

2.1.2.3. Powder X-Ray Diffraction

The variety of crystalline structures on solid materials can be studied using a large number of distinct diffraction patterns formed upon interaction with different types of coherently scattered monochromatic waves (e.g. x-rays), whose lengths are commensurate with the lattice spacing of the crystalline structure. Each material has a specific powder diffraction pattern, and powder X-Ray diffraction (PXRD), which is the 'fingerprint' of a crystalline material, allowing the verification of its composition, purity and structure [186].

In scope of this thesis, this technique confirms the absence of structural changes in the MOF upon impregnation with IL, if the IL@MOF spectrum presents specific peaks found in pristine ZIF-8. Said spectra were obtained using a Rigaku MinFlex II apparatus and the measurements for the composites were carried out between 2 θ values of 2° and 50° with a step of 0.02°, whilst the measurements for the pristine MOF were carried out between 2 θ values of 2° and 60° with a step of 0.02°.

2.1.2.4. Fourier Transform Infrared Spectroscopy

Fourier Transform Infrared Spectroscopy (FT-IR) is an analytical technique that allows the identification of organic/inorganic substances in a compound, measuring the infrared radiation (IR) absorbed by component, transmittance (%), as a function of the wavenumber (cm⁻¹).

Since each infrared absorbed band corresponds and identifies specific molecular species [187], this technique allows the confirmation a successful impregnation, if bands of both the IL and pristine MOF are visible in the spectrum of the composite. The utilized equipment was a FT-IR Spectrometer Spectrum two model (Perkin Elmer).

2.1.3. Experimental Methodology

The adsorption and desorption isotherms were obtained using a static gravimetric method, where the measuring cell (usually with around 0.3 g of adsorbent) is coupled to a suspension magnet instead of hanging directly at the micro-balance, allowing the measurements to be transmitted without contact from the closed cell to a highly accurate Sartorius balance, located outside and under ambient atmosphere, as illustrated in Figure 2.3.

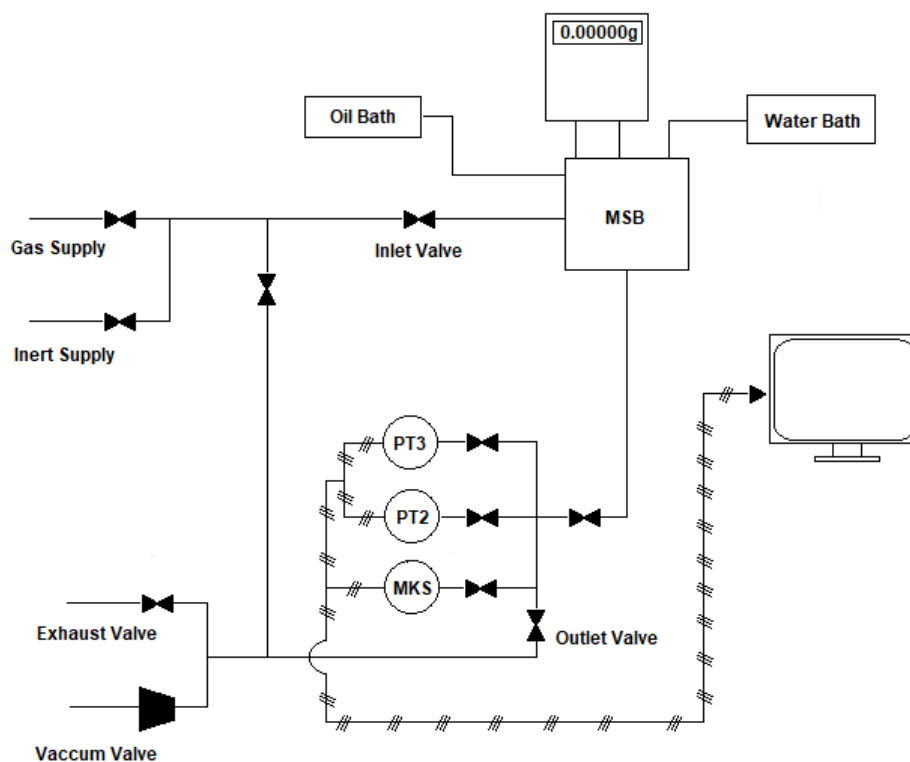


Figure 2.3. Scheme of the adsorption operating unit: MSB - high-pressure magnetic-suspension microbalance; MKS – pressure transducer for 0-1bar; PT2 – pressure transducer for 0-10 bar; PT3 – pressure transducer for 0-35 bar [40].

Because the adsorbent is constantly surrounded by gas, the balance can only register an ‘apparent’ weight, with it being the difference between the sample’s ‘real’ weight and the associated buoyancy force, including the porous volume of the sample [85].

To make sure that there are no gas leaks in the system that could cause instability and adulterate the obtained results, a pressure of approximately 16 bar of He (99.999% purity, Praxair) is set for 24 hours. If the pressure in the system remains constant, and no gas leaks are observed, the degasification process can be initiated.

Degasification, under vacuum for 3-4 hours at the temperature of 100°C, ensures the absence of unwanted molecular species in the system that could disrupt the process of adsorption and adulterate the obtained results. Following degasification, and while still under vacuum, the temperature is set to 30°C. After equilibrium is reached, with no noticeable variations in pressure, temperature and mass, the 'apparent' weight of the sample is registered, along with the operating conditions.

Pressurizing the system in consecutive steps disturbs the pre-established equilibrium stages, and when a new equilibrium under isothermal conditions is reached, a new value for the 'apparent' weight of the sample can be registered, as well as the pressure and temperature of the system. The number of points desired to obtain the adsorption isotherm determines the number of times the pressurization process is repeated. When the maximum desired pressure is reached, a stepwise depressurization of the measurement cell is done, to recheck the previously measured data and obtain a desorption curve [184].

The gases used in adsorption equilibrium measurements were CO₂ (99.998% purity, Praxair) and CH₄ (99.95% purity, Praxair). Regarding the utilized equipment, the ISOSORP 2000 high-pressure magnetic-suspension microbalance (Rubotherm GmbH, Bochum, Germany) has a resolution of 10⁻⁵ g, an uncertainty of ≤0.002% and a reproducibility of ≤3x10⁻⁵ g for a maximum load of 25 g. Temperature measurements were obtained using a four-wire Pt100 probe (RS Amidata, Spain) and its control, within 0.1°C of the set-point value, was done using a thermostatic oil bath F32 HL (Julabo GmbH, Germany) and a water bath ENK6-CT 2000-00053 (J. P. Selecta, Spain).

The variables of interest were recorded using an in-house developed software (BioCTR) and subatmospheric pressure inside the microbalance was reached using an Edwards RV5 vacuum pump. Pressure measurements were obtained using a Baratron model 627D (MKS Instruments GmbH, Germany) for 0-1bar (accurate to 0.12% of the measured value) and Omegadyne Inc. (Sunbury, OH, USA) models with an accuracy of 0.05% of full scale: PX01C2-150A5T for 0-10 bar and PX01C1-500A5T for 0-35 bar.

2.1.4. Adsorption Quantities

The first quantity to consider when studying adsorption isotherms is net adsorption, q_{net} (mol/kg), and it represents the difference between the amount of gas present in the measurement cell, with and without the adsorbent [103]. The mathematical expression to calculate this quantity is represented in equation (7).

$$q_{\text{net}} = \frac{m - m_s - m_h + V_h \rho_g}{m_s} \quad (7)$$

Where m is the 'apparent' mass weighed by the balance; m_s is the mass of adsorbent measured in vacuum after degasification; V_h and m_h are the volume and mass, respectively, of all components of the measuring cell that contribute to buoyancy effects; and ρ_g is the gas density for each point of the experiments' different temperature and pressure values [184,188].

Secondly, there is excess adsorption, q_{exc} (mol/kg) which is the difference between the excess number of gas molecules present in the measurement cell containing the adsorbent, and the number of gas molecules that would be present if all the system's volume was available to be occupied by the gas in its bulk state. For this quantity, the skeletal density is considered and the Gibbs dividing line separates the bulk phase from the solid phase, including the adsorbent and the monolayer of adsorbed molecules [103].

$$q_{exc} = q_{net} + V_s \rho_g = q_{net} + \frac{\rho_g}{\rho_s} \quad (8)$$

It can be obtained using expression (8), where V_s represents the volume of the adsorbent disregarding its pore volume, determined through Helium (He) pycnometry [103,184,188].

Lastly, in total adsorption, q_t (mol/kg), the solid phase – separated from the bulk phase by the Gibbs dividing line – includes the amount of adsorbed gas molecules, plus the molecules that were not adsorbed and linger inside the pore volume, meaning that both the material's skeletal density and pore volume are key factors in its determination. It can be calculated using equation (9) where V_p is the pore volume of the adsorbent impenetrable by the molecules of adsorbate [184].

$$q_t = q_{ex} + V_p \rho_g = q_{net} (V_p + V_s) \rho_g \quad (9)$$

Besides the adsorption quantities, that help quantify the adsorption capacity of a certain material, the ideal selectivity represents its affinity to preferably adsorb a specific gas, in comparison to other gaseous species. In scope of this thesis, the ideal selectivity was calculated with expression (10) and it refers to the selectivity of the IL@MOF composite to preferably adsorb CO₂ instead of CH₄.

$$S_{CO_2/CH_4} = \frac{q_{t CO_2}}{q_{t CH_4}} \quad (10)$$

In order to obtain the ideal selectivity, the Sips adsorption model was used to predict the total amount adsorption isotherm, q_t (mol/kg), using to expression (11).

$$q_t = \frac{q_s (bp)^{\frac{1}{n}}}{1 + (bp)^{\frac{1}{n}}} \quad (11)$$

The Solver add-in from Microsoft Excel was used to minimize the sum of the differences between the predicted and the experimental adsorbed amounts, by readjusting q_s , b and P parameters for both CO₂ and CH₄ data, allowing the calculation, for the desired pressure range, of the ideal selectivity.

In expression (11), q_t represents the specific total amount adsorbed, q_s represents the maximum specific adsorbed amount and p is the total pressure. Also, n is the heterogeneity parameter and a higher n is associated with a more heterogeneous system. Regarding the affinity constant, b , one concludes that a higher value is associated with more adsorbate molecules being attracted to the surface of the adsorbent.

In addition, a polynomial fitting (order 4) was used to predict the total amount adsorption isotherm, q_t (mol/kg), even though it does not have parameters that meaningfully describe physical adsorption. The obtained variables for each fitting were compared, as further detailed in section 3.1.4.

2.2. Gas Permeation in Mixed-Matrix Membranes

2.2.1. Materials and Preparation

The mixed-matrix membranes were prepared using the solvent evaporation method, and the selection of filler/s, solvent and polymer was of the utmost importance. The chosen polymer was Matrimid®5218 (Hunstman, USA) since it is an affordable material with high thermal and mechanical stabilities, that make it one of the most common materials used as structural composites, adhesives and membranes in gas separation processes [178].

The solvent used was dichloromethane, CH₂Cl₂ (>99.9% purity, Sigma Aldrich), due to its ability to dissolve Matrimid®5218, and because it is more environmental-friendly than the alternatives *i.e.* chloroform and dimethylformamide [189,190].

The selected fillers were the IL@MOF composites [C₆MIM][NTf₂]@ZIF-8 and [C₂MIM][Ac]@ZIF-8 which have shown interesting CH₄ and CO₂ uptake capacity and CO₂/CH₄ ideal selectivity, as reported in reference [1].

Table 2.3, shows the mass of IL and ZIF-8 in each membrane and Table 2.4 shows a list of the ILs used to synthesize the IL@MOF composites, as well as the polymer used in MMMs.

Table 2.3. IL and ZIF-8 loading for each composite acting as filler.

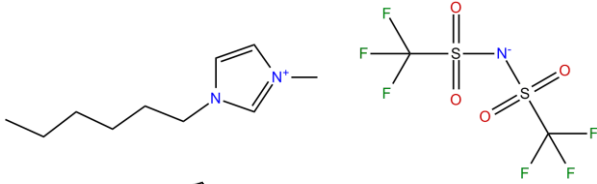
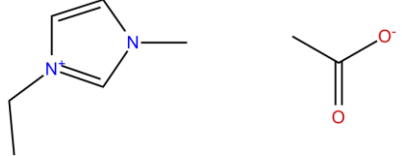
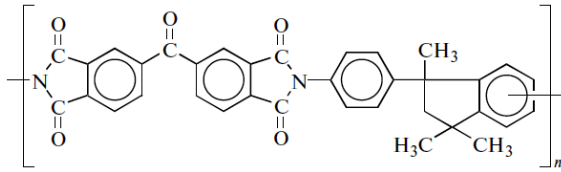
Filler (wt%)	Filler Mass (g)	[C ₆ MIM][NTf ₂]@ZIF-8		[C ₂ MIM][Ac]@ZIF-8	
		IL (g)	ZIF-8 (g)	IL (g)	ZIF-8 (g)
10	0.0250	0.0042	0.0208	0.0018	0.0232
15	0.0375	0.0063	0.0312	0.0027	0.0348
20	0.0500	0.0084	0.0416	0.0036	0.0464
25	0.0625	0.0105	0.0520	0.0044	0.0581
30	0.0750	0.0126	0.0624	0.0053	0.0697

To produce a MMM, two vials are needed. On the first vial, 2.25 mL of dichloromethane (CH₂Cl₂) are added to 0.25 g of Matrimid®5218, while on a second vial the same volume of CH₂Cl₂ is added to the mass of filler correspondent to its desired weight percentage: 10 wt% = 0.025 g; 15 wt% = 0.0375 g; 20 wt% = 0.05 g; 25 wt% = 0.065 g; 30 wt% = 0.075 g. The filler wt% corresponds to equation 12.

$$Filler \text{ (wt\%)} = \frac{m_{filler}}{m_{polymer}} \times 100\% \quad (12)$$

Afterwards, both vials are sealed, and the mixtures are submitted to an ultrasonic bath for 4 hours, and posteriorly stirred for 24 hours on a magnetic stirrer at 600 rpm. After the 24 hours, the Matrimid®5218 solution is poured into the vial containing the filler solution, which is then sealed and stirred for 1 hour at 600 rpm. After stirring, the solution is poured into a round teflon petri dish and placed in a desiccator until the solvent has completely evaporated.

Table 2.4. Chemical Formula, nomenclature, name, molecular weight and structure of the chosen ILs to synthesize the IL@MOF composites, and the polymer used in MMMs.

Formula	Nomenclature	Name	M _w (g/mol)	Structure
C ₁₂ H ₁₉ F ₆ N ₃ O ₄ S ₂	[C ₆ MIM][NTf ₂]	1-hexyl-3-methylimidazolium bis[(trifluoromethyl)sulfonyl]imide	447.41	
C ₈ H ₁₄ N ₂ O ₂	[C ₂ MIM][Ac]	1-ethyl-3-methylimidazolium acetate	170.21	
-	Matrimid®5218	5(6)-amino-1-(4' aminophenyl)-1,3-trimethylindane	-	

The ILs structure was retrieved from the NIST Ionic Liquids Database - ILThermo [182] and the structure of Matrimid®5218 was obtained from reference [194].

2.2.2. Characterization Techniques

To evaluate the structural/chemical properties of the IL@MOF MMMs, two characterization techniques were conducted: contact angle measurements and evaluation of mechanical properties.

2.2.2.1. Contact Angles

The contact angle between a drop of water on the surface of a solid, is the equilibrium established between the drop and three interfacial tensions *i.e.* solid-gas (γ_{SG}), solid-liquid (γ_{SL}) and liquid-gas (γ_{LG}), as seen in Figure 2.4.

Knowing the value of the contact angle allows the conclusion of the hydrophobic behavior of the synthesized membranes, with them being considered hydrophilic when the contact angle is inferior to 90° and hydrophobic when the angle is superior to 90° , when using water [191].

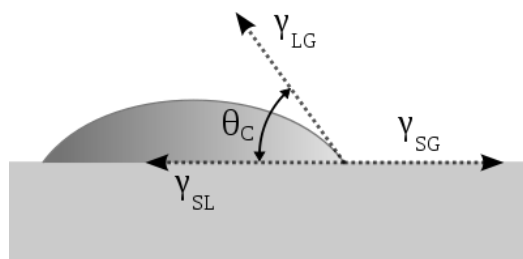


Figure 2.4. Illustration of the three tensions involved in the determination of a contact angle in a solid's surface. Adapted from reference [195].

These measurements were done using the KSV (CAM2008) software, which is an optical system that captures several pictures of the drop of water on the membrane surface, and calculates the contact angle of both left and right side. The software captured 10 frames of the water's drop on the membranes' surface and each sample was measured 3 times, with the final value being an average of said 3 measurements.

2.2.2.2. Mechanical Properties

In this thesis, the mechanical properties of the prepared MMMs were evaluated by puncture tests, to determine their resistance until breakdown or deformation [192]. These measurements were performed with the help of Professor Vítor Alves, at Instituto Superior de Agronomia (ISA), using a texturometer analyzer (TA XT – Plus Texture Analyzer – Stable Micro Systems, UK). The samples with 3x3 cm in dimensions were tested at room temperature.

The results obtained by the perforation of the membrane's sample, at the speed of $1 \text{ mm}\cdot\text{s}^{-1}$, by using a texturometer analyzer's probe diameter of 2 mm, as well as the calibration of the equipment, were registered and controlled using an ISA-built-in software. The experiments were repeated 3 times for each membrane sample. Figure 2.5 shows an example of the curves obtained, showing the Force (N) as a function of distance (mm).

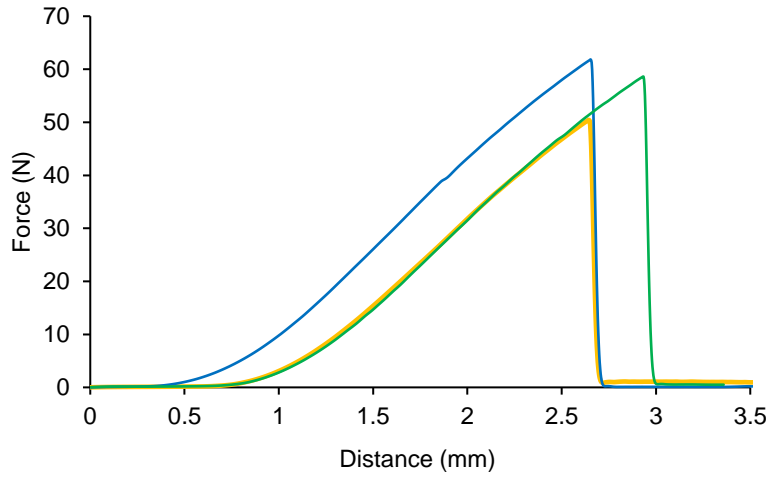


Figure 2.5. Illustrative example of the curves obtained for Run 1 (see Table 2.5), where the three colours represent three replicas.

According to expressions (13) and (14) the tensile strength (σ) of each membrane sample is obtained using the cross-sectional area (S_c), and force (F) obtained measurements and registered by the probe.

$$\sigma = \frac{F}{S_c} \quad (13)$$

$$S_c = \pi \times r^2 \quad (14)$$

2.2.3. Experimental Methodology

Gas permeation experiments are performed in a permeation cell that is divided into two compartments, each corresponding to the feed and permeate. The cell is submerged into a water bath heated up to 30°C, controlled by a thermostat (Julabo ED, Germany), and a transducer (Druck PCDR 910 models 99166 and 991675, UK, with accuracies of ± 0.008 bar) is connected to each compartment to measure the pressure, as illustrated in Figure 2.6.

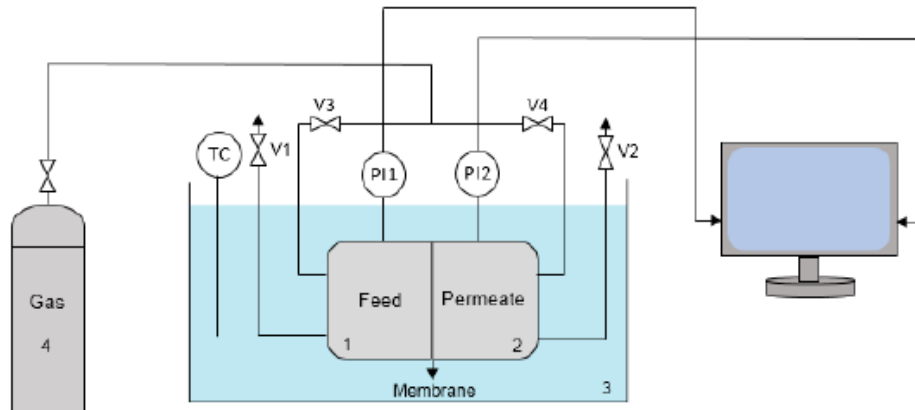


Figure 2.6. Illustration of the permeation apparatus: 1 - feed compartment, 2 - permeate compartment, 3 - water bath, 4 - gas feed, TC - temperature controller, PI1 & PI2 - pressure indicators, V1 & V2 - exhaust valves, V3 & V4 - inlet valves [40].

Before starting the experiment, the thickness of the membrane is measured using a micrometer (Elcometer). Afterwards, the membrane is placed on the white circle between the cell's two compartments, as seen in Figure 2.7 (a), and it is closed and sealed as presented in Figure 2.7 (b).

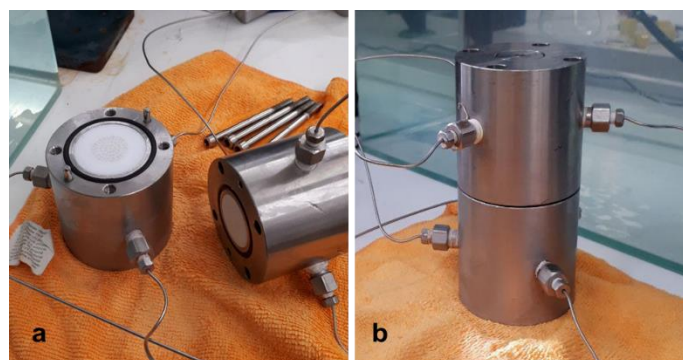


Figure 2.7. Illustration of the gas permeation measurement cell (a) opened and (b) sealed.

The first step, after placing the cell in the water bath, is to purge the entire system with the gas of interest, keeping all the valves opened to ensure the absence of other gaseous species. Posteriorly, the exhaust valves are closed and a pressure of 0.7 bar is settled, after which the inlet valves are also closed, allowing the pressure inside the cell to stabilize. Following pressure stabilization, the driving force is applied by rapidly opening and closing the exhaust valve of the permeate compartment, which will cause the pressure to gradually increase in said compartment, while simultaneously decreasing in the feed's compartment. Figure 2.8 shows an example for the feed and permeate pressure values obtained throughout the experiment.

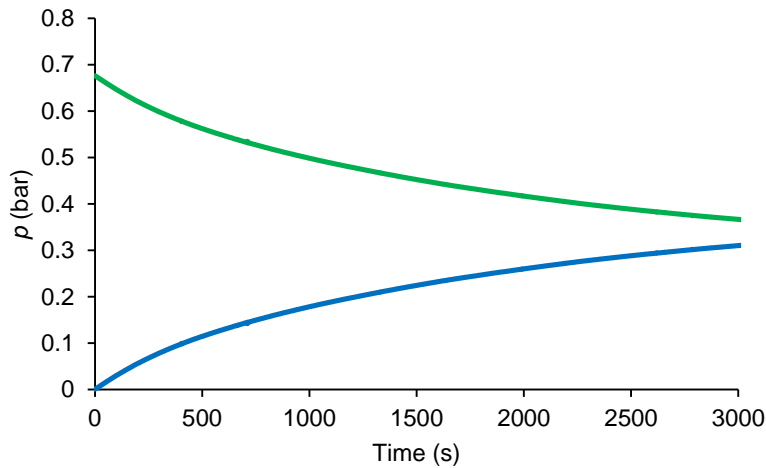


Figure 2.8. Illustrative example of the Feed (green) and Permeate (blue) curves obtained for CO₂ Run 9 (see Table 2.5).

To calculate the CH₄ and CO₂ MMMs' permeability and selectivity, the initial moment (t_0) is considered when the driving force is applied to the system. The analysis of the pressure data in both compartments, registered with PicoLog software, is done with equation (15) where β is the cell's geometric parameter, Δp_0 is the difference of pressure at t_0 , Δp is the variation of pressure through time, P is the permeability, t is time and l is the membrane's thickness.

$$\frac{1}{\beta} \times \ln\left(\frac{\Delta p_0}{\Delta p}\right) = P \times \frac{t}{l} \quad (15)$$

Hence, the graphic representation of $\frac{1}{\beta} \times \ln\left(\frac{\Delta p_0}{\Delta p}\right)$ as a function of $\frac{t}{l}$ allows the determination of the permeability (P) values for each gas, which corresponds to the slope of the obtained curve. Figure 2.9 is an example of the obtained curve, with the permeability value being the slope of the obtained linear equation.

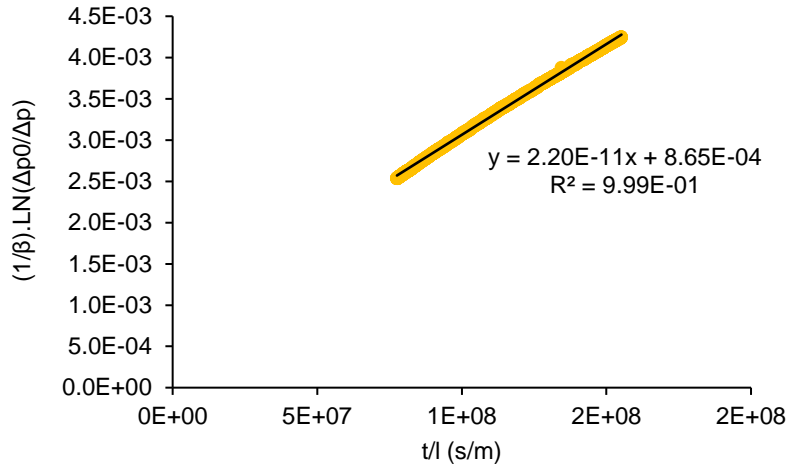


Figure 2.9. Illustrative example of the curve obtained for CO₂, Run 12 (see Table 2.5).

In addition, β can be obtained using equation (16) where A is the area of the membrane, V_{Feed} is the volume of the feed compartment and V_{Perm} is the volume of the permeate compartment.

$$\beta = A \times \left(\frac{1}{V_{\text{Feed}}} + \frac{1}{V_{\text{Perm}}} \right) \quad (16)$$

The calibration of the unit was done using a PDMS membrane with the thickness of 1.20×10^{-4} m and known N₂ permeability of 2.075×10^{-10} m².s⁻¹. The prementioned protocol for membrane permeation was followed, considering that this time the slope of the graphical representation of $\frac{1}{P} \times \ln\left(\frac{\Delta p_0}{\Delta p}\right)$ as function of $\frac{t}{l}$ is β (β (GP₁) = 106.26 cm⁻¹ and β (GP₂) = 109.17 cm⁻¹).

Lastly, with the obtained permeability values, for the same membrane tested with different gases, it is possible to obtain the value of the ideal CO₂/CH₄ selectivity, $\alpha_{\text{CO}_2/\text{CH}_4}$, as seen in equation (17) where P_{CO_2} is the permeability of CO₂ and P_{CH_4} is the permeability of CH₄.

$$\alpha_{\text{CO}_2/\text{CH}_4} = \frac{P_{\text{CO}_2}}{P_{\text{CH}_4}} \quad (17)$$

Table 2.5 shows the planification of the permeation experiments set in this work, where pristine Matrimid®5218, Matrimid®5218/ZIF-8 and Matrimid®5218/IL@ZIF-8 MMMs were assessed.

Table 2.5. Work plan and summary of the conducted permeation experiments.

Material	Filler Loading (wt%)	Run	Gases	Observations
Matrimid®5218 (Batch I)	-	1	CH ₄ and CO ₂	Control
Matrimid®5218 (Batch II)	-	2	CH ₄ and CO ₂	Test reproducibility with different membranes
ZIF-8	10	3	CH ₄ and CO ₂	-
	20	4	CH ₄ and CO ₂	-
	30	5	CH ₄ and CO ₂	-
Matrimid®5218/[C ₂ MIM][Ac]@ZIF-8	10	6	CH ₄ and CO ₂	-
	15	7	CH ₄ and CO ₂	-
	20	8	CH ₄ and CO ₂	-
	25 (Batch I)	9	CH ₄ and CO ₂	Control
	25 (Batch II)	10	CH ₄ and CO ₂	Test reproducibility with the same membrane
	30	11	CH ₄ and CO ₂	-
Matrimid®5218/[C ₆ MIM][NTf ₂]@ZIF-8	10	12	CH ₄ and CO ₂	-
	15	13	CH ₄ and CO ₂	-
	20	14	CH ₄ and CO ₂	-
	25	15	CH ₄ and CO ₂	-
	30	16	CH ₄ and CO ₂	-

3. Results and Discussion

3.1. IL@MOF Composites

No thermogravimetric analysis (TGA) was conducted for the composite materials, since both ZIF-8 and ILs have degradation temperatures above 100°C.

3.1.1. He Pycnometry

The determined values for the matrix density of the utilized MOF and the IL@MOF composites, considering the experimental protocol described in chapter 2.1.3 and the mathematical background presented in chapter 2.1.2.1, are listed in Table 3.1.

Table 3.1. Experimental determined values for the density of the solid matrix of the IL@MOF composites.

Material	ρ_s (g/cm ³)
ZIF-8	1.49
[N ₁ 2OH 2OH 2OH][NTf ₂]@ZIF-8	1.42
[C ₄ MIM] ₂ [Co(SCN) ₄]@ZIF-8	1.34
[C ₄ MIM][FeCl ₄]@ZIF-8	1.33

The obtained value for the solid matrix of the pristine ZIF-8 was 1.49 g/cm³ which is in accordance with the reported literature value of 1.518(3) g/cm³ [193]. It is possible to see that all the density values obtained for the composites are lower than the observed value for the ZIF-8, which means that the impregnation of the IL in the MOF affected its solid matrix density. However, because this parameter is obtained with both the slope and intercept of the apparent mass as function of the helium density, small errors in these values might change the linear fitting, impacting the obtained density values. The obtained plots for each composite are presented in Appendix A.

3.1.2. N₂ Adsorption-Desorption Isotherms at 77K

The determination of the specific surface area of the prepared composite samples was performed using N₂ adsorption-desorption equilibrium measurements at 77 K. Through Figure 3.1, it is possible to confirm that the obtained isotherms for the composites are Type I, which considering IUPAC definition is characteristic of microporous materials [100]. It is also possible to see that the uptake capacity decreased 33% in the [N₁₂OH 2OH 2OH][NTf₂]@ZIF-8 composite and about 66% in the [C₄MIM][FeCl₄]@ZIF-8 and [C₄MIM]₂[Co(SCN)₄]@ZIF-8 composites, comparing with pristine ZIF-8. In addition, the ZIF-8 isotherm is close to literature data reported by Kinik *et al.* [28].

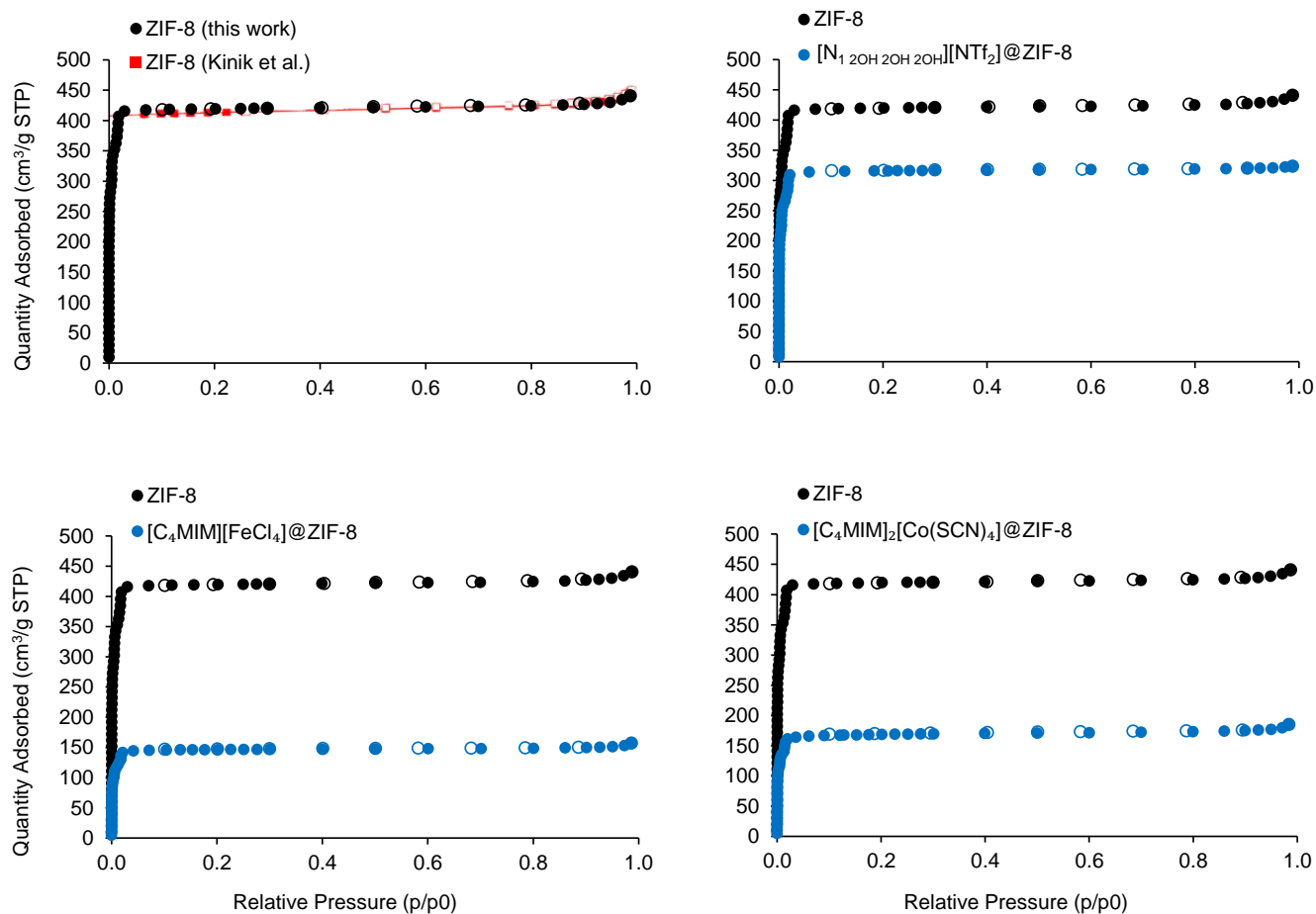


Figure 3.1. N₂ adsorption-desorption isotherms at 77 K for the ZIF-8 used in this thesis (black), literature ZIF-8 data (red) and the IL@MOF composites (blue).

The obtained BET, and Langmuir, specific surface area and the total pore volume for each material is listed on Table 3.2.

Table 3.2. Values for BET specific surface and its c constant; Langmuir specific surface area, total pore volume and partial pressure, obtained using *MicroActive* software.

Sample	BET Specific Surface Area (m ² /g)	c	Langmuir Specific Surface Area (m ² /g)	Total Pore Volume (cm ³ /g)	p/p ₀
ZIF-8	1907 ± 81	407	2008 ± 83	0.67	0.97
[N ₁ 2OH 2OH 2OH][NTf ₂]@ZIF-8	1658 ± 79	171	1732 ± 88	0.49	0.97
[C ₄ MIM] ₂ [Co(SCN) ₄]@ZIF-8	817 ± 48.77	249	847 ± 52	0.28	0.97
[C ₄ MIM][FeCl ₄]@ZIF-8	691 ± 41	270	717 ± 45	0.24	0.97

It is possible to see that due to the IL impregnation, the $[N_{1,2OH,2OH,2OH}][NTf_2]@ZIF-8$ composite shows a loss of 13.06% in BET specific surface area, and 26.87% in total pore volume, considering the pristine ZIF-8, whilst the $[C_4MIM][FeCl_4]@ZIF-8$ composite presents a loss of 63.77% in BET specific surface area and 64.29% in total pore volume. The composite $[C_4MIM]_2[Co(SCN)_4]@ZIF-8$ presents a BET specific surface area loss of 57.16% and a total pore volume loss of 58.20%.

A non-local density functional theory (NLDFT) analysis was conducted, with *MicroActive* software, to determine the pore size distribution for the composites, in comparison with ZIF-8, as represented in Figure 3.2.

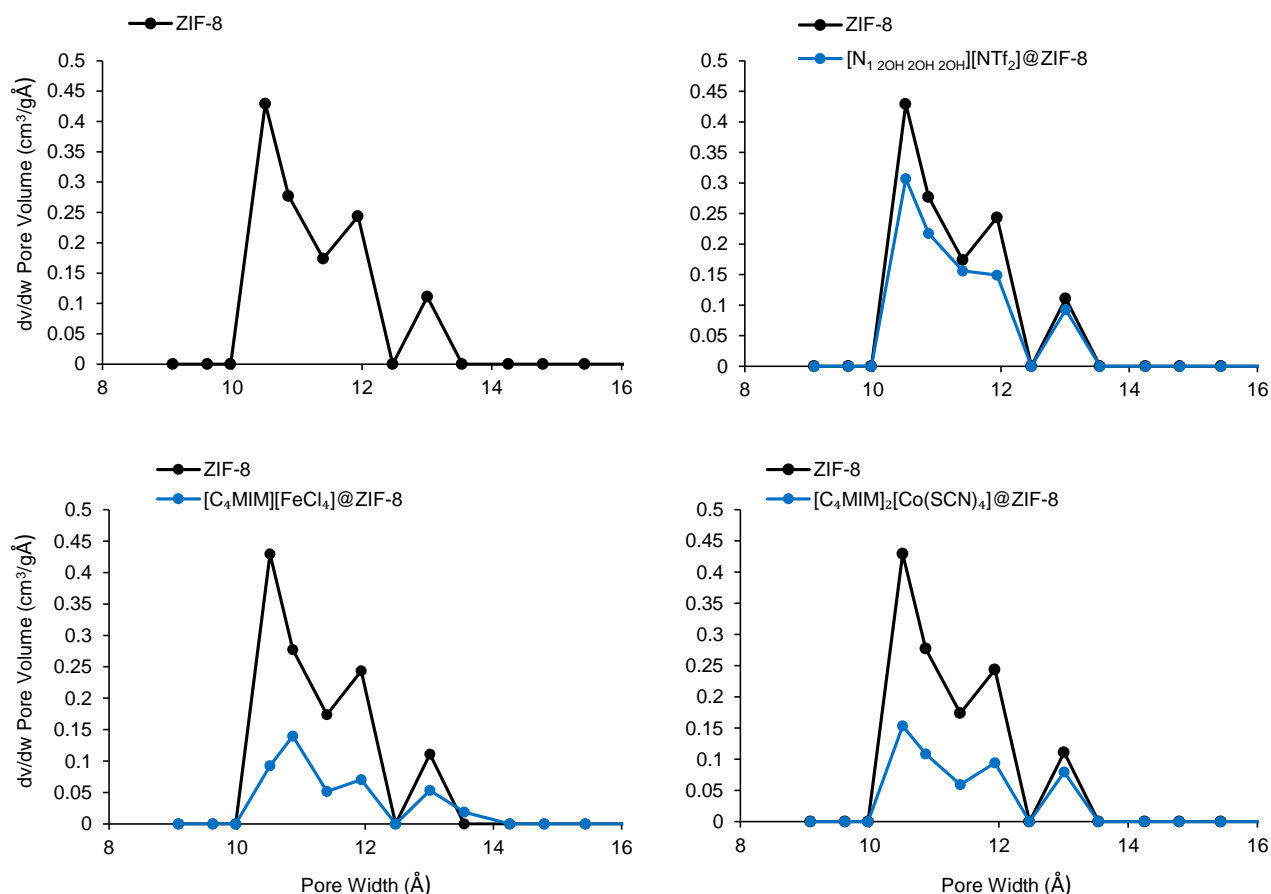


Figure 3.2. Pore size distribution obtained through NLDFT analysis of the ZIF-8 and the IL@ZIF-8 composites.

Figure 3.2 shows a decrease on the available pore volume, which, with the obtained results depicted in Figure 3.1, indicates that total pore volume/quantity suffered a loss in comparison with the pristine ZIF-8, due to the IL impregnation. Moreover, it further accentuates the fact that these are microporous materials, according to IUPAC classification, since they have pores smaller than 20 Å (2 nm) [100].

3.1.3. Powder X-Ray Diffraction

As previously mentioned in section 2.1.2.3, PXRD allows the verification of the absence of structural changes in the MOF upon the IL impregnation, which can be confirmed by comparing the spectra of each composite with the one of the pristine ZIF-8. It can also show if the prepared materials are crystalline or amorphous. The atoms of crystalline materials are periodically arranged in a 3D space, resulting in the presence of high and narrow intensity peaks in PXRD spectra, whilst in amorphous compounds the atoms are randomly arranged, causing the appearance of randomly distributed and wider peaks [194].

As shown in Figure 3.3, the results presented for ZIF-8 are in accordance with PXRD data reported for this material [152], as well as with literature sources stating that ZIF-8 is a crystalline material, since there are high and narrow intensity peaks presented in the obtained spectrums [195–197]. In the obtained PXRD results, the characteristic peaks of ZIF-8 are present in all the synthesized composites, which allows the conclusion that these materials are also crystalline.

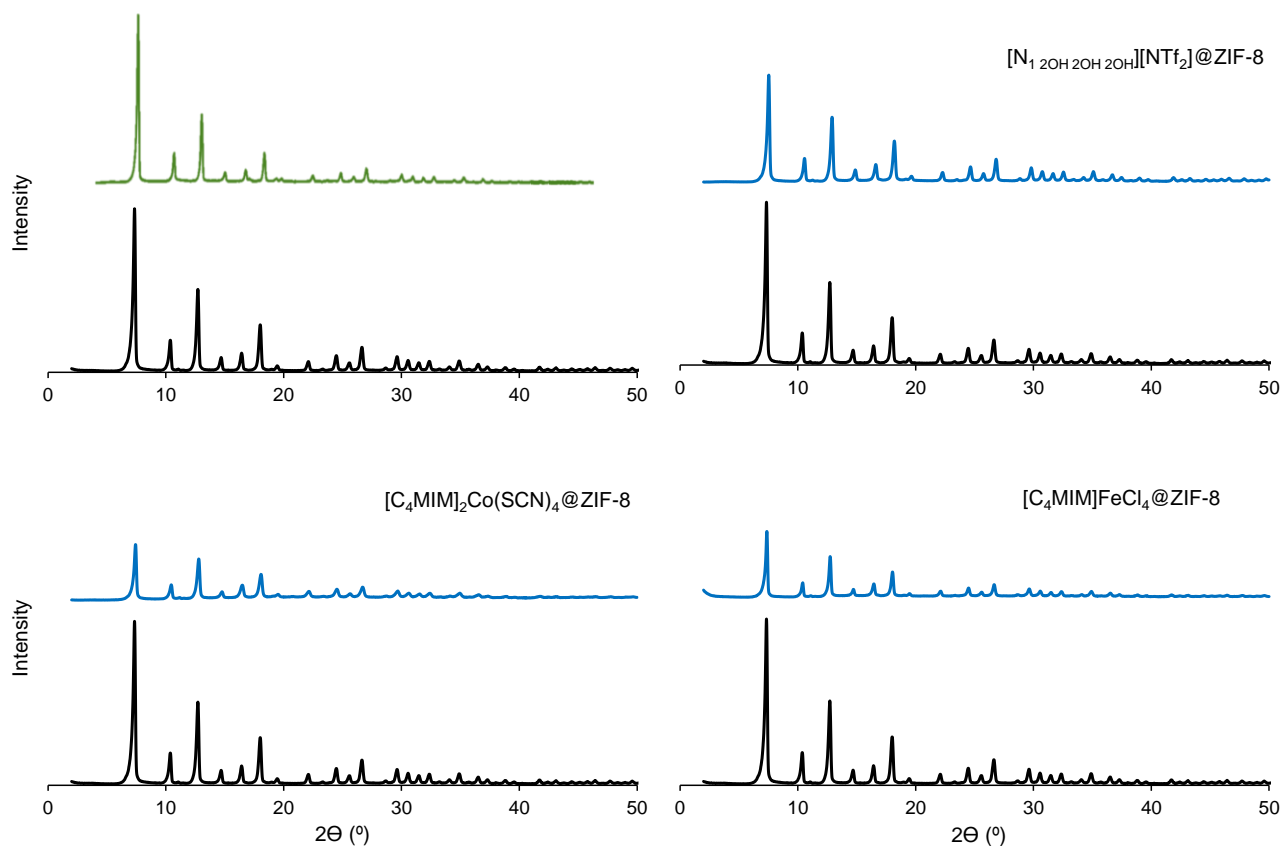


Figure 3.3. PXRD spectra for the ZIF-8 reported in literature [152] (**green**), the ZIF-8 used in this thesis (**black**), and for the synthesized IL@MOF composites (**blue**).

3.1.4. Fourier Transform Infrared Spectroscopy

As mentioned in chapter 2.1.2.4, FT-IR allows the identification of organic/inorganic species in a certain material since each infrared band, present on the plot of transmittance as a function of the wavenumber, corresponds to a specific molecular species. Therefore it is possible to confirm the success of the IL impregnation in the MOF, if bands of the first can be found in the spectra of the composite.

The FT-IR spectra for the $[N_{1.2}OH_{2.0}H_{2.0}H_{2.0}][NTf_2]@ZIF-8$ composite illustrated in Figure 3.4, shows the presence of bands correspondent to the $[NTf_2]^-$ anion: between $1250-1190\text{ cm}^{-1}$ (presumed to be C-F₃ stretch) and 1060 cm^{-1} (characteristic of N-S stretch) [198], which corroborate the conclusion of a successful IL impregnation.

In Figure 3.4 the obtained FT-IR spectra for the $C_4[MIM]_2[Co(SCN)_4]@ZIF-8$ composite, shows a band between $2150-1990\text{ cm}^{-1}$ (characteristic of the N=C=S isothiocyanate stretch) [199] found in the pristine IL, allowing the conclusion that this was also a successful impregnation.

For $[C_4MIM][FeCl_4]@ZIF-8$, and according to literature [199], it is probable that a characteristic band for a metal-halogen stretch bond, specifically metal-Cl can be found between $610-220\text{ cm}^{-1}$, depending on the strength of the bond, the mass of the metal atom and the its valence state. However, in scope of this thesis, the limit wavenumber for which the measurement was conducted was 450 cm^{-1} , making it impossible to validate the successfulness of the IL impregnation through this technique. Nonetheless, the results presented for the N₂ adsorption-desorption isotherms at 77K for this composite allow said conclusion.

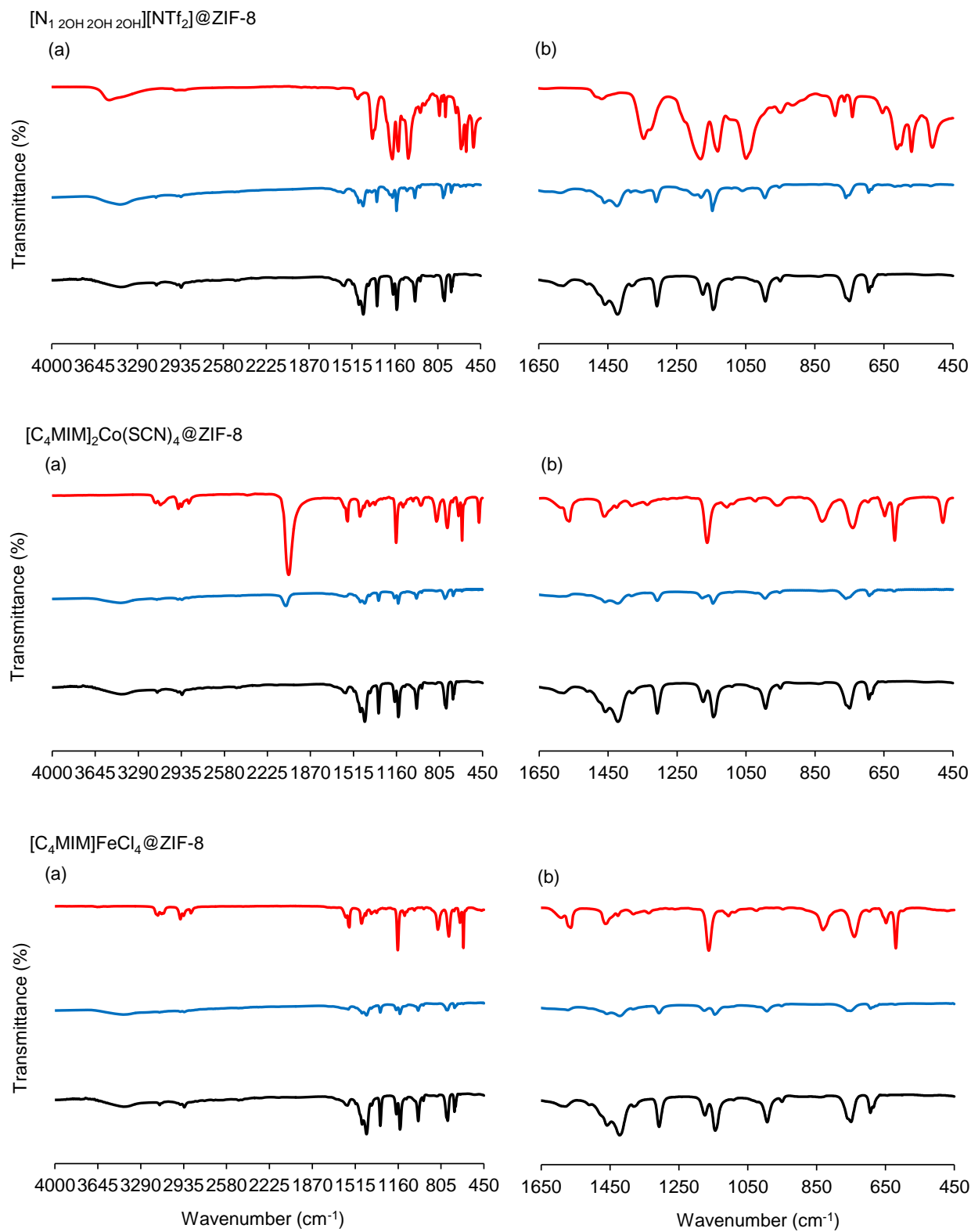


Figure 3.4. Obtained FT-IR spectra for the studied ILs (**red**), the ZIF-8 (**black**) and the synthesized IL@MOF composites (**blue**) between (a) 4000-450 cm⁻¹ and (b) 1650-450 cm⁻¹.

3.1.4. Adsorption Equilibria for CO₂ and CH₄

In order to assess the performance of the prepared IL@ZIF-8 composites, in terms of CH₄ and CO₂ adsorption capacity as well as CO₂/CH₄ ideal selectivity, adsorption equilibrium measurements were conducted at 30°C and between 0 and 16 bar. Table 3.3 shows the Sips adsorption isotherm model parameters for ZIF-8 and each composite, as well as their Average Relative Error (%).

Table 3.3. Sips adsorption model parameters and Average Relative Error (%) for ZIF-8 and each IL@ZIF-8 composite.

Samples	CH ₄				CO ₂			
	q _s (mol/kg)	b	n	ARE (%)	q _s (mol/kg)	b	n	ARE (%)
ZIF-8	10.15	0.031	0.962	0.71	12.92	0.083	0.870	4.34
[N ₁ 2OH 2OH 2OH][NTf ₂]@ZIF-8	8.62	0.028	0.985	2.17	10.27	0.091	0.860	3.62
[C ₄ MIM][FeCl ₄]@ZIF-8	4.79	0.035	0.977	1.20	6.72	0.093	0.890	4.64
[C ₄ MIM] ₂ [Co(SCN) ₄]@ZIF-8	4.42	0.032	0.994	3.33	6.45	0.075	0.909	5.29

However, the Sips adsorption model did not provide an accurate fitting of the experimental data, especially for CO₂ at subatmospheric pressure, as exemplified in Figure 3.5, which could have an unpredictable impact in the selectivity of these materials.

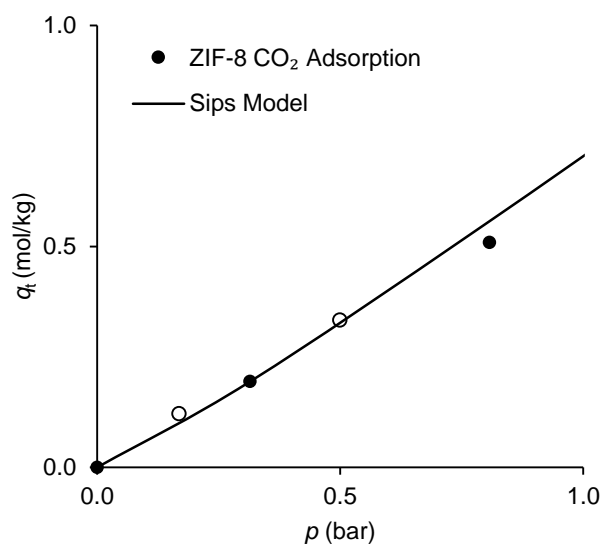


Figure 3.5. Example of the poor fitting provided by the Sips model for CO₂ adsorption by ZIF-8, between 0 and 1 bar. Open symbols are desorption and close symbols are adsorption. Straight line represents the Sips fitting.

In order to overcome the poor fitting provided by the Sips model, a polynomial adjustment (order 4) was used, and its parameters are presented in Appendix B. Figure 3.6 shows the CH₄ and CO₂ adsorption/desorption isotherms for ZIF-8 and the IL@ZIF-8 composites.

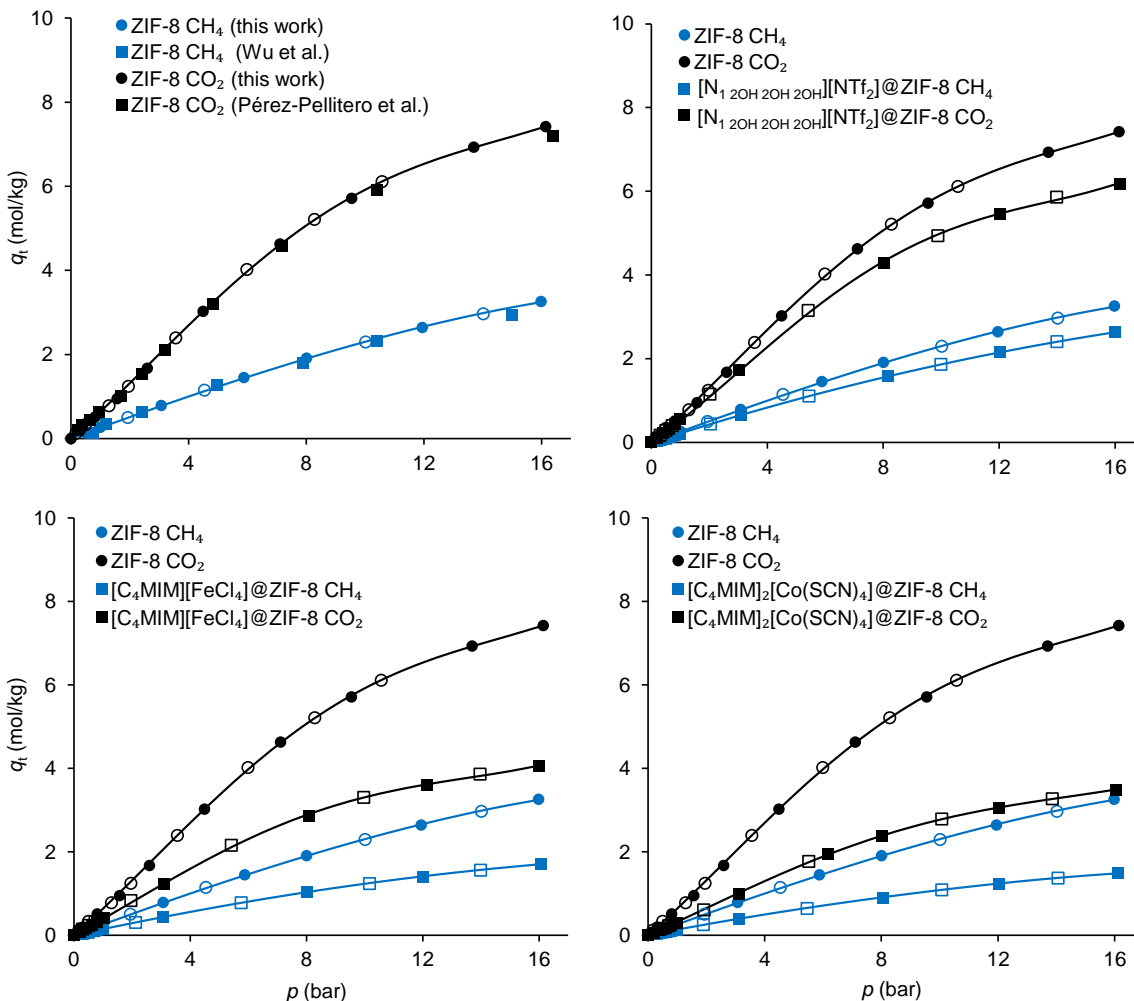


Figure 3.6. CH₄ and CO₂ adsorption/desorption isotherms at 30°C for ZIF-8 and its comparison with literature, and the IL@ZIF-8 composites. Open symbols are desorption and close symbols are adsorption. Straight lines represent the polynomial fitting.

The adsorbed amount was represented in total adsorption (q_t) since it takes into account the solid matrix density and its total pore volume. Considering the N₂ adsorption-desorption at 77 K, all the composites suffered a total pore volume loss, which justifies the general lower adsorption capacity verified in the IL@ZIF-8 composites. Figure 3.7 shows a comparison between the CO₂ and CH₄ uptake capacities for each composite. The potential use of these composites to capture CO₂ from biogas can be evaluated by analysing their capacity towards the adsorption of both CO₂ and CH₄. At 8 bar the difference between CO₂ and CH₄ adsorption capacity of [C₄MIM]₂[Co(SCN)₄]₂@ZIF-8 and [C₄MIM][FeCl₄]₂@ZIF-8 is merely 1.47 mol/kg and 1.85 mol/kg, respectively.

On the other hand, for $[N_{1.2OH.2OH.2OH}][NTf_2]@ZIF-8$ this difference is 2.77 mol/kg, which considering that PSA processes for biogas upgrading to biomethane usually operate between 3 and 10 bar [200], means that this composite has a greater potential for CO_2 adsorption than the other composites.

However, as seen in Figure 3.7, all the prepared IL@ZIF-8 composites have lower CO_2 and CH_4 uptake capacity than the pristine ZIF-8. Tables 3.4 and 3.5 show the percentage of capacity loss for both CH_4 and CO_2 , in all the composites at 1 and 16 bar, respectively.

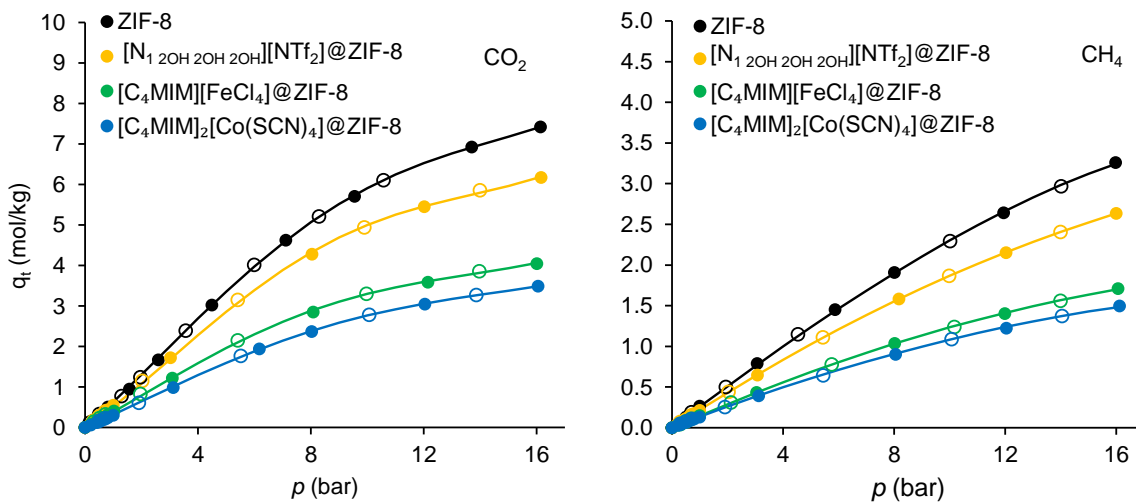


Figure 3.7. CH_4 and CO_2 adsorption-desorption isotherms at 30°C for ZIF-8 and the studied ILs. Open symbols are desorption and closed symbols are adsorption. Straight lines represent the polynomial fitting.

Table 3.4. CH_4 and CO_2 uptake capacity at 30°C for ZIF-8 and the IL@ZIF-8 composites, as well as the percentage of capacity loss at 1 bar using ZIF-8 as reference.

q_t (mol/Kg) at 1 bar							
ZIF-8		$[N_{1.2OH.2OH.2OH}][NTf_2]@ZIF-8$		$[C_4MIM][FeCl_4]@ZIF-8$		$[C_4MIM]_2[Co(SCN)_4]@ZIF-8$	
CH_4	CO_2	CH_4	CO_2	CH_4	CO_2	CH_4	CO_2
0.26	0.64	0.22	0.51	0.15	0.39	0.13	0.32
Capacity Loss (%)		14.78	19.11	42.86	38.84	48.03	49.77

Table 3.5. CH_4 and CO_2 uptake capacity at 30°C for ZIF-8 and the IL@ZIF-8 composites, as well as the percentage of capacity loss at 16 bar using ZIF-8 as reference.

q_t (mol/Kg) at 16 bar							
ZIF-8		$[N_{1.2OH.2OH.2OH}][NTf_2]@ZIF-8$		$[C_4MIM][FeCl_4]@ZIF-8$		$[C_4MIM]_2[Co(SCN)_4]@ZIF-8$	
CH_4	CO_2	CH_4	CO_2	CH_4	CO_2	CH_4	CO_2
3.25	7.39	2.64	6.16	1.70	4.07	1.48	3.49
Capacity Loss (%)		18.82	16.60	47.69	45.00	54.47	52.83

As can be seen in Tables 3.4 and 3.5, the percentage of capacity loss for CO₂ uptake by all the composites ranges between 19-50% at 1 bar, and 17-53% at 16 bar. Nonetheless, and despite the loss in adsorption capacity, due to the impregnation with IL that partially occupied pore volume, it is also important to evaluate the ideal selectivity of each composite to adsorb CO₂.

Figure 3.8 shows the CO₂/CH₄ ideal selectivity of these composites and their comparison with the pristine ZIF-8 and the [C₂MIM][Ac]@ZIF-8 composite prepared and characterized by T. Ferreira [1]. And as can be seen from this comparison, the composite [C₄MIM][FeCl₄]@ZIF-8 surpasses the pristine ZIF-8 with an increase in CO₂/CH₄ ideal selectivity of 7.16-7.60% at subatmospheric pressure and 5.42% at 5 bar. However, below 5 bar its ideal selectivity is still lower than that of the [C₂MIM][Ac]@ZIF-8 composite. The remaining composites do not show significant improvements in CO₂/CH₄ ideal selectivity when compared with ZIF-8 between 0 and 5 bar.

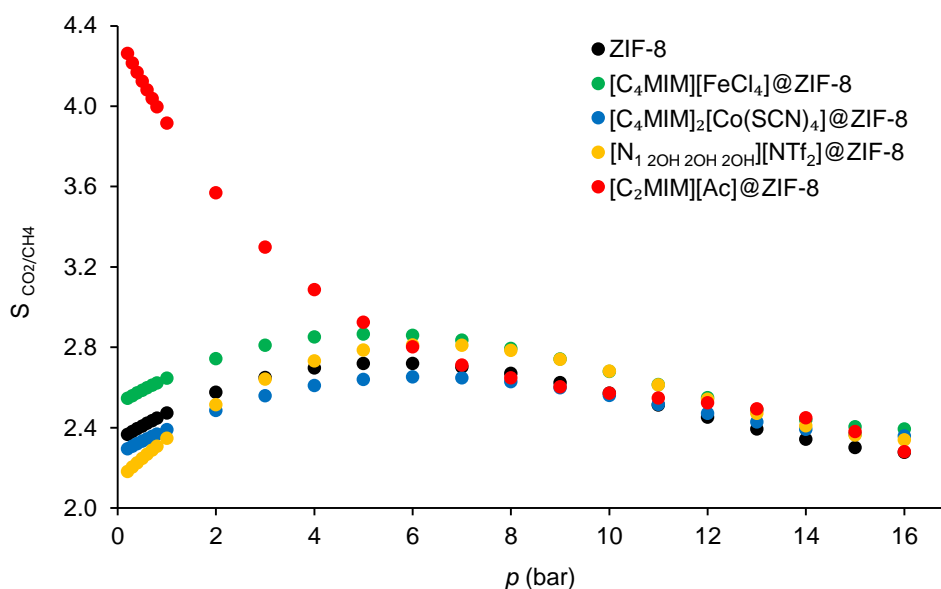


Figure 3.8. Ideal CO₂/CH₄ selectivity at 30°C for ZIF-8 and the IL@ZIF-8 composites, compared with [C₂MIM][Ac] reported by T. Ferreira [1], and using a polynomial fitting.

Nonetheless, above 5 bar these composites show an increase in ideal selectivity, with [C₄MIM][FeCl₄]@ZIF-8 showing the highest CO₂/CH₄ ideal selectivity between 10 and 16 bar, with values of 2.68 and 2.39, respectively, representing an increase of 4.24% and 5.14% in comparison with ZIF-8. Also, in the same pressure range, [N_{1,2OH,2OH,2OH}][NTf₂]@ZIF-8 shows higher ideal selectivity than the pristine ZIF-8, with this difference representing an increase of 4.28% and 2.74% at 10 and 16 bar, respectively, which can be explained by the affinity of the anion [NTf₂]⁻ in the solubilisation of CO₂ [100-102].

As previously mentioned, PSA processes for biogas upgrade to biomethane operate between 3 and 10 bar, which means that the slight increase in CO₂/CH₄ ideal selectivity presented by these materials between 5 and 16 bar, could be an indicator of their potential use in adsorption separation processes.

However, the previously discussed CO₂ uptake capacity results, show that the prepared IL@ZIF-8 composites are not suited to be used as alternative adsorbents, since they do not show an improvement in CO₂ uptake capacity, when compared with the pristine ZIF-8.

3.2. Mixed-Matrix Membranes

3.2.1. Contact Angles

As previously mentioned in section 2.2.2.1, the value of the contact angle helps to qualify a membrane when it comes to its hydrophobicity/hydrophilicity. When using water, a surface is considered hydrophilic when the contact angle is inferior to 90° and hydrophobic when said angle is superior to 90° [191]. As presented in Figure 3.9, the contact angle obtained for a pristine Matrimid®5218 membrane was 86° which is close to reported literature value of 84° [201], making it a slightly hydrophilic membrane.

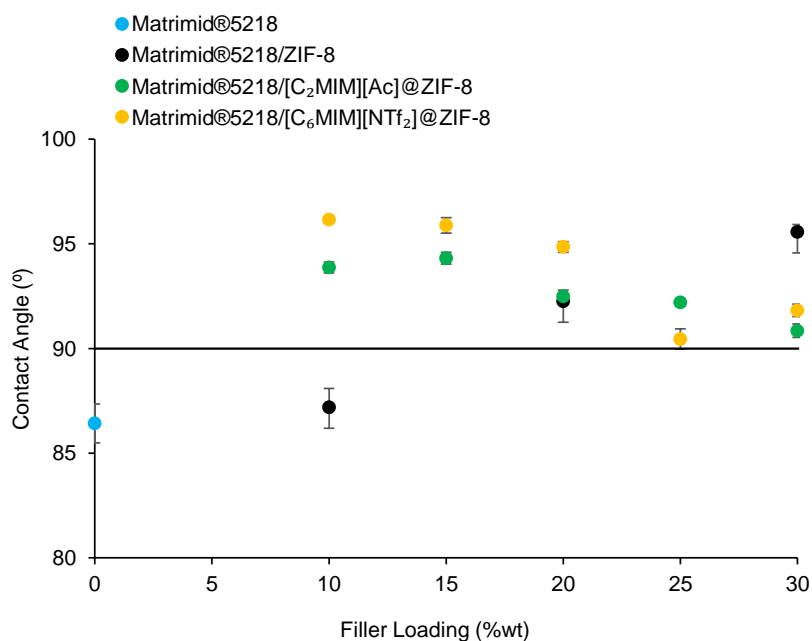


Figure 3.9. Obtained contact angles for Matrimid®5218, Matrimid®5218/ZIF-8, Matrimid®5218/[C₆MIM][NTf₂]@ZIF-8 and Matrimid®5218/[C₂MIM][Ac]@ZIF-8.

The obtained results for 20 wt% and 30 wt% Matrimid®5218/ZIF-8 are expected, considering the hydrophobic nature of ZIF-8 [202], whilst the contact angle for its 10 wt% loading can be explained by the influence of the pristine hydrophilic Matrimid®5218, that is present in the MMM in a larger amount.

Results for Matrimid®5218/[C₆MIM][NTf₂]/ZIF-8 are also consistent with literature data, due to the prementioned ZIF-8 hydrophobicity, and considering the fact the [C₆MIM][NTf₂] IL is extremely hydrophobic [203,204]. The contact angles for Matrimid®5218/[C₂MIM][Ac]/ZIF-8 are also within expected, even though [C₂MIM][Ac] is a hydrophilic IL [205]. A possible explanation for this, is that the presence of the IL – that represents only a small percentage of the filler – was not enough to counteract the hydrophobicity of the MOF.

3.2.2. Mechanical Properties

Puncture tests, previously described in section 2.2.2.2, were conducted to determine the tensile strength, σ , of the prepared membranes. Usually, when performing such tests the elongation of the membrane is determined as well. However, since all the membranes broke upon the application of force, instead of suffering an elongation, this part of the test was not determined.

As it is known, Matrimid®5218 is a polymer with good mechanical properties [206] and therefore, this test aimed to observe the changes in the membranes upon the incorporation with different loadings of ZIF-8 and the IL@MOF composites [C₆MIM][NTf₂]/ZIF-8 and [C₂MIM][Ac]/ZIF-8. Due to differences on thickness of the synthesized membranes, and to ensure a proper comparison between the obtained results, the tensile strength, obtained using equations 12 and 13, was normalized, by dividing the obtained tensile strength value by each membrane's thickness.

The average non-normalized tensile strength value obtained for the pristine Matrimid®5218 membrane with no filler is 18.13 ± 0.88 MPa (see Table 3.6) for a thickness of 125.60 ± 1.54 μ m, which, considering the error margins, is very close to reported literature values for this polymer, of approximately 14.89 ± 4.00 MPa for a membrane with a thickness value of 120 ± 15 μ m [207].

Table 3.6. Puncture test results for the Matrimid®5218/ZIF-8 membranes.

Filler Loading (%)	Matrimid®5218/ZIF-8			
	0	10	20	30
Thickness (μ m)	125.60 ± 1.54	69.60 ± 1.19	62.40 ± 1.04	81.20 ± 2.16
σ (MPa)	18.13 ± 0.88	4.34 ± 0.14	1.47 ± 0.06	1.40 ± 0.16
Normalized σ (MPa/mm)	144.36 ± 7.23	62.32 ± 2.21	23.49 ± 1.05	17.28 ± 2.00

As can be seen in Table 3.6, when filling the polymeric matrix with the MOF, the tensile strength of the new membranes is lower than that of the pristine Matrimid®5218. It is also possible to observe that an increment in ZIF-8 loading causes the tensile strength of the membranes' to decrease.

This can be explained by the rigid crystalline structure of MOFs, whose particles might be agglomerated in the polymeric matrix, acting as stress concentrators and causing plastic deformation in the matrix [212,213]. A possible way to verify said hypothesis is by conducting an Energy-Dispersive X-Ray (EDS) analysis, to determine the presence and quantify the distribution of chemical elements on the synthesized membranes [214,215]. Scanning Electron Microscopy (SEM) can also be used to analyse the morphology of the membranes [216,217], allowing the evaluation of the dispersion level of the ZIF-8 in the polymeric structure. Based on these results, it is important to note that the incorporation of ZIF-8 in the polymeric matrix of the Matrimid®5218 is not advantageous when considering the mechanical properties of Matrimid®5218-based membranes, since it turns them more fragile and rigid.

Tables 3.7 and 3.8 show the puncture tests results for the MMMs incorporating IL@ZIF-8 composites, which are lower than the non-normalized tensile strength value obtained for the Matrimid®5218 membrane, which means that none of the synthesized MMM exceed the flexibility and ductility properties of the pristine polymer membrane [210].

Table 3.7. Puncture test results for the Matrimid®5218/[C₆MIM][NTf₂]/ZIF-8 membranes.

Matrimid®5218/[C ₆ MIM][NTf ₂]/ZIF-8					
Filler Loading (%)	10	15	20	25	30
Thickness (µm)	74.80 ± 1.66	70.80 ± 0.91	72.00 ± 2.19	66.80 ± 1.66	88.00 ± 1.26
σ (MPa)	3.74 ± 0.28	2.02 ± 0.17	1.92 ± 0.07	1.06 ± 0.04	1.36 ± 0.05
Normalized σ (MPa/mm)	50.03 ± 3.88	28.52 ± 2.43	26.71 ± 1.26	15.85 ± 0.70	15.49 ± 0.62

Table 3.8. Puncture test results for the Matrimid®5218/[C₂MIM][Ac]/ZIF-8 membranes.

Matrimid®5218/[C ₂ MIM][Ac]/ZIF-8					
Filler Loading (%)	10	15	20	25	30
Thickness (mm)	69.60 ± 3.07	65.20 ± 1.66	57.20 ± 0.91	52.00 ± 0.98	73.20 ± 1.66
σ (MPa)	2.44 ± 0.22	1.84 ± 0.09	1.04 ± 0.29	0.70 ± 0.12	0.98 ± 0.09
Normalized σ (MPa/mm)	34.99 ± 3.47	28.27 ± 1.64	18.26 ± 5.17	13.44 ± 2.24	13.38 ± 1.25

The tensile strength for Matrimid®5218/[C₆MIM][NTf₂]/@ZIF-8 is higher than the puncture strength for Matrimid®5218/[C₂MIM][Ac]/@ZIF-8, for the same loadings, which is an indicator that the presence of the IL [C₆MIM][NTf₂] turns the membranes more flexible. It is also noticeable that the normalized tensile strength of the Matrimid®5218/[C₆MIM][NTf₂]/@ZIF-8 and Matrimid®5218/[C₂MIM][Ac]/@ZIF-8 membranes decreases as the IL@MOF loading increases, which is expected due to the saturation of the polymeric matrix with filler loading.

Reported literature results show that in general, the flexibility of polymer/IL@MOF membranes is higher than that of polymer/MOF membranes, due to the stiffness of the surrounding matrix that results in a smaller tendency for cracks to develop in that area. On the other hand, when the surface chemistry of the molecules softens the surrounding matrix, more cracks/debonding might develop in the interphase region [208], causing a loss of flexibility/elasticity. Considering this, and the fact that Matrimid®5218/ZIF-8 membranes presented higher tensile strength than Matrimid®5218/IL@ZIF-8 membranes, it can be concluded that the polymer-filler interfacial structures are tougher/stiffer in the first. Another possible explanation, is the fact that at higher IL@ZIF-8 loadings, and consequently higher IL loadings, the intra-chain crystallisation becomes more important than the inter-chain crystallisation, that is relevant for network formation, which results in a loss of mechanical strength and elasticity [209].

3.2.3. CO₂ and CH₄ Permeation

It is important to refer that the obtained results for CO₂ and CH₄ permeability and ideal selectivity were obtained through equations 15 and 17, respectively. Tables 3.9 and 3.10, present the CO₂/CH₄ ideal selectivity and CH₄ and CO₂ permeability results for Matrimid®5218/[C₂MIM][Ac]/@ZIF-8 (Runs 8 and 9) and Matrimid®5218/[C₆MIM][NTf₂]/@ZIF-8 (Runs 12 and 14) since these are the only membranes that presented trusted results in gas permeation assays.

The remaining ones (see Table 2.5.) should be repeated due to experimental complications, such as the membrane size (that was too small to properly cover the measurement cell) and eventual gas leaks in the permeate compartment, that might have caused disturbances in the measured pressure.

Table 3.9. CO₂/CH₄ ideal selectivity and CH₄ and CO₂ permeability results for Matrimid®5218/[C₂MIM][Ac]/@ZIF-8.

Filler Loading (wt%)	Matrimid®5218/[C ₂ MIM][Ac]/@ZIF-8	
	20 (Run 8)	25 (Run 9)
P_{CO_2} (Barrer)	63.31 ± 0.19	720.68 ± 0.78
P_{CH_4} (Barrer)	1.07 ± 0.002	11.17 ± 0.008
α_{CO_2/CH_4}	59.03	64.49

Table 3.10. CO₂/CH₄ ideal selectivity and CH₄ and CO₂ permeability results for Matrimid®5218/[C₆MIM][NTf₂]/ZIF-8.

Matrimid®5218/[C ₆ MIM][NTf ₂]/ZIF-8		
Filler Loading (wt%)	10 (Run 12)	20 (Run 14)
P_{CO_2} (Barrer)	11.85 ± 0.02	101.72 ± 0.13
P_{CH_4} (Barrer)	0.93 ± 0.0005	2.84 ± 0.002
$\alpha_{\text{CO}_2/\text{CH}_4}$	12.75	35.84

According to the data in Tables 3.9 and 3.10, all the membranes show a higher CO₂ permeability in contrast with CH₄. A possible explanation for this is the diffusion-solution mechanism that describes gas transport in non-porous membranes, translated through equation 17, where the permeability (P) depends on the solubility (S) and diffusivity (D) coefficients of a specific gas [210].

$$P = D \times S \quad (17)$$

In polymers, the CO₂ solubility coefficient is higher than that of CH₄ [211,212] which in addition to its lower energy barrier for diffusion, explains why it presents higher diffusivity and solubility rates through the ZIF-8's porous network and the Matrimid®5218 polymeric structure [212,213], and consequently higher permeability. In addition, and despite ZIF-8 having cavities of 1.1 nm connected by narrow windows of 0.34 nm, upon IL impregnation its structure might suffer structural changes that favour the transport of smaller molecules like CO₂ (kinetic diameter of 0.33 nm) instead of larger molecules like CH₄ (kinetic diameter of 0.38 nm) [213,214].

A general tendency for a paired growth in both permeability and selectivity with loading increase, can be justified not only by the absence of non-selective voids and a good polymer-filler compatibility [215], but also by the presence of ZIF-8, which has a high CO₂ uptake capacity, and by the influence of the IL in terms of affinity to favour CO₂ solubility instead of CH₄.

The [NTf₂]⁻ anion has been proved to have a good CO₂ affinity [100-102], just like the [C₂MIM][Ac] [1] which help explain the results obtained for these MMMs, as depicted in Figure 3.10, showing the ideal CO₂/CH₄ selectivities as function of the CO₂ permeability for the studied membranes, as well as literature values for Matrimid®5218 [219] and Matrimid®5218/ZIF-8 [220] in comparison with the CO₂/CH₄ Robeson Upper Bound at 30°C [166].

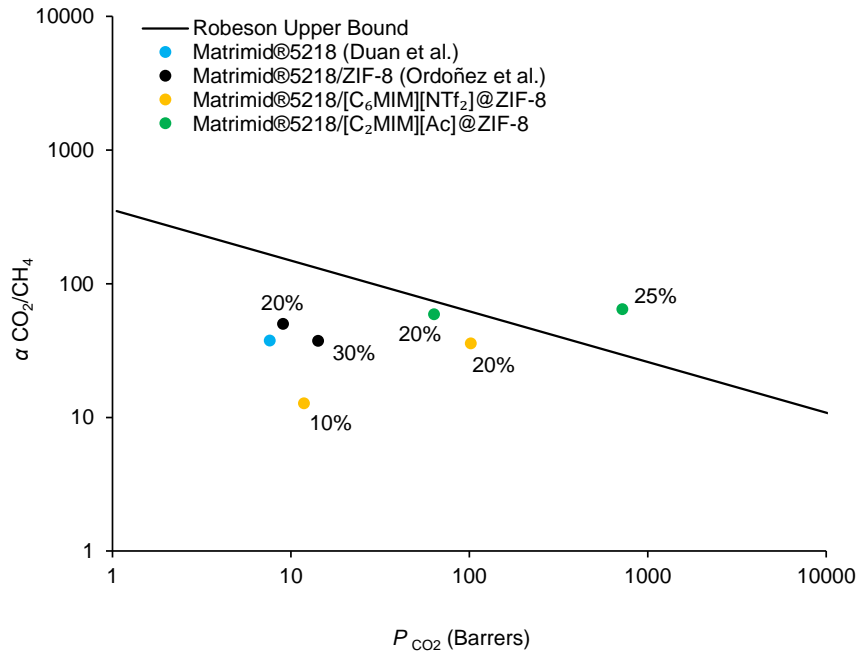


Figure 3.10. CO₂/CH₄ selectivity as function of the CO₂ permeability (Barrers) at 30°C.

The extremely encouraging results obtained for Matrimid®5218/[C₂MIM][Ac]@ZIF-8 25 wt% are in accordance with the good adsorption equilibria results reported by T. Ferreira [1] where this composite presented the highest CO₂ uptake capacity. The fact that this membrane surpasses the CO₂/CH₄ Robeson Upper Bound is a good indicator that it is a promising improvement over the reported literature data so far. However, its poor results in mechanical properties show that there is a need for optimization on what concerns its ductility/flexibility, and consequently its physical resistance to stress.

4. Conclusion

One of the goals of this thesis was to assess the CO₂ uptake capacity and CO₂/CH₄ selectivity of three brand-new IL@MOF composites: [N₁ 2OH 2OH 2OH][NTf₂]₂@ZIF-8, [C₄MIM]₂[Co(SCN)₄]₂@ZIF-8 and [C₄MIM][FeCl₄]₂@ZIF-8, for a feasible application in biogas upgrading processes. The prepared IL@ZIF-8 composites were fully characterized in order to understand the effect of the IL in the structure of ZIF-8.

He pycnometry showed that the IL@ZIF-8 composites have lower solid matrix density values than the pristine ZIF-8, which allows the conclusion of a successful IL impregnation. N₂ adsorption-desorption at 77 K, alongside NLDFT analysis, showed that all composited have a Type I isotherm and pores smaller than 20 Å, which according to IUPAC classification is a characteristic of microporous materials [100]. It also showed that upon IL impregnation, the IL@ZIF-8 composites suffered a loss in BET specific surface area and pore volume. For [N₁ 2OH 2OH 2OH][NTf₂]₂@ZIF-8 the loss in BET specific surface area and total pore volume was of 13.06% and 26.87%, respectively. For [C₄MIM][FeCl₄]₂@ZIF-8 these losses were more drastic, with BET surface area and total pore volume suffering a decrease of 63.77% and 64.29%, respectively. The composite [C₄MIM]₂[Co(SCN)₄]₂@ZIF-8 presented a BET specific surface area loss of 57.16% and a total pore volume loss of 58.20%.

In Powder X-Ray Diffraction (PXRD), and due to an organized atomic 3D structure, crystalline materials present high and narrow intensity peaks. Since the characteristic peaks of ZIF-8, a crystalline material, were present in all the synthesized composites, PXRD allowed the conclusion that these materials are also crystalline. Fourier Transform Infrared Spectroscopy (FT-IR) showed the presence of infrared bands, characteristic of each IL on the plot of transmittance as a function of the wavenumber of the [N₁ 2OH 2OH 2OH][NTf₂]₂@ZIF-8 and [C₄MIM]₂[Co(SCN)₄]₂@ZIF-8 composites, which is a further indicator of a successful IL impregnation.

Adsorption equilibria, conducted through a static gravimetric method at the temperature of 30°C and in the pressure range of 0-16 bar showed that for both CH₄ and CO₂ uptake capacity none of the prepared IL@ZIF-8 composites surpass the pristine ZIF-8 due to the IL impregnation that partially occupied pore volume and surface area. All the composites suffered losses in CO₂ uptake capacity between 19-50% at 1 bar, and between 17-53% at 16 bar, when compared with the pristine ZIF-8.

When it comes to ideal selectivity, the obtained results indicate that up to 5 bar, none of the composites surfaced the [C₂MIM][Ac]₂@ZIF-8 prepared by T. Ferreira. However, the composite [C₄MIM][FeCl₄]₂@ZIF-8 surpasses the pristine ZIF-8 with an increase of 7.16-7.60% at subatmospheric pressure and 5.42% at 5 bar.

Between 10 and 16 bar, the [C₄MIM][FeCl₄]/ZIF-8 composite presented the highest CO₂/CH₄ ideal selectivity with values of 2.68 and 2.39 for 10 and 16 bar, respectively, which represent an increase of 4.24% and 5.14% regarding the pristine ZIF-8. Furthermore, [N_{1,2OH,2OH,2OH}][NTf₂]/ZIF-8 also showed higher ideal selectivity values than the pristine ZIF-8, with increases of 4.28% and 2.74% for 10 and 16 bar, respectively.

In parallel, this thesis also aimed to test the CO₂ permeability and CO₂/CH₄ ideal selectivity in Matrimid®5218-based mixed-matrix membranes with the [C₆MIM][NTf₂]/ZIF-8 and [C₂MIM][Ac]/ZIF-8 composites, reported by T. Ferreira, as fillers. For this, the membranes were prepared using the solvent evaporation method and posteriorly characterized for their mechanical properties and hydrophobicity.

Gas permeation experiments showed that all the membranes have higher CO₂ permeability than CH₄, which can be explained by CO₂ having a higher solubility coefficient in polymers, and by its lower energy barrier for diffusion. Both permeability and selectivity increase with the filler loading, not only due to the absence of non-selective voids and good polymer-filler compatibility, but also, and more importantly, due to the presence of ZIF-8 which has a high CO₂ uptake capacity and to the influence of the ILs that have a good affinity towards CO₂ solubility. The obtained results for the Matrimid®5218/[C₂MIM][Ac]/ZIF-8 membrane that surpasses the Robeson Upper Bound, show that this polymer/filler combination is an improvement over the reported literature data so far when it comes to establishing a good trade-off relationship between permeability and selectivity.

As for the mechanical properties of the prepared MMMs, the ones containing ZIF-8 as filler were more fragile and rigid than the pristine Matrimid®5218, due to the agglomeration of ZIF-8 particles in the polymeric matrix that act as stress concentrators and can cause plastic deformation in the matrix, and thus the incorporation of this MOF in this polymeric matrix is not advantageous. Usually the flexibility of a membrane is enhanced upon incorporation with an IL. However, when the membranes were loaded with IL@MOF composites, it was verified a loss of elasticity and mechanical strength.

Despite the promising results obtained in the gas permeation experiments, the optimization of the mechanical properties of these membranes is of the utmost importance for a future application in industrial gas separation processes.

5. Future Work

After the developed work in this thesis, regarding adsorption equilibria for the composites $[N_{1,2OH,2OH}][NTf_2]@ZIF-8$, $[C_4MIM]_2[Co(SCN)_4]@ZIF-8$ and $[C_4MIM][FeCl_4]@ZIF-8$, and the membranes Matrimid@5218/ $[C_6MIM][NTf_2]@ZIF-8$ and Matrimid@5218/ $[C_2MIM][Ac]@ZIF-8$, and considering the fact that there are hundreds of IL@MOFs' possible combinations, there are some aspects that can be further investigated, as follows:

- (1) Test adsorption for the utilized materials, with a binary mixture that represents the typical biogas stream;
- (2) Incorporate higher IL loadings in IL@MOF composites to study its effect and impacts regarding both adsorption and gas permeation;
- (3) Perform gas permeation in higher pressure/temperature ranges to evaluate the performance differences of the membranes (partially) studied in this thesis;
- (4) Conduct a FT-IR analysis on the reported membranes, to understand the existent bonds between filler and matrix;
- (5) Test IL impregnation in different MOFs that might have better CO_2 uptake capacity and selectivity;
- (6) Synthesize, for a posterior IL@MOF composite creation, an IL with an $[Ac]^-$ anion and a $[N_{1,2OH,2OH,2OH}]^+$ cation and test its adsorption and gas permeation performance;
- (7) Test all the utilized composites, on adsorption and gas permeation with membranes, for CO_2/N_2 mixtures;
- (8) Try different polymeric matrixes

6. References

- [1] T. Ferreira, (2017). Thesis: Hybrid Ionic Liquids/Metal Organic Frameworks for CO₂/CH₄ Separation.
- [2] American Association for the Advancement of Science, (2009). Letter to US Senator,. Available: <https://botany.org/Resources/ClimateLetter20091021.pdf> [Accessed January 9th].
- [3] Union of Concerned Scientists, (2014). Global Warming Impacts,. Available: <https://www.ucsusa.org/our-work/global-warming/science-and-impacts/global-warming-impacts#.WseLL4jwbWV> [Accessed January 9th].
- [4] National Geographic, (2015). Effects of Global Warming,. Available: <https://www.nationalgeographic.com/environment/global-warming/global-warming-effects/> [Accessed January 9th].
- [5] Intergovernmental Panel on Climate Change, (2015). Climate Change 2014 – Synthesis Report, pp. 2–26.
- [6] World Meteorological Organization, (2017). Greenhouse Gas Bulletin, *World Meteorological Organization Bulletin*. pp. 1–4.
- [7] National Oceanic and Atmospheric Association, (2018). ENSO: Recent Evolution, Current Status and Predictions,. Available: http://www.cpc.ncep.noaa.gov/products/analysis_monitoring/lanina/ [Accessed January 9th].
- [8] M.P. Chipperfield et al., (2017). Detecting recovery of the stratospheric ozone layer, *Nature*. vol. 549, pp. 211–218.
- [9] National Aeronautics and Space Administration (NASA), (1998). Greenhouse Gases: Refining the Role of Carbon Dioxide,. Available: https://www.giss.nasa.gov/research/briefs/ma_01/ [Accessed January 10th].
- [10] V.J. Fabry *et al.*, (2015). Impacts of ocean acidification on marine fauna and ecosystem processes, *Journal of Marine Science*. vol. 65, pp. 414–432.
- [11] J. Tollefson, (2017). CO₂ emissions set to spike in 2017, *Nature*. vol. 551, pp. 283.
- [12] J. Tollefson, (2017). Trump says no to climate pact, *Nature*. vol. 546, pp. 198.
- [13] United Nations: Climate Change, (2015). Paris Agreement - Status of Ratification,. Available: http://unfccc.int/paris_agreement/items/9444.php [Accessed January 16th].
- [14] R.B. Jackson *et al.*, (2017). Warning signs for stabilizing global CO₂ emissions, *Environmental Research Letters*. vol. 12, pp. 1–4.
- [15] J.C.M. Pires *et al.*, (2011). Recent developments on carbon capture and storage: An overview, *Chemical Engineering Research and Design*. vol. 89, pp. 1446–1460.
- [16] International Energy Agency, (2017). Global Carbon Dioxide Emissions 1980-2016, pp. 1–996. Available: <https://www.iea.org/newsroom/energysnapshots/global-carbon-dioxide-emissions-1980-2016.html> [Accessed January 10th].

- [17] Nina Chestney, (2018). Global carbon emissions hit record high in 2017,. Available: <https://www.reuters.com/article/us-energy-carbon-ia/global-carbon-emissions-hit-record-high-in-2017-idUSKBN1GY0RB> [Accessed September 9th].
- [18] NOAA Research News, (2018). Another Climate Milestone on Mauna Loa,. Available: <https://research.noaa.gov/article/ArtMID/587/ArticleID/2362/Another-climate-milestone-falls-at-NOAA's-Mauna-Loa-observatory> [Accessed September 9th].
- [19] Intergovernmental Panel on Climate Change, (2007). Climate Change 2007 - The Physical Science Basis.
- [20] Intergovernmental Panel on Climate Change, (2013). Climate Change 2013 – The Physical Science Basis.
- [21] D. Shang *et al.*, (2017). Ionic liquids in gas separation processing, *Current Opinion in Green and Sustainable Chemistry*. vol. 5, pp. 74–81.
- [22] I.A.A.C. Esteves and J.P.B. Mota, (2007). Gas Separation by a Novel Hybrid Membrane/Pressure Swing Adsorption Process, *Industrial & Engineering Chemistry Research*. vol. 46, pp. 5723–5733.
- [23] I.A.A.C. Esteves and J.P.B. Mota, (2007). Hybrid Membrane/PSA Processes for CO₂/N₂ Separation, *Adsorption Science & Technology*. vol. 25, pp. 693–716.
- [24] B. Guo *et al.*, (2006). Adsorption of Carbon Dioxide on Activated Carbon, *Journal of Natural Gas Chemistry*. vol. 15, pp. 223–229.
- [25] F. Akhtar *et al.*, (2017). Thin zeolite laminates for rapid and energy-efficient carbon capture, *Nature – Scientific Reports*. vol. 7, pp. 3–8.
- [26] A. Elsayed *et al.*, (2014). Experimental and numerical investigation of the effect of pellet size on the adsorption characteristics of activated carbon/ethanol, *Energy Procedia*. vol. 61, pp. 2327–2330.
- [27] F. Rouquerol *et al.*, (1999). Adsorption by Powders and Porous Solids: Principles, Methodology and Applications.
- [28] F.P. Kinik *et al.*, (2016). [BMIM][PF₆] Incorporation Doubles CO₂ Selectivity of ZIF-8: Elucidation of Interactions and Their Consequences on Performance, *ACS Applied Materials and Interfaces*. vol. 8, pp. 30992–31005.
- [29] P. Llewellyn *et al.*, (2008). High Uptakes of CO₂ and CH₄ in Mesoporous Metal Organic Frameworks MIL-100 and MIL-101, *Langmuir*. vol. 24, pp. 7245–7250.
- [30] I. Cota and F. Fernandez Martinez, (2017). Recent advances in the synthesis and applications of metal organic frameworks doped with ionic liquids for CO₂ adsorption, *Coordination Chemistry Reviews*. vol. 361, pp. 189–204.
- [31] S. Cavenati *et al.*, (2008). Metal organic framework adsorbent for biogas upgrading, *Industrial & Engineering Chemistry Research*. vol. 47, pp. 6333–6335.
- [32] E. Adatoz *et al.*, (2015). Opportunities and challenges of MOF-based membranes in gas separations, *Separation and Purification Technology*. vol. 152, pp. 207–237.

- [33] P.P. Radecki *et al.*, (1999). Emerging Separation and Separative Reaction Technologies for Process Waste Reduction - Adsorption and Membrane Systems.
- [34] S.S. Hosseini *et al.*, (2016). Recent progress in development of high performance polymeric membranes and materials for metal plating wastewater treatment: A review, *Journal of Water Process Engineering*. vol. 9, pp. 78–110.
- [35] W. Li *et al.*, (2015). Metal-organic framework composite membranes: Synthesis and separation applications, *Chemical Engineering Science*. vol. 135, pp. 232–257.
- [36] M. Rezakazemi *et al.*, (2014). State-of-the-art membrane based CO₂ separation using mixed matrix membranes (MMMs): An overview on current status and future directions, *Progress in Polymer Science*. vol. 39, pp. 817–861.
- [37] H.B. Tanh Jeazet *et al.*, (2016). Increased Selectivity in CO₂/CH₄ Separation with Mixed-Matrix Membranes of Polysulfone and Mixed-MOFs MIL-101(Cr) and ZIF-8, *European Journal of Inorganic Chemistry*. pp. 4363–4367.
- [38] B. Zornoza *et al.*, (2013). Metal organic framework based mixed matrix membranes: An increasingly important field of research with a large application potential, *Microporous and Mesoporous Materials*. vol. 166, pp. 67–78.
- [39] I. Erucar *et al.*, (2013). Recent advances in metal-organic framework-based mixed matrix membranes, *Chemistry - An Asian Journal*. vol. 8, pp. 1692–1704.
- [40] I. Ferreira, (2017). Thesis: Carbon dioxide capture using mixed matrix membranes with metal-organic frameworks supporting ionic liquids.
- [41] W. Zhang *et al.*, (2018). Fabrication of mixed-matrix membranes with MOF-derived porous carbon for CO₂ separation, *AIChE Journal*. vol. 64, pp. 3400–3409.
- [42] P.S. Goh *et al.*, (2011). Recent advances of inorganic fillers in mixed matrix membrane for gas separation, *Separation and Purification Technology*. vol. 81, pp. 243–264.
- [43] A.J. Fletcher *et al.*, (2005). Flexibility in metal-organic framework materials: Impact on sorption properties, *Journal of Solid State Chemistry*. vol. 178, pp. 2491–2510.
- [44] G. Férey and C. Serre, (2009). Large breathing effects in three-dimensional porous hybrid matter: Facts, analyses, rules and consequences, *Chemical Society Reviews*. vol. 38, pp. 1380–1399.
- [45] BP, (2015). Statistical Review of World Energy June 2015, *British Petroleum*. pp. 48.
- [46] S. Faramawy *et al.*, (2016). Natural gas origin, composition, and processing: A review, *Journal of Natural Gas Science and Engineering*. vol. 34, pp. 34–54.
- [47] ChemEngineering, (2016). Flue Gas,. Available: <https://chemenginring.wikispaces.com/Fluegas> [Accessed July 4th].
- [48] Union of Concerned Scientists, (2014). Environmental Impacts of Natural Gas,. Available: <https://www.ucsusa.org/clean-energy/coal-and-other-fossil-fuels/environmental-impacts-of-natural-gas#.W1RwD6tjO01> [Accessed June 9th].

- [49] P. Luis, (2016). Use of monoethanolamine (MEA) for CO₂ capture in a global scenario: Consequences and alternatives, *Desalination*. vol. 380, pp. 93–99.
- [50] X. He and M.B. Hägg, (2014). Energy efficient process for CO₂ capture from flue gas with novel fixed-site-carrier membranes, *Energy Procedia*. vol. 63, pp. 174–185.
- [51] S. Achinas *et al.*, (2017). A Technological Overview of Biogas Production from Biowaste, *Engineering*. vol. 3, pp. 299–307.
- [52] G. Leonzio, (2016). Upgrading of biogas to bio-methane with chemical absorption process: Simulation and environmental impact, *Journal of Cleaner Production*. vol. 131, pp. 364–375.
- [53] W.L. McCabe *et al.*, (1993). Unit Operations of Chemical Engineering, pp. 1130.
- [54] L.M. Galán Sánchez *et al.*, (2007). Solvent Properties of Functionalized Ionic Liquids for CO₂ Absorption, *Chemical Engineering Research and Design*. vol. 85, pp. 31–39.
- [55] J.R. Li *et al.*, (2014). Carbon dioxide capture-related gas adsorption and separation in metal-organic frameworks, *Coordination Chemistry Reviews*. vol. 255, pp. 1791–1823.
- [56] M. Wang *et al.*, (2011). Post-combustion CO₂ capture with chemical absorption: A state-of-the-art review, *Chemical Engineering Research and Design*. vol. 89, pp. 1609–1624.
- [57] R. Smith, (2005). Chemical Process Design and Integration, John Wiley & Sons, INC, .
- [58] E.B. Rinker *et al.*, (2000). Absorption of Carbon Dioxide in Aqueous Blends of Diethanolamine and Methylethanolamine, *Industrial & Engineering Chemistry Research*. vol. 39, pp. 4346–4356. Available: http://rochelle.che.utexas.edu/files/2015/02/Chakravarti_Thesis_1992.pdf.
- [59] M. Fürhacker *et al.*, (2003). Aerobic biodegradability of methyldiethanolamine (MDEA) used in natural gas sweetening plants in batch tests and continuous flow experiments, *Chemosphere*. vol. 52, pp. 1743–1748.
- [60] H.A. Rangwala *et al.*, (1992). Absorption of CO₂ into aqueous tertiary amine/mea solutions, *The Canadian Journal of Chemical Engineering*. vol. 70, pp. 482–490.
- [61] A.A. Khan *et al.*, (2016). Experimental investigation of sorption characteristics of capturing carbon dioxide into piperazine activated aqueous 2-amino-2-methyl-1-propanol solution in a packed column, *International Journal of Greenhouse Gas Control*. vol. 44, pp. 217–226.
- [62] U.E. Aronu *et al.*, (2009). Solvent selection for carbon dioxide absorption, *Energy Procedia*. vol. 1, pp. 1051–1057.
- [63] J. Dupont, (2011). From molten salts to ionic liquids: A “nano” journey, *Accounts of Chemical Research*. vol. 44, pp. 1223–1231.
- [64] Z. Lei *et al.*, (2017). Introduction: Ionic Liquids, *Chemical Reviews*. vol. 117, pp. 6633–6635.
- [65] C. Ye *et al.*, (2001). Room-temperature ionic liquids: A novel versatile lubricant, *Chemical Communications*. vol. 21, pp. 2244–2245.
- [66] J.S. Wilkes, (2002). A short history of ionic liquids - From molten salts to neoteric solvents, *Green Chemistry*. vol. 4, pp. 73–80.
- [67] A. Arce *et al.*, (2006). Mutually immiscible ionic liquids, *Chemical Communications*. vol. 2, pp. 2548–2550.

- [68] J. Holbrey *et al.*, (2003). Solubility and Solvation in Ionic Liquids, *ChemInform*. vol. 34,.
- [69] J. Vila *et al.*, (2006). Great increase of the electrical conductivity of ionic liquids in aqueous solutions, *Fluid Phase Equilibria*. vol. 247, pp. 32–39.
- [70] K. Ghandi, (2014). A Review of Ionic Liquids, Their Limits and Applications, *Green and Sustainable Chemistry*. vol. 4, pp. 44–53.
- [71] M. Alhamami *et al.*, (2009). Ionic-liquid materials for the electrochemical challenges of the future, *Nature Materials*. vol. 8, pp. 621–629.
- [72] J. Wang *et al.*, (2016). Recent development of ionic liquid membranes, *Green Energy & Environment*. vol. 1, pp. 43–61.
- [73] K. Fujie and H. Kitagawa, (2016). Ionic liquid transported into metal-organic frameworks, *Coordination Chemistry Reviews*. vol. 307, pp. 382–390.
- [74] F. Rantwijk and R. Sheldon, (2007). Biocatalysis in Ionic Liquids, *Chemical Reviews*. vol. 107, pp. 2757–2785.
- [75] J. Qu *et al.*, (2009). Ionic Liquids as Novel Lubricants and Additives for Diesel Engine Applications, *Tribology Letters*. vol. 35, pp. 181–189.
- [76] K.N. Marsh *et al.*, (2004). Room temperature ionic liquids and their mixtures - A review, *Fluid Phase Equilibria*. vol. 219, pp. 93–98.
- [77] J.P. Hallett and T. Welton, (2011). Room-temperature ionic liquids: Solvents for synthesis and catalysis, *Chemical Reviews*. vol. 111, pp. 3508–3576.
- [78] C. Yue *et al.*, (2011). Synthesis and application of task-specific ionic liquids used as catalysts and/or solvents in organic unit reactions, *Journal of Molecular Liquids*. vol. 163, pp. 99–121.
- [79] B.E. Gurkan *et al.*, (2010). Equimolar CO₂ Absorption by Anion-Functionalized Ionic Liquids, *Journal of the American Chemical Society*. vol. 132, pp. 2116–2117.
- [80] B. Wu *et al.*, (2017). Poly (ionic liquid)-Based Breath Figure Films: A New Kind of Honeycomb Porous Films with Great Extendable Capability, *Nature - Scientific Reports*. vol. 7, pp. 1–15.
- [81] W. Qian *et al.*, (2017). Frontiers in poly(ionic liquid)s: Syntheses and applications, *Chemical Society Reviews*. vol. 46, pp. 1124–1159.
- [82] S. Wickramanayake *et al.*, (2014). Mechanically robust hollow fiber supported ionic liquid membranes for CO₂ separation applications, *Journal of Membrane Science*. vol. 470, pp. 52–59.
- [83] A.A. Shamsuri and D.K. Abdullah, (2010). Ionic Liquids: Preparations and Limitations, *Makara, Sains*. vol. 14, pp. 101–106.
- [84] A.E. Samir, (2011). Ionic Liquids Recycling for Reuse, *Ionic Liquids - Classes and Properties*. pp. 239–272.
- [85] J.U. Keller and R. Staudt, (2005). Gas adsorption equilibria: Experimental Methods and Adsorptive Isotherms.
- [86] D.D. Do, (1998). Adsorption Analysis: Equilibria and Kinetics.

- [87] S. Goldberg, (2005). Equations and models describing adsorption processes in soils, *Chemical Processes in Soils*. vol. 8, pp. 489–517.
- [88] Micromeritics Instrument Corporation, (2014). Gas Adsorption Theory,. Available: http://www.micromeritics.com/Repository/Files/Gas_Adsorption_Theory_poster.pdf [Accessed January 15th].
- [89] J. Coca *et al.*, (1985). Mass Transfer Operations: Absorption and Extraction, *Encyclopedia of Life Support Systems*. vol. 2,.
- [90] P. Webb, (2003). Introduction to Chemical Adsorption Analytical Techniques and their Applications to Catalysis, *MIC Technical Publications*. vol. 13, pp. 1–4.
- [91] R. Fernandez-Prini, (1982). Le Chatelier's Principle and the Prediction of the Effect of Temperature on solubilities, *Journal of Chemical Education*. vol. 59, pp. 550–553.
- [92] J.M. Thomas, (1961). The existence of endothermic adsorption, *Journal of Chemical Education*. vol. 38, pp. 138.
- [93] Effect of pressure on adsorption of a gas, (2015). Available: <https://chemistry.stackexchange.com/questions/61164/effect-of-pressure-on-adsorption-of-a-gas> [Accessed January 20th].
- [94] D.Y.C. Leung *et al.*, (2014). An overview of current status of carbon dioxide capture and storage technologies, *Renewable and Sustainable Energy Reviews*. vol. 39, pp. 426–443.
- [95] M. Mulholland and M.A. Latifi, (2009). Predictive Control of Pressure Swing Adsorption, in: Proc. 17th Int. Conf. Process Control '09, : pp. 323–331.
- [96] L. Jiang *et al.*, (2018). Performance exploration of temperature swing adsorption technology for carbon dioxide capture, *Energy Conversion and Management*. vol. 165, pp. 396–404.
- [97] M.A. Kalbassi *et al.*, (1998). Temperature Swing Adsorption, US5846295.
- [98] D.M. Ruthven *et al.*, (1994). Pressure Swing Adsorption.
- [99] K.S.W. Sing, (1985). Reporting physisorption data for gas/solid systems with special reference to the determination of surface area and porosity, *Pure and Applied Chemistry*. vol. 57, pp. 603–619.
- [100] M. Thommes *et al.*, (2015). Physisorption of gases, with special reference to the evaluation of surface area and pore size distribution (IUPAC Technical Report), *Pure and Applied Chemistry*. vol. 87, pp. 1051–1069.
- [101] K.S. Knaebel, (2004). Adsorbent Selection, *Albright's Chemical Engineering Handbook*. vol. 20, pp. 1119–1171.
- [102] American Physical Society, J. Willard Gibbs, (n.d.). Available: <https://www.aps.org/programs/outreach/history/historicsites/gibbs.cfm> [Accessed April 6th].
- [103] S. Gumma and O. Talu, (2010). Net adsorption: A thermodynamic framework for supercritical gas adsorption and storage in porous solids, *Langmuir*. vol. 26, pp. 17013–17023.
- [104] S. Gumma and O. Talu, (2003). Gibbs dividing surface and helium adsorption, *Adsorption*. vol. 9, pp. 17–28.

- [105] I.A.A.C. Esteves, (2005). Thesis: Gas Separation Processes by Integrated Adsorption and Permeation Technology.
- [106] R.H. Perry *et al.*, (1997). Chemical Engineers' Handbook.
- [107] Engineering 360 – IEEE, (2018). Absorbents and Adsorbents Information,. Available: https://www.globalspec.com/learnmore/materials_chemicals_adhesives/chemicals_raw_materials/desiccants_absorbents [Accessed January 20th].
- [108] National Programme on Technology Enhanced Learning, (2009). Surface Characterization Techniques,. Available: <http://nptel.ac.in/courses/122101001/downloads/lec-37.pdf> [Accessed February 26th].
- [109] A. Itodo *et al.*, (2010). Estimation of Specific Surface Area using Langmuir Isotherm Method, *Journal of Applied Sciences and Environmental Management*. vol. 14, pp. 141–145.
- [110] M.S. Mavens, (2012). The Importance of Surface Area in Adsorbents,. Available: <http://hengyeusa.com/community/the-importance-of-surface-area-and-adsorbents> [Accessed January 20th].
- [111] M.J. Ndolomingo and R. Meijboom, (2016). Determination of the surface area and sizes of supported copper nanoparticles through organothiol adsorption - Chemisorption, *Applied Surface Science*. vol. 390, pp. 224–235.
- [112] R.T. Yang, (2003). Adsorbents, Fundamentals and Applications, John Wiley & Sons, INC, .
- [113] B. Jha and D.N. Singh, (2016). Fly Ash Zeolites: Advanced Structured Materials, vol. 78,.
- [114] M. Alhamami *et al.*, (2014). A review on breathing behaviors of metal-organic-frameworks (MOFs) for gas adsorption, *Materials*. vol. 7, pp. 3198–3250.
- [115] A.C. Tella and I.Y. Aaron, (2012). Syntheses and Applications of Metal-Organic Frameworks Materials: A Review Frameworkds, *Acta Chimica and Pharmaceutica Indica*. vol. 2, pp. 75–81.
- [116] K.K. Gangu *et al.*, (2016). A review on contemporary Metal-Organic Framework materials, *Inorganica Chimica Acta*. vol. 446, pp. 61–74.
- [117] S. Ma and H.-C. Zhou, (2010). Gas storage in porous metal–organic frameworks for clean energy applications, *Chem. Commun*. vol. 46, pp. 44–53.
- [118] K. Sumida *et al.*, (2012). Carbon dioxide capture in metal-organic frameworks, *Chemical Reviews*. vol. 112, pp. 724–781.
- [119] M.P. Suh *et al.*, (2011). Hydrogen storage in metal-organic frameworks, *Chemical Reviews*. vol. 112, pp. 782–835.
- [120] Y. He *et al.*, (2014). Methane storage in metal-organic frameworks, *Chemical Society Reviews*. vol. 43, pp. 5657–5678.
- [121] J. Lee *et al.*, (2009). Metal-organic framework materials as catalysts, *Chemical Society Reviews*. vol. 38, pp. 1450–1459.
- [122] M. Yoon *et al.*, (2012). Homochiral metal-organic frameworks for asymmetric heterogeneous catalysis, *Chemical Reviews*. vol. 112, pp. 1196–1231.

- [123] J. Liu *et al.*, (2014). Applications of metal-organic frameworks in heterogeneous supramolecular catalysis, *Chemical Society Reviews*. vol. 43, pp. 6011–6061.
- [124] L. Ma *et al.*, (2009). Enantioselective catalysis with homochiral metal-organic frameworks, *Chemical Society Reviews*. vol. 38, pp. 1248–1256.
- [125] M.D. Allendorf *et al.*, (2009). Luminescent metal-organic frameworks, *Chemical Society Reviews*. vol. 38, pp. 1330–1352.
- [126] Z. Hu *et al.*, (2014). Luminescent metal-organic frameworks for chemical sensing and explosive detection, *Chemical Society Reviews*. vol. 43, pp. 5815–5840.
- [127] L.E. Kreno *et al.*, (2012). Metal-Organic Framework Materials as Chemical Sensors, *Chemical Reviews*. vol. 112, pp. 1105–1125.
- [128] P. Ramaswamy *et al.*, (2014). MOFs as proton conductors-challenges and opportunities, *Chemical Society Reviews*. vol. 43, pp. 5913–5932.
- [129] J.M. Taylor *et al.*, (2010). Facile proton conduction via ordered water molecules in a phosphonate metal-organic framework, *Journal of the American Chemical Society*. vol. 132, pp. 14055–14057.
- [130] J.A. Hurd *et al.*, (2009). Anhydrous proton conduction at 150°C in a crystalline metal-organic framework, *Nature Chemistry*. vol. 1, pp. 705–710.
- [131] P. Horcajada *et al.*, (2012). Metal-Organic Frameworks in Biomedicine, pp. 1232–1268.
- [132] P. Horcajada *et al.*, (2010). Porous metal-organic-framework nanoscale carriers as a potential platform for drug delivery and imaging, *Nature Materials*. vol. 9, pp. 172–178.
- [133] J. Della Rocca *et al.*, (2011). Nanoscale metal-organic frameworks for biomedical imaging and drug delivery, *Accounts of Chemical Research*. vol. 44, pp. 957–968.
- [134] C.A. Trickett *et al.*, (2017). The chemistry of metal-organic frameworks for CO₂ capture, regeneration and conversion, *Nature Reviews Materials*. vol. 2, pp. 17045.
- [135] A.R. Millward and O.M. Yaghi, (2005). Metal Organic Frameworks with Exceptionally High Capacity for Storage of Carbon Dioxide at Room Temperature, *Journal of the American Chemical Society*. vol. 127, pp. 17998–17999.
- [136] K. Vikrant *et al.*, (2017). Metal-organic frameworks (MOFs): Potential and challenges for capture and abatement of ammonia, *Journal of Materials Chemistry A*. vol. 5, pp. 2215–2221.
- [137] J. Zhang *et al.*, (2016). Synthesis, Photoluminescence, and Gas Adsorption Properties of a New Furan-Functionalized MOF and Direct Carbonization for Synthesis of Porous Carbon, *Crystal Growth and Design*. vol. 16, pp. 475–482.
- [138] B. Mu *et al.*, (2010). Gas adsorption study on mesoporous metal-organic framework UMCM-1, *Journal of Physical Chemistry C*. vol. 114, pp. 6464–6471.
- [139] V. Finsy *et al.*, (2009). Separation of CO₂/CH₄ mixtures with the MIL-53(Al) metal-organic framework, *Microporous and Mesoporous Materials*. vol. 120, pp. 221–227.
- [140] H. Wu *et al.*, (2010). Highly selective CO₂ capture by a flexible microporous metal-organic framework (MMOF) material, *Chemistry - A European Journal*. vol. 16, pp. 13951–13954.

- [141] D. Wu *et al.*, (2013). Direct calorimetric measurement of enthalpy of adsorption of carbon dioxide on CD-MOF-2, a green metal-organic framework, *Journal of the American Chemical Society*. vol. 135, pp. 6790–6793.
- [142] J.J. Gassensmith *et al.*, (2011). Strong and reversible binding of carbon dioxide in a green metal-organic framework, *Journal of the American Chemical Society*. vol. 133, pp. 15312–15315.
- [143] R.A. Smaldone *et al.*, (2010). Metalorganic frameworks from edible natural products, *Angewandte Chemie - International Edition*. vol. 49, pp. 8630–8634.
- [144] S. Han *et al.*, (2011). Imprinting chemical and responsive micropatterns into metal-organic frameworks, *Angewandte Chemie - International Edition*. vol. 50, pp. 276–279.
- [145] D. Danaci *et al.*, (2015). Assessment of ZIF materials for CO₂ capture from high pressure natural gas streams, *Chemical Engineering Journal*. vol. 280, pp. 486–493.
- [146] N. De Acha *et al.*, (2017). Detection of Ethanol in Human Breath Using Optical Fiber Long Period Grating Coated with Metal-Organic Frameworks, *Proceedings*. vol. 1, pp. 474.
- [147] I. Dincer, (2018). Comprehensive Energy Systems - Catalysts: Metal-Organic Frameworks, in: 1st ed., Elsevier, .
- [148] K.S. Park *et al.*, (2006). Exceptional chemical and thermal stability of zeolitic imidazolate frameworks, *Proceedings of the National Academy of Sciences of the United States of America*. vol. 103, pp. 10186–91.
- [149] I.U. Khan *et al.*, (2018). Economical, environmental friendly synthesis, characterization for the production of zeolitic imidazolate framework-8 (ZIF-8) nanoparticles with enhanced CO₂ adsorption, *Arabian Journal of Chemistry*. vol. 8, pp. 0–11.
- [150] M. Du *et al.*, (2016). Adsorption mechanism on metal organic frameworks of Cu-BTC, Fe-BTC and ZIF-8 for CO₂ capture investigated by X-ray absorption fine structure, *RSC Adv*. vol. 6, pp. 62705–62716.
- [151] B. Chen *et al.*, (2014). Zeolitic imidazolate framework materials: Recent progress in synthesis and applications, *Journal of Materials Chemistry A*. vol. 2, pp. 16811–16831.
- [152] K.Y.A. Lin and H.A. Chang, (2014). Efficient adsorptive removal of humic acid from water using zeolitic imidazole framework-8 (ZIF-8), *Water, Air, and Soil Pollution*. vol. 226, pp. 2–17.
- [153] W.H. Chen *et al.*, (2018). Biocatalytic cascades driven by enzymes encapsulated in metal-organic framework nanoparticles, *Nature Catalysis*. vol. 2018,.
- [154] K.B. Sezginel *et al.*, (2016). Tuning the Gas Separation Performance of CuBTC by Ionic Liquid Incorporation, *Langmuir*. vol. 32, pp. 1139–1147.
- [155] E.R. Cooper *et al.*, (2004). Ionic liquids and eutectic mixtures as solvent and template in synthesis of zeolite analogues, *Nature*. vol. 430, pp. 1012–1016.
- [156] D.N. Dybtsev *et al.*, (2004). Synthesized From an Ionic Liquid Medium, vol. 3, pp. 1594–1595.

- [157] R.E. Morris, (2009). Ionothermal synthesis - Ionic liquids as functional solvents in the preparation of crystalline materials, *Chemical Communications*. pp. 2990–2998.
- [158] Q.X. Luo *et al.*, (2014). Molecular size- and shape-selective Knoevenagel condensation over microporous Cu₃(BTC)₂ immobilized amino-functionalized basic ionic liquid catalyst, *Applied Catalysis A: General*. vol. 478, pp. 81–90.
- [159] M. Ji *et al.*, (2013). Organic electron-rich N-heterocyclic compound as a chemical bridge: Building a Brønsted acidic ionic liquid confined in MIL-101 nanocages, *Journal of Materials Chemistry A*. vol. 1, pp. 6530–6534.
- [160] IEA Bioenergy, (2017). Annual Report 2017, *International Energy Agency: Paris, France*. pp. 140.
- [161] M.R. Riazi and D. Chiaramonti, (2017). Biofuels Production and Processing Technology.
- [162] X.Y. Chen *et al.*, (2015). Membrane gas separation technologies for biogas upgrading.
- [163] D. Nevstrueva, Thesis: Preparation of Polysulfone Membranes, (n.d.).
- [164] T. Yang and T.S. Chung, (2013). High performance ZIF-8/PBI nano-composite membranes for high temperature hydrogen separation consisting of carbon monoxide and water vapor, *International Journal of Hydrogen Energy*. vol. 38, pp. 229–239.
- [165] J.E. Cadotte, (1981). Interacially synthesized reverse osmosis membrane, US4277344.
- [166] L.M. Robeson, (2008). The upper bound revisited, *Journal of Membrane Science*. vol. 320, pp. 390–400.
- [167] H. Verweij, (2012). Inorganic membranes, *Current Opinion in Chemical Engineering*. vol. 1, pp. 156–162.
- [168] Y. Zhang *et al.*, (2013). Current status and development of membranes for CO₂/CH₄ separation: A review, *International Journal of Greenhouse Gas Control*. vol. 12, pp. 84–107.
- [169] C.M. Zimmerman *et al.*, (1997). Tailoring mixed matrix composite membranes for gas separations, *Journal of Membrane Science*. vol. 137, pp. 145–154.
- [170] B. Zornoza *et al.*, (2009). Mesoporous silica sphere-polysulfone mixed matrix membranes for gas separation, *Langmuir*. vol. 25, pp. 5903–5909.
- [171] B. Zornoza *et al.*, (2011). Hollow silicalite-1 sphere-polymer mixed matrix membranes for gas separation, *Separation and Purification Technology*. vol. 77, pp. 137–145.
- [172] T.H. Bae *et al.*, (2009). Facile high-yield solvothermal deposition of inorganic nanostructures on zeolite crystals for mixed matrix membrane fabrication, *Journal of the American Chemical Society*. vol. 131, pp. 14662–14663.
- [173] O.G. Nik *et al.*, (2011). Amine-functionalized zeolite FAU/EMT-polyimide mixed matrix membranes for CO₂/CH₄ separation, *Journal of Membrane Science*. vol. 379, pp. 468–478.
- [174] X.Y. Chen *et al.*, (2016). Mixed matrix membranes based on silica nanoparticles and microcellular polymers for CO₂/CH₄ separation, *Journal of Cellular Plastics*. pp. 1–23.
- [175] A.L. Khan *et al.*, (2012). SPEEK and functionalized mesoporous MCM-41 mixed-matrix membranes for gas Separation, *Procedia Engineering*. vol. 44, pp. 1902–1905.

- [176] H.B. Tanh Jeazet *et al.*, (2012). Metal-organic frameworks in mixed-matrix membranes for gas separation, *Dalton Transactions*. vol. 41, pp. 14003–14027.
- [177] S. Shahid, (2015). Thesis: Polymer-Metal Organic Frameworks (MOFs) Mixed Matrix Membranes for Gas Separation Applications.
- [178] F. Dorosti *et al.*, (2014). Fabrication and characterization of Matrimid/MIL-53 mixed matrix membrane for CO₂/CH₄ separation, *Chemical Engineering Research and Design*. vol. 92, pp. 2439–2448.
- [179] T.T. Moore and W.J. Koros, (2005). Non-ideal effects in organic-inorganic materials for gas separation membranes, *Journal of Molecular Structure*. vol. 739, pp. 87–98.
- [180] Y. Ban *et al.*, (2015). Confinement of Ionic Liquids in Nanocages: Tailoring the Molecular Sieving Properties of ZIF-8 for Membrane-Based CO₂ Capture, *Angewandte Chemie - International Edition*. vol. 54, pp. 15483–15487.
- [181] L.M. Robeson, (1991). Correlation of separation factor versus permeability for polymeric membranes, *Journal of Membrane Science*. vol. 62, pp. 165–185.
- [182] NIST, Ionic Liquids Database - ILThermo, (n.d.). Available: <https://ilthermo.boulder.nist.gov><https://ilthermo.boulder.nist.gov> [Accessed June 19th].
- [183] T. Peng Chee *et al.*, (2017). Size Control and Stability Study of Zeolitic Imidazolate Framework-8 to Prepare Mixed Matrix Membrane, *Journal of Physical Science*. vol. 28, pp. 215–226.
- [184] B.C.R. Camacho *et al.*, (2015). Adsorption equilibrium of carbon dioxide and nitrogen on the MIL-53(Al) metal organic framework, *Separation and Purification Technology*. vol. 141, pp. 150–159.
- [185] K. Sing, (2001). The use of nitrogen adsorption for the characterisation of porous materials, *Colloids and Surfaces A: Physicochemical and Engineering Aspects*. vol. 187–188, pp. 3–9.
- [186] V. Pecharsky and P. Zavalij, (2016). Fundamentals of Powder Diffraction and Structural Characterization of Materials.
- [187] Materials Evaluation and Engineering, (2014). Fourier Transform-Infrared Spectroscopy, in: *Handb. Anal. Methods Mater.*, : pp. 19–20.
- [188] A.L. Myers and P.A. Monson, (2014). Physical Adsorption of Gases: The Case for Absolute Adsorption as the Basis for Thermodynamic Analysis, vol. 20, pp. 591–622.
- [189] Special Chem, Matrimid@5218, (n.d.). Available: <https://adhesives.specialchem.com/product/p-huntsman-matrimid-5218> [Accessed July 6th].
- [190] P.S. Tin *et al.*, (2003). Effects of cross-linking modification on gas separation performance of Matrimid membranes, *Journal of Membrane Science*. vol. 225, pp. 77–90.
- [191] Kino, Contact angle, wetting, and spreading, (n.d.). Available: <http://www.surface-tension.org/article/60.html> [Accessed June 7th].
- [192] AMETEK, Puncture strength testing, (n.d.). Available: <https://www.ametektest.com/learningzone/testtypes/puncture-testing> [Accessed June 7th].

- [193] S. Cao *et al.*, (2013). Hierarchical bicontinuous porosity in metal-organic frameworks templated from functional block co-oligomer micelles, *Chemical Science*. vol. 4, pp. 3573–3577.
- [194] B.D. Cullity, (1978). Elements of Diffraction.
- [195] X. Gong *et al.*, (2017). ZIF-8-Based Membranes for Carbon Dioxide Capture and Separation, *ACS Sustainable Chemistry and Engineering*. vol. 5, pp. 11204–11214.
- [196] Y.R. Lee *et al.*, (2015). ZIF-8: A comparison of synthesis methods, *Chemical Engineering Journal*. vol. 271, pp. 276–280.
- [197] J. Tatarko, (2015). Thesis: The production, properties and applications of the zinc imidazolate, ZIF-8.
- [198] K. Hanke *et al.*, (2015). Understanding the ionic liquid [NC₄₁₁₁][NTf₂] from individual building blocks: An IR-spectroscopic study, *Physical Chemistry Chemical Physics*. vol. 17, pp. 8518–8529.
- [199] G. Socrates, (2001). Infrared and Raman characteristic group frequencies.
- [200] I. Angelidaki *et al.*, (2018). Biogas upgrading and utilization : Current status and perspectives, *Biotechnology Advances*. vol. 36, pp. 452–466.
- [201] L.Y. Jiang and T.S. Chung, (2009). β -Cyclodextrin containing Matrimid®-nanocomposite membranes for pervaporation application, *Journal of Membrane Science*. vol. 327, pp. 216–225.
- [202] K. Zhang *et al.*, (2013). Exploring the framework hydrophobicity and flexibility of ZIF-8: From biofuel recovery to hydrocarbon separations, *Journal of Physical Chemistry Letters*. vol. 4, pp. 3618–3622.
- [203] M.G. Freire *et al.*, (2008). Mutual Solubilities of Water and the [C_nMIM][Tf₂N] Hydrophobic Ionic Liquids, *The Journal of Physical Chemistry B*. vol. 112, pp. 1604–1610.
- [204] P. Yee *et al.*, (2013). State of hydrophobic and hydrophilic ionic liquids in aqueous solutions: Are the ions fully dissociated?, *Journal of Physical Chemistry B*. vol. 117, pp. 12556–12566.
- [205] S. Wang *et al.*, (2013). Syntheses, crystal structures of two coordination polymers constructed from imidazole-based dicarboxylate ligands containing alkyl group, *Inorganic Chemistry Communications*. vol. 30, pp. 115–119.
- [206] R. Castro-Muñoz *et al.*, (2018). Matrimid® 5218 in preparation of membranes for gas separation: Current state-of-the-art, *Chemical Engineering Communications*. vol. 205, pp. 161–196.
- [207] N. Sanches, (2012). Thesis: Desenvolvimento de Membranas para Separação de Gases contendo MOFs (Metal Organic Frameworks), pp. 56. Available: <http://hdl.handle.net/10362/7729>.
- [208] H. Li *et al.*, (2016). Simultaneous enhancement of mechanical properties and CO₂ selectivity of ZIF-8 mixed matrix membranes: Interfacial toughening effect of ionic liquid, *Journal of Membrane Science*. vol. 511, pp. 130–142.

- [209] P. Bernardo *et al.*, (2012). Gas transport properties of Pebax®/room temperature ionic liquid gel membranes, *Separation and Purification Technology*. vol. 97, pp. 73–82.
- [210] A.F. Ismail *et al.*, (2005). Understanding the Solution-Diffusion Mechanism in Gas Separation Membrane for Engineering Students, *Regional Conference on Engineering Education*. pp. 155–159.
- [211] O. Vopička *et al.*, Mixed gas sorption in glassy polymeric membranes: CO₂/CH₄ mixtures in a polymer of intrinsic microporosity (PIM-1)., vol. 39, (n.d.).
- [212] M. Mulder, (2003). Basic principles of membrane technology, 2nd ed., Kluwer Academic Publishers, .
- [213] L. Zhang *et al.*, (2014). Adsorption and Diffusion of CO₂ and CH₄ in Zeolitic Imidazolate Framework-8: Effect of Structural Flexibility, *The Journal of Physical Chemistry C*. pp. 140411102121001.
- [214] J. Yang *et al.*, (2012). Adsorption of CO₂, CH₄, and N₂ on gas diameter grade ion-exchange small pore zeolites, *Journal of Chemical and Engineering Data*. vol. 57, pp. 3701–3709.
- [215] S. Shahid and K. Nijmeijer, (2014). Performance and plasticization behavior of polymer-MOF membranes for gas separation at elevated pressures, *Journal of Membrane Science*. vol. 470, pp. 166–177.
- [216] S.N.V.K. Aki *et al.*, (2004). High-Pressure Phase Behavior of Carbon Dioxide with Imidazolium-Based Ionic Liquids, *Journal of Physical Chemistry*. vol. 108, pp. 20355–20365.
- [217] E.K. Shin *et al.*, (2008). High-pressure solubilities of carbon dioxide in ionic liquids: 1-Alkyl-3-methylimidazolium bis(trifluoromethylsulfonyl)imide, *Journal of Supercritical Fluids*. vol. 45, pp. 282–292.
- [218] S. Raeissi and C.J. Peters, (2009). Carbon Dioxide Solubility in the Homologous 1-Alkyl-3-methylimidazolium Bis (trifluoromethylsulfonyl) imide Family, *Journal of Chemical & Engineering Data*. vol. 54, pp. 382–386.
- [219] C. Duan *et al.*, (2014). Post-treatment effect on gas separation property of mixed matrix membranes containing metal organic frameworks, *Journal of Membrane Science*. vol. 466, pp. 92–102.
- [220] M.J.C. Ordoñez *et al.*, (2010). Molecular sieving realized with ZIF-8/Matrimid® mixed-matrix membranes, *Journal of Membrane Science*. vol. 361, pp. 28–37.

7. Appendixes

7.1. Appendix A – He Pycnometry Data

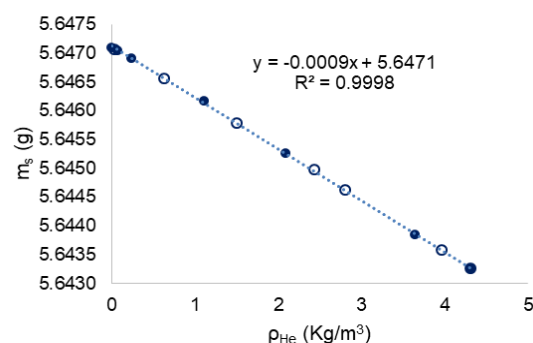
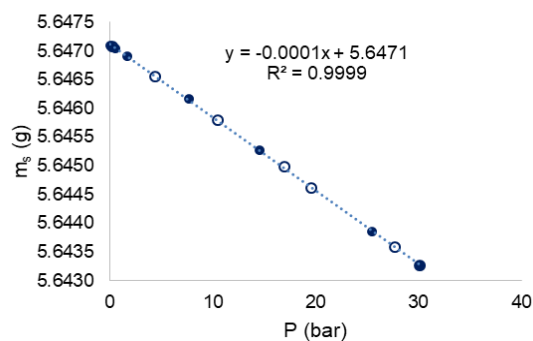
Before measuring the data related to He Pycnometry in the gravimetric unit, the sampler holder's mass and volume has to be determined, with a blank measurement. These results are listed below.

	Sample Holder 1	Sample Holder 2
Mass (g)	5.35086	6.32864
Volume (cm ³)	0.68146	0.80339

Afterwards, the He pycnometry measurements were performed and the plots in this appendix represent the apparent mass (m_s) as function He density (ρ_{He}) for the measured composites [N₁ 2OH 2OH][NTf₂]₂@ZIF-8, [C₄MIM]₂[Co(SCN)₄]₂@ZIF-8 and [C₄MIM][FeCl₄]₂@ZIF-8. The trendline presented solely describes the adsorption points. The value of its intercept is the solid's matrix mass (discounting the mass of the sample holder) and its slope is the solid's matrix's volume (discounting the volume of the sample holder). The values of the He density at different pressure and temperatures were obtained from reference [107].

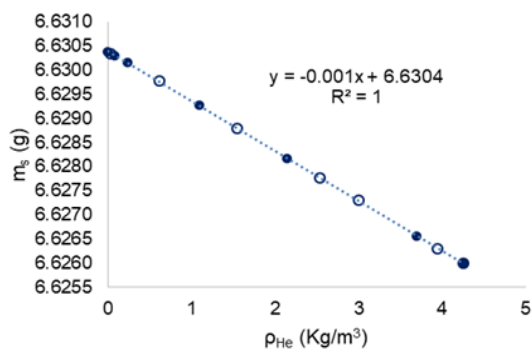
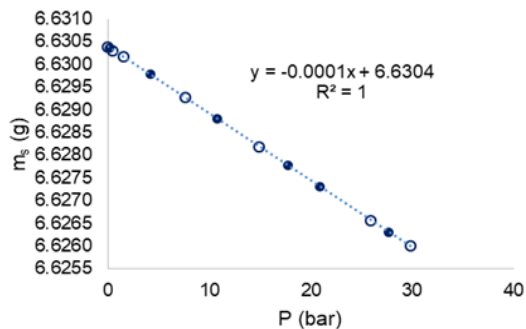
- [N₁ 2OH 2OH 2OH][NTf₂]₂@ZIF-8

T (°C)	P (bar)	m_s (g)	ρ_{He} (kg/cm ³)
59.98	0.00000	5.64710	0.0000
60.09	0.50280	5.64704	0.0726
60.06	1.65333	5.64691	0.2387
60.05	7.67774	5.64617	1.1058
60.00	14.50018	5.64527	2.0831
59.92	25.42915	5.64386	3.6379
59.88	30.13225	5.64326	4.3030
59.98	27.68904	5.64358	3.9569
60.11	19.56491	5.64462	2.8040
60.10	16.92759	5.64498	2.4287
60.08	10.47257	5.64579	1.5066
60.08	4.40385	5.64656	0.6351
60.12	0.19490	5.64707	0.0282
59.91	0.00000	5.64706	0.0000



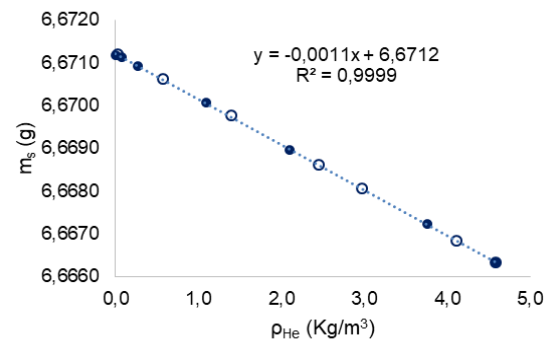
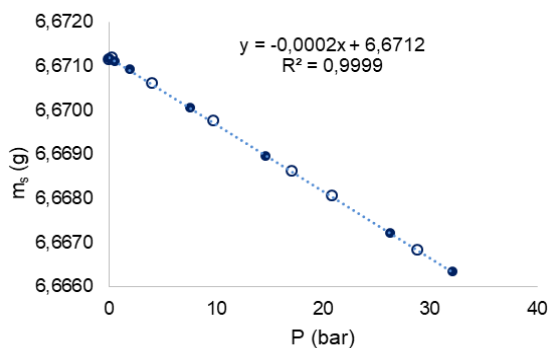
- $[\text{C}_4\text{MIM}]_2[\text{Co}(\text{SCN})_4]@\text{ZIF-8}$

T (°C)	P (bar)	m_s (g)	ρ_{He} (kg/cm ³)
60.00	0.00000	6.63038	0.0000
60.13	0.49980	6.63030	0.0722
60.12	1.57938	6.63016	0.2280
60.06	7.60413	6.62928	1.0952
60.03	14.92695	6.62817	2.1438
59.94	25.85300	6.62656	3.6977
59.88	29.84647	6.62599	4.2627
59.98	27.64865	6.62630	3.9512
60.05	20.93120	6.62730	2.9987
60.05	17.72959	6.62777	2.5433
60.11	10.78561	6.62879	1.5513
60.01	4.23062	6.62978	0.6103
60.06	0.19720	6.63035	0.0285
59.92	0.00000	6.63031	0.0000



- $[\text{C}_4\text{MIM}][\text{FeCl}_4]@\text{ZIF-8}$

T (°C)	P (bar)	m_s (g)	ρ_{He} (kg/cm ³)
59.96	0.00000	6.67118	0.0000
60.07	0.54580	6.67112	0.0788
60.08	1.88827	6.67093	0.2726
60.04	7.60653	6.67006	1.0957
60.01	14.58094	6.66897	2.0945
59.88	26.26607	6.66722	3.7568
59.89	32.08629	6.66634	4.5784
59.99	28.78884	6.66684	4.1121
60.07	20.77325	6.66806	2.9761
60.08	17.04837	6.66862	2.4460
60.12	9.69609	6.66976	1.3951
60.06	3.97813	6.67063	0.5738
60.09	0.19860	6.67120	0.0287
59.88	0.00000	6.67116	0.0000



7.2. Appendix B – Polynomial Fitting Parameters

Table 7.1 presents the obtained parameters upon fitting the adsorption equilibria experimental data with a polynomial (order 4) adjustment.

Table 7.1. Parameters of the polynomial fitting.

Samples	CH ₄						CO ₂					
	a	b	c	d	e	ARE (%)	a	b	c	d	e	ARE (%)
ZIF-8	-2.52E-06	-3.11E-05	-2.43E-03	2.60E-01	0	1.23	1.46E-04	-5.05E-03	3.43E-02	6.07E-01	0	2.52
[N ₁ 2OH 2OH 2OH][NTf ₂]@ZIF-8	1.21E-06	-3.21E-05	-3.44E-03	2.23E-01	0	1.55	1.81E-04	-6.06E-03	4.49E-02	4.76E-01	0	4.44
[C ₄ MIM][FeCl ₄]@ZIF-8	6.18E-07	-3.10E-05	-2.38E-03	1.50E-01	0	0.99	9.62E-05	-3.01E-03	1.59E-02	3.76E-01	0	4.87
[C ₄ MIM] ₂ [Co(SCN) ₄]@ZIF-8	-4.04E-06	1.24E-04	-3.78E-03	1.38E-01	0	3.41	5.76E-05	-1.89E-03	9.61E-03	3.21E-01	0	2.41